NASA CONTRACTOR REPORT

NASA CR-2305

AN EXPERIMENTAL INVESTIGATION OF VORTEX STABILITY, TIP SHAPES, COMPRESSIBILITY, AND NOISE FOR HOVERING MODEL ROTORS

by James L. Tangler, Robert M. Wohlfeld, and Stan J. Miley

Prepared by
BELL HELICOPTER COMPANY
Fort Worth, Texas 76101
for Langley Research Center

NATIONAL AERONAUTICS AND SPACE ADMINISTRATION • WASHINGTON, D. C. • SEPTEMBER 1973

1. Report No.	2. Government Accession No.	3. Recipient's Catalog No.
NASA CR-2305		

4. Title and Subtitle	5. Report Date
AN EXPERIMENTAL INVESTIGATION OF VORTEX STABILITY, TIP SHAPES, COMPRESSIBILITY, AND NOISE FOR HOVERING MODEL ROTORS*	September 1973
	6. Performing Organization Code
7. Author(s)	8. Performing Organization Report No.
James L. Tangler, Robert M. Wohlfeld, and Stan J. Miley	299-099-641
	10. Work Unit No.
9. Performing Organization Name and Address	
Bell Helicopter Company Fort Worth, TX 76101	11. Contract or Grant No. NAS1-10946
	13. Type of Report and Period Covered
12. Sponsoring Agency Name and Address	Contractor Report
National Aeronautics and Space Administration Washington, D.C. 20546	14. Sponsoring Agency Code

15. Supplementary Notes

*The contract research effort which has lead to the results in this report was financially supported by USAAMRDL (Langley Directorate).

This is a final report.

16. Abstract

Schlieren methods of flow visualization and hot-wire anemometry for velocity measurements were used to investigate the wakes generated by hovering model propellers and rotors. The research program was directed toward investigating (1) the stability of the tip vortex, (2) the effects produced by various tip shapes on performance and tip vortex characteristics, and (3) the shock formation and noise characteristics associated with various tip shapes. A free-wake analysis was also conducted for comparison with the vortex stability experimental results.

Schlieren photographs showing wake asymmetry, interaction, and instability are presented along with a discussion of the effects produced by the number of blades, collective pitch, and tip speed. Two hot-wire anemometer techniques, used to measure the maximum circumferential velocity in the tip vortex, are discussed. These were used in conjunction with the schlieren system to relate the tip vortex characteristics of three tip shapes investigated to their measured performance. Schlieren photographs illustrating the three-dimensional spiral shock formation produced at the rotor tip are presented along with a comparison of the effects produced by airfoil profile and tip shape.

17. Key Words (Suggested by Author(s))	18. Distribution Statement
Hovering rotor, wake flow, schlieren photography, spiral shock waves, tip shapes	Unclassified - Unlimited

19. Security Classif. (of this report)	20. Security Classif. (of this page)	21. No. of Pages	22. Price*
Unclassified	Unclassified	85	Domestic, $3.75 Foreign, $6.25

*For sale by the National Technical Information Service, Springfield, Virginia 22151

TABLE OF CONTENTS

TABLE OF CONTENTS (CONTINUED)

SYMBOLS

b	number of blades
c	blade chord
C_T	rotor thrust coefficient, thrust/$\pi R^2 \rho (\Omega R)^2$
C_Q	rotor torque coefficient, torque/$\pi R^3 \rho (\Omega R)^2$
M_T	blade tip Mach number
r	radius of a spanwise station from center of rotation
R	blade radius
Re	Reynolds number at blade tip based on chord
V_r	wake induced radial velocity component
V_t	wake induced tangential velocity component
V_z	wake induced axial velocity component
V_θ	maximum circumferential velocity in vortex
V_τ	translational velocity of vortex
x,y,z	fixed axis system rectangular coordinates
Γ	circulation of a vortex
θ	blade collective pitch angle
ρ	air density
ψ	blade azimuth angle relative to x-axis
ψ_W	azimuth angle measured from a blade to a point on the trailing helical tip vortex filament that originates from the blade
ω	angular velocity at which two vortices revolve about their centroid of vorticity
Ω	rotor angular velocity

LIST OF FIGURES

LIST OF FIGURES (CONTINUED)

LIST OF FIGURES (CONTINUED)

LIST OF FIGURES (CONTINUED)

AN EXPERIMENTAL INVESTIGATION OF VORTEX STABILITY, TIP SHAPES, COMPRESSIBILITY, AND NOISE FOR HOVERING MODEL ROTORS

By James L. Tangler, Robert M. Wohlfeld,
and Stan J. Miley
Bell Helicopter Company

I. INTRODUCTION

A hovering rotor blade generates a continuous vortex sheet, the outboard portion of which immediately rolls up into a discrete vortex at the blade's tip as shown in Figure 1.

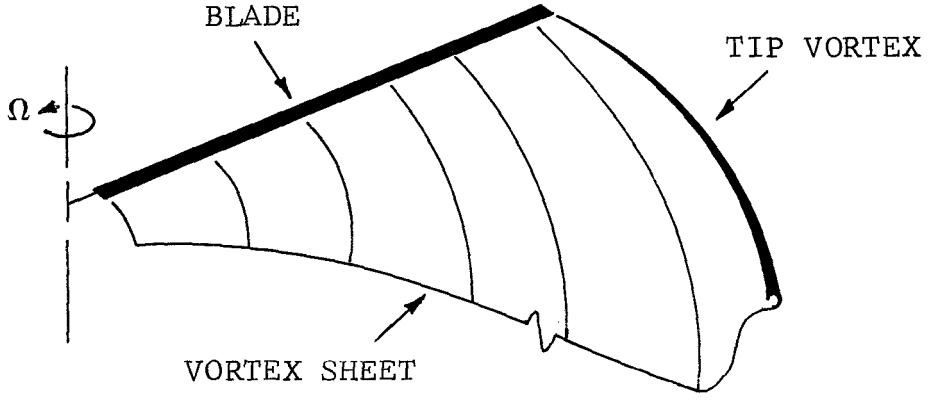

Figure 1. Wake Generated by a Rotor Blade.

The tip vortex and the remaining portion of the vortex sheet travel downward in a smoothly contracting helical pattern determined by the induced velocity field generated by both the wake and the bound blade vorticity. The vortex sheet travels downstream at a much faster rate than the tip vortex. In the region of maximum wake contraction the strong interaction between adjacent tip vortices from neighboring rotor blades alters the trajectory of the vortices causing them to move downward at an irregular rate. Thereafter, vortex instability occurs, which eventually results in vortex diffusion and breakup. This process differs considerably from the classical concept of a smoothly contracting wake that moves downstream in an orderly manner.

Most studies on vortex stability have dealt with the tip vortex pair generated by fixed-wing aircraft. Various factors and mechanisms responsible for the instability and decay of a vortex pair have been reported in References 1 through 3. An

early investigation of the motion and stability of a helical vortex was conducted by Levy and Forsdyke (Ref. 4). They found that a helical vortex was stable only if the tangent of the helical pitch angle exceeds 0.3. Based on their finding the wake generated by a hovering propeller or rotor would be unstable since each has a pitch less than this value.

A free-wake analysis developed by Crimi (Ref. 5) can be used to calculate the trajectory of the tip vortex generated by a rotor. Using his method in the hover mode for a two-bladed rotor, he notes evidence of nonperiodic wake behavior occurring between two to three revolutions of the wake below the rotor.

Tanner and Wohlfeld (Ref. 6) applied the schlieren method of flow visualization to rotating systems, and studied the path followed by the tip vortex generated by model propellers. They observed that the wake became unstable several revolutions below the rotor, and that there was a high degree of mixing between the vortex sheet generated by a blade and the tip vortex from the previous blade.

Extensive analytical and experimental investigations of helicopter hover performance and wake geometry characteristics have been conducted by Landgrebe (Refs. 7 through 9). During these investigations he found evidence of wake instability which increased with distance below the rotor. He also found that small errors in predicting the wake geometry close to the rotor can result in large errors in performance predictions. This was particularly true for rotors having more than two blades.

Recently Widnall (Ref. 10) theoretically investigated the stability of a helical vortex filament. The results of this investigation showed that a helical vortex filament has several modes of instability.

Several investigators have looked at the effects produced by blade tip shape on tip vortex characteristics and performance. McCormick et.al. (Ref. 11) conducted wind-tunnel tests to determine the vortex characteristics associated with several tips. Results from this investigation showed that a 60 deg swept-aft tip substantially reduced the maximum circumferential velocity in the tip vortex over that of a square tip.

R. Spivey (Ref. 12) investigated the effects of profile and planform shape on tip aerodynamics and found that sweeping the leading edge of the tip aft 70 deg reduced the power required in forward flight. Further wind-tunnel studies by W. Spivey (Ref. 13) found that both a swept-aft and double-swept tip provided performance improvements over a square tip for a wide range of conditions.

Recently the wake generated by a hovering rotor has been surveyed using hot-film and hot-wire anemometer techniques. Boatwright (Ref. 14) surveyed the wake generated by a full-scale rotor using a split-film total vector anemometer to obtain three-component wake velocity measurements. Cook (Ref. 15) investigated the structure of the tip vortex generated by a full-scale single-bladed rotor using a hot-wire anemometer.

The prediction of hover performance requires an accurate description of the flow field in which the rotor will operate. Although significant progress has been made in defining the flow field for a wide range of conditions, detailed knowledge about various aspects of the wake is required to further refine presently available hover performance methods. Those areas in which insufficient knowledge is available concern (1) the stability of the tip vortex, (2) the rate at which the tip vortex decays, and (3) the effects produced by tip geometry on the characteristics of the tip vortex. These areas also pertain to the analysis of aerodynamic noise and wake induced vibratory loads on an aircraft's fuselage and lifting surfaces.

The purpose of this research program was to develop experimental techniques (utilizing the schlieren method of flow visualization and hot-wire method of velocity measurement) for studying the wake of small-scale rotors in hover. These techniques were directed toward:

(1) Determining what factors and mechanisms are involved in vortex interaction and instability and how these phenomena are manifested.

(2) Analyzing the performance and flow field characteristics of a square, swept, and double-swept tip shape.

(3) Investigating the shock formation and noise characteristics associated with various airfoil profiles and tip shapes.

II. EXPERIMENTAL APPARATUS

2.1 Model Rotor Facility

The test facility used for this investigation was located in a large room at Bell Helicopter Company as shown in Figure 2. The facility included two model rotor hover test rigs and a schlieren system for visualizing the rotor's flow field.

2.1.1 Primary hover test rig. - The primary hover test rig is shown in Figure 3. The rotor was mounted in an inverted position so that the wake propagated upward. This position eliminated any ground effect or test stand interference with the wake. The electric drive motor was rated at 5.96 kilowatts at 20,000 rpm and was driven by a variable frequency power supply. Through a 3.33:1 speed reduction system the rpm was reduced to 6000 for driving the 35 cm radius rotor shown. This rpm corresponded to a maximum tip speed of 214 m/sec. Because of the motor's power limitation this tip speed could not be achieved at high collective pitch settings. Consequently, it was necessary to limit rotor tip speeds to 152 m/sec so that the complete collective pitch range of the rotors could be utilized. Wake studies at tip speeds greater than 152 m/sec were conducted using 16.5 and 20.3 cm radius propellers and rotors without the speed reduction system.

Rotor thrust measurements were obtained from a small strain-gaged cantilever beam mounted inside the base of the test stand. The complete rotor and drive system was mounted to a steel shaft that was free to slide up and down inside the test stand base. The bottom of the shaft was supported by the end of the cantilever beam. One ball bearing provided point contact between the end of the cantilever beam and the center of the shaft supporting the rotor and drive system. Torque measurements were obtained from a strain-gaged moment arm located about half-way up the test stand. Both thrust and torque measurements were recorded on an X-Y plotter.

A traversing mechanism located above the rotor in the region of the wake was used to position a hot-wire anemometer probe. The probe could be positioned radially with a motor-driven lead screw. The vertical position had to be changed manually.

2.1.2 One-bladed hover test rig. - The secondary test rig, shown in Figure 4, was used for taking velocity measurements of the tip vortex generated by a single-bladed rotor. The rotor was powered by a 187 watt variable speed electric motor controlled by a variac. A telescoping, traversing mechanism that rotates with the blade was used to position the hot-wire

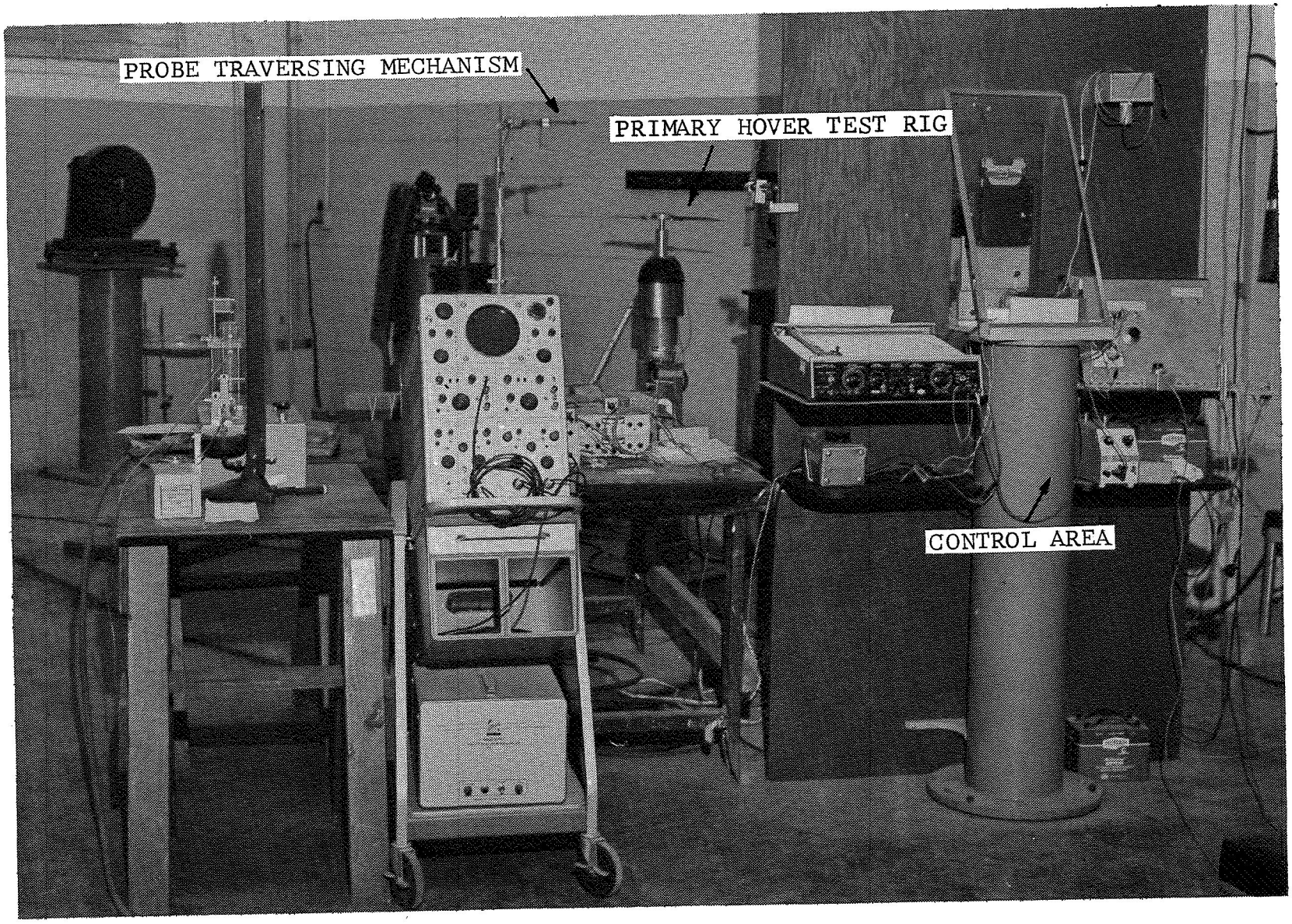

Figure 2. Model Rotor Hover Facility.

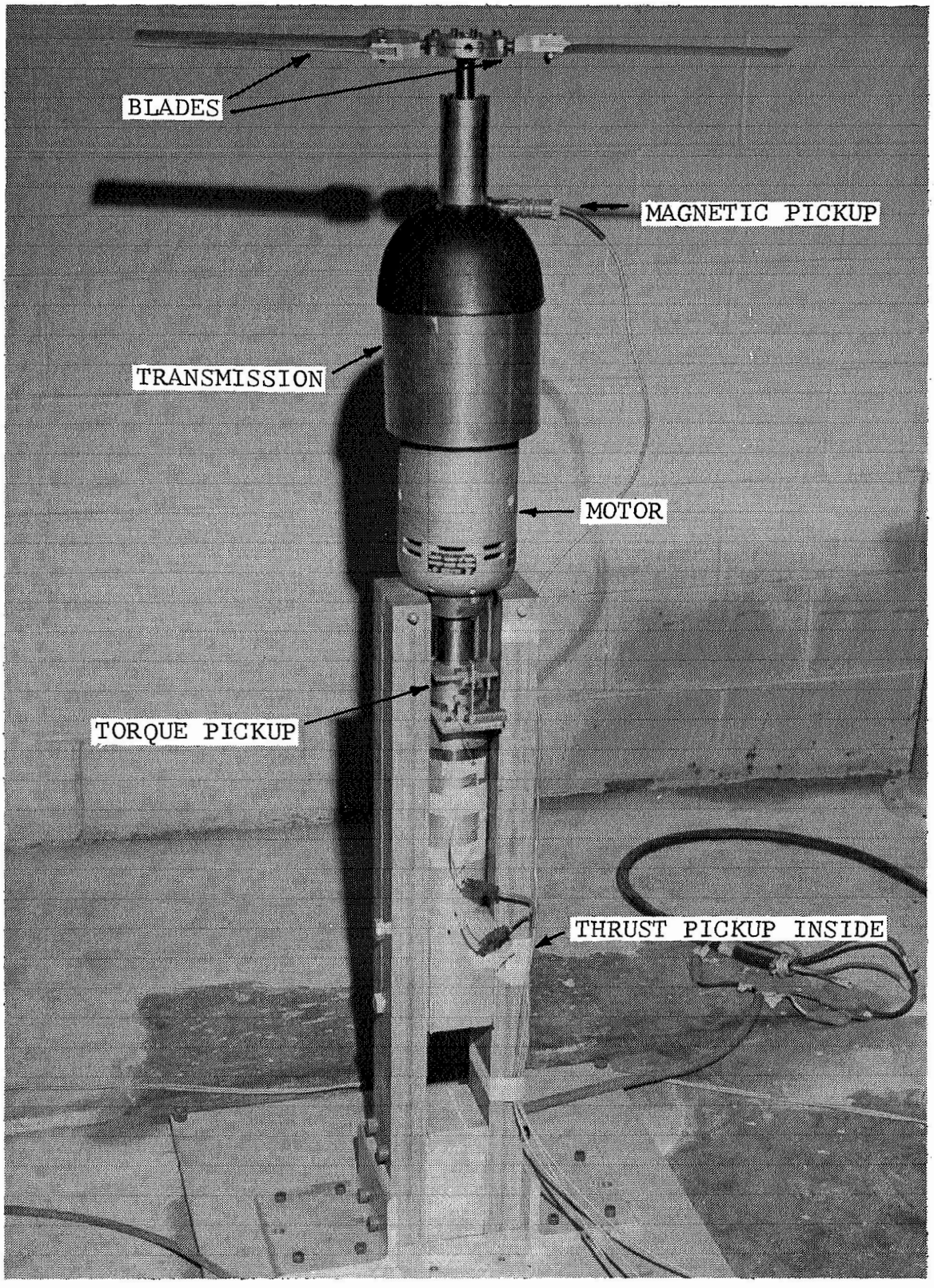

Figure 3. Primary Hover Test Rig.

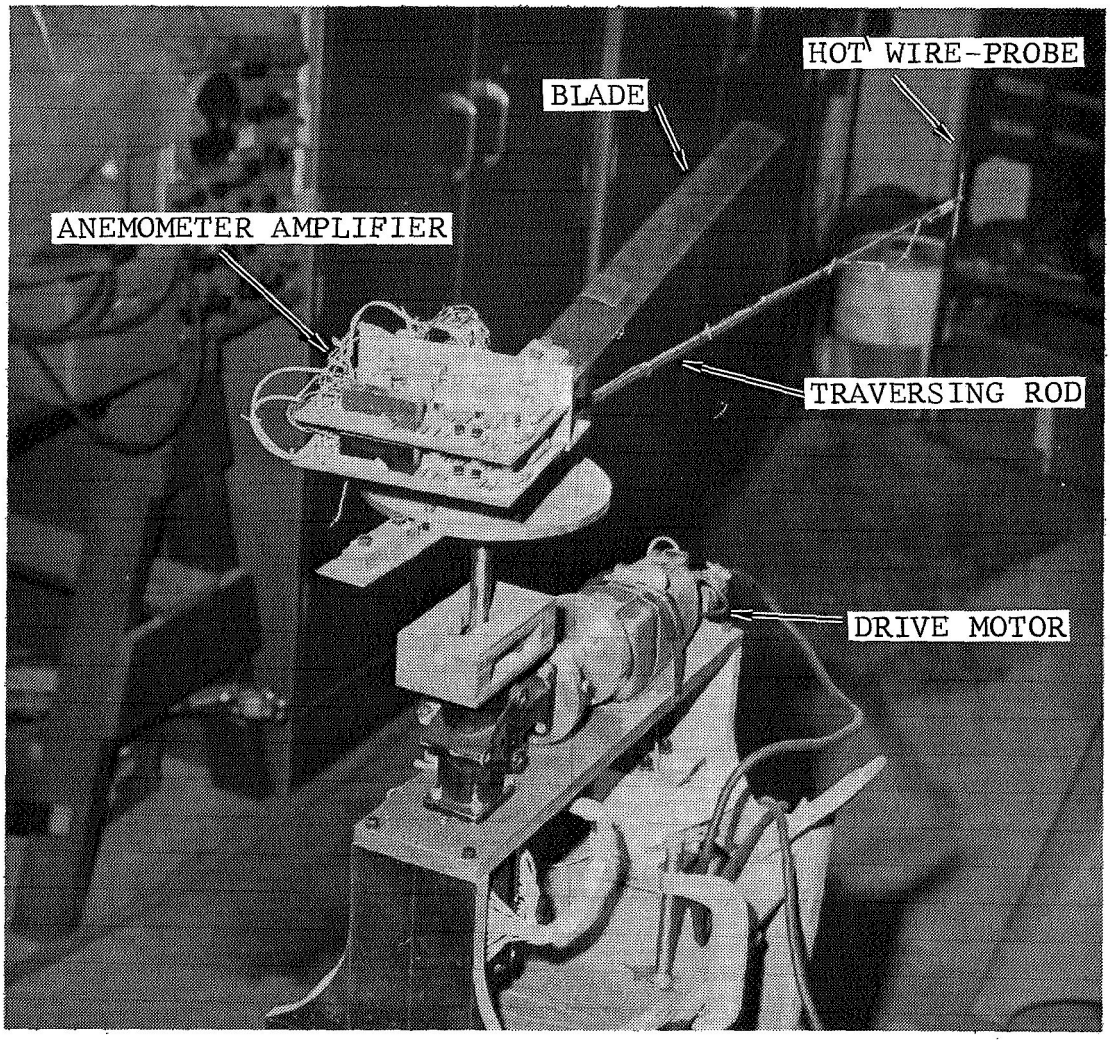

Figure 4. One-Bladed Hover Test Rig.

in the tip vortex. Its azimuth, relative to the blade, was changed manually. The signal from the hot-wire was fed into the hub-mounted anemometer amplifier. Wires from the amplifier passed down the hollow driveshaft to the slip ring unit at the bottom of the test stand. From there the signal was fed into a linearizer and then monitored on an oscilloscope.

2.2 Schlieren System

Figure 5 is a schematic of the schlieren system developed by Bell Helicopter Company to visualize the flow generated by small-scale rotors.

The unique feature of this system is the electronically controlled stroboscopic light source used to make the rotating system appear motionless. It consists of a magnetic pickup that receives one signal per revolution from the rotor shaft. The signal is fed into a preamplifier, a pulse-shaping Schmitt trigger circuit, an adjustable time-delay circuit, and an output stage as shown in the block diagram. With the adjustable time-delay circuit the wake can be visualized with the rotor at any azimuth, ψ, with respect to the focal plane.

2.3 Model Rotors

Because of the broad requirements of this investigation model rotors of various sizes were required. In Table I, these rotors are categorized into three groups based on their use in this report.

TABLE I

MODEL ROTOR GROUPS

Rotor Group	Use
1	Section III (Vortex Stability Investigation)
2	Section IV (Tip Shape Investigation)
3	Section V (Compressibility and Noise Investigation)

2.3.1 Rotor Group 1. - This group consisted of two small fixed-pitch propellers and four small fixed-pitch rotors shown in Figure 6. With these small propellers and rotors

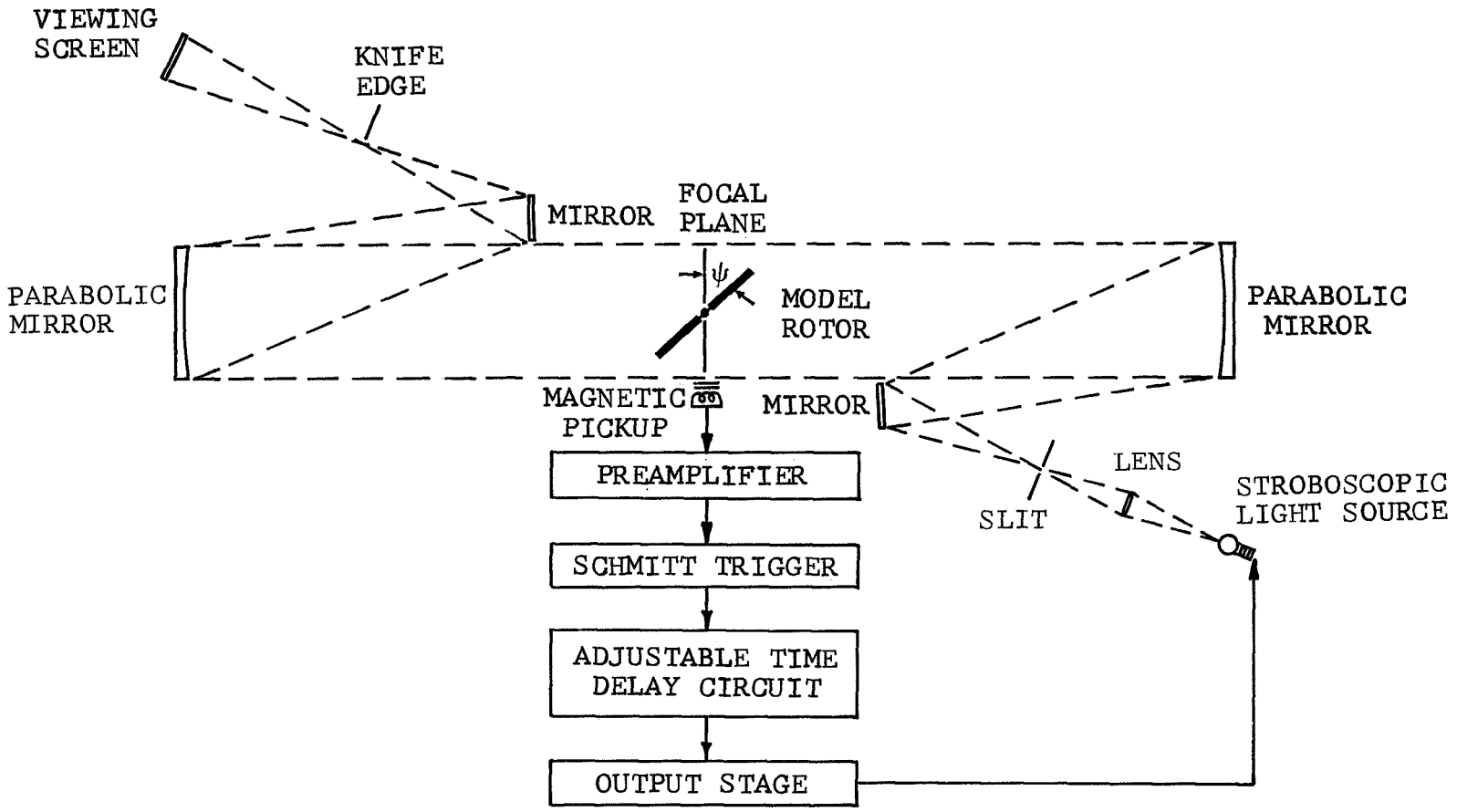

Figure 5. Schematic of Schlieren System.

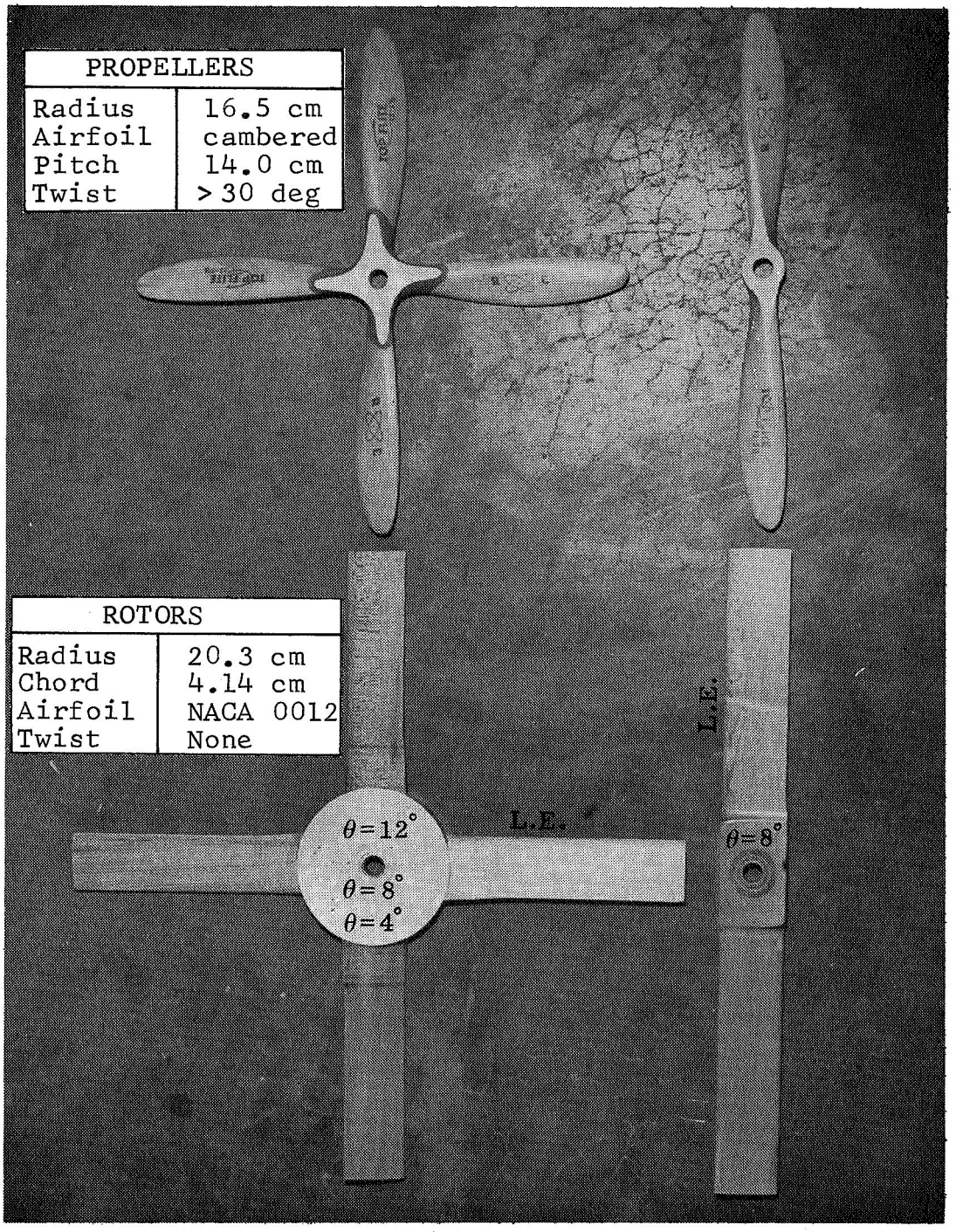

Figure 6. Model Propellers and Rotors Used for the Vortex Stability Investigation (Rotor Group 1).

their complete wake could be observed with the schlieren system for the vortex stability investigation.

2.3.2 Rotor Group 2. - This group consisted of three larger model rotors with a square, swept, and double-swept tip shape as shown in Figure 7. The performance and wake characteristics associated with these rotors were investigated. The blades, which were machined from hard maple and covered with a layer of fiberglass, were rigidly mounted into the hub. Their collective pitch was varied manually. The 58 deg swept and double-swept tip shapes were fabricated onto standard, square tip blades. The blade area was kept constant in each case so that a sufficiently valid performance comparison could be made between the blades. Consequently, the blade's radius at the trailing edge for the swept and double-swept tip was slightly larger than that of the square tip blade, while their leading edge radius was slightly smaller. On both the swept and double-swept tip the sweep was terminated slightly before the trailing edge.

In addition to these blades, this group also included a single mahogany rotor blade shown in Figure 4, that was used for the tip vortex analysis conducted with the stationary hot-wire probe. The blade had a 72.4 cm radius, 4.14 cm constant chord, zero twist, and a NACA 0012 airfoil profile.

2.3.3 Rotor Group 3. - Group 3 consisted of three small fixed-pitch rotors with a square, swept, and double-swept tip shape as shown in Figure 8. A second square tip rotor identical to that shown, except it had a Wortmann FX 69-H-098 airfoil, was also included in this group. These small rotors were ideal for the compressibility and noise portion of the investigation because of their low power requirement which enabled them to be operated at high tip Mach numbers.

2.4 Hot-Wire Anemometer

Constant-temperature, hot-wire anemometers were used for taking velocity measurement in the wake. Originally it was anticipated that velocity measurements would be taken with an X-configuration probe. This proved to be impractical since the size of the X-probe was approximately equal to the diameter of the vortex core being measured. Because of this, the spatial resolution was too poor to further pursue its use with small-scale rotors. Consequently, a probe with a single platinum-iridium wire 17.80 microns in diameter and 4.0 mm in length was used for taking velocity measurements in the wake. The signal from the hot-wire was conditioned by a linearizer through which the output voltage was made nearly proportional to the flow velocity. The output voltage was then monitored on an oscilloscope.

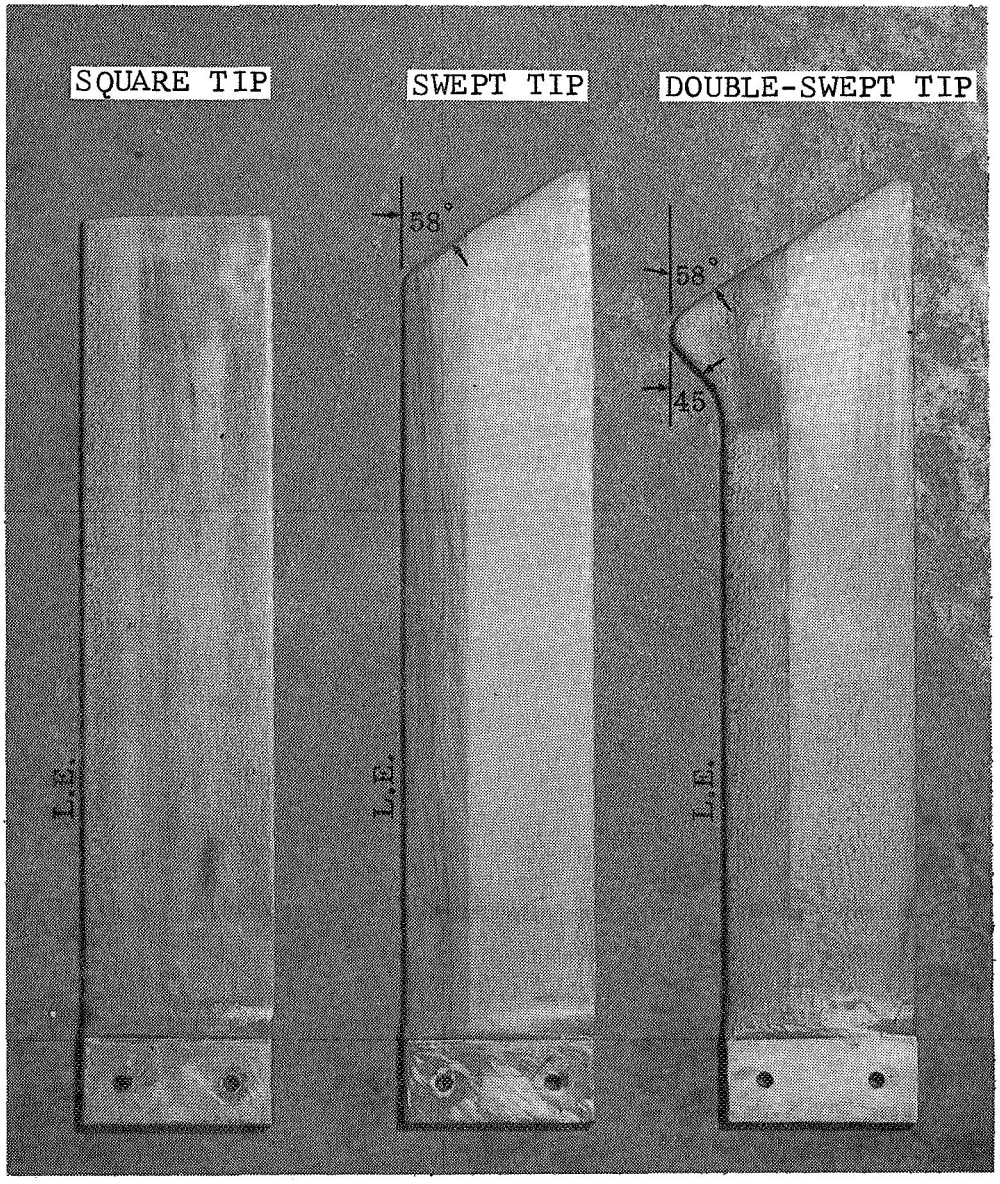

Radius	35.0 cm
Chord	5.71 cm
Airfoil	NACA 0012
Pitch	Variable
Twist	None

Figure 7. Model Rotors Used for the Tip Shape Investigation (Rotor Group 2).

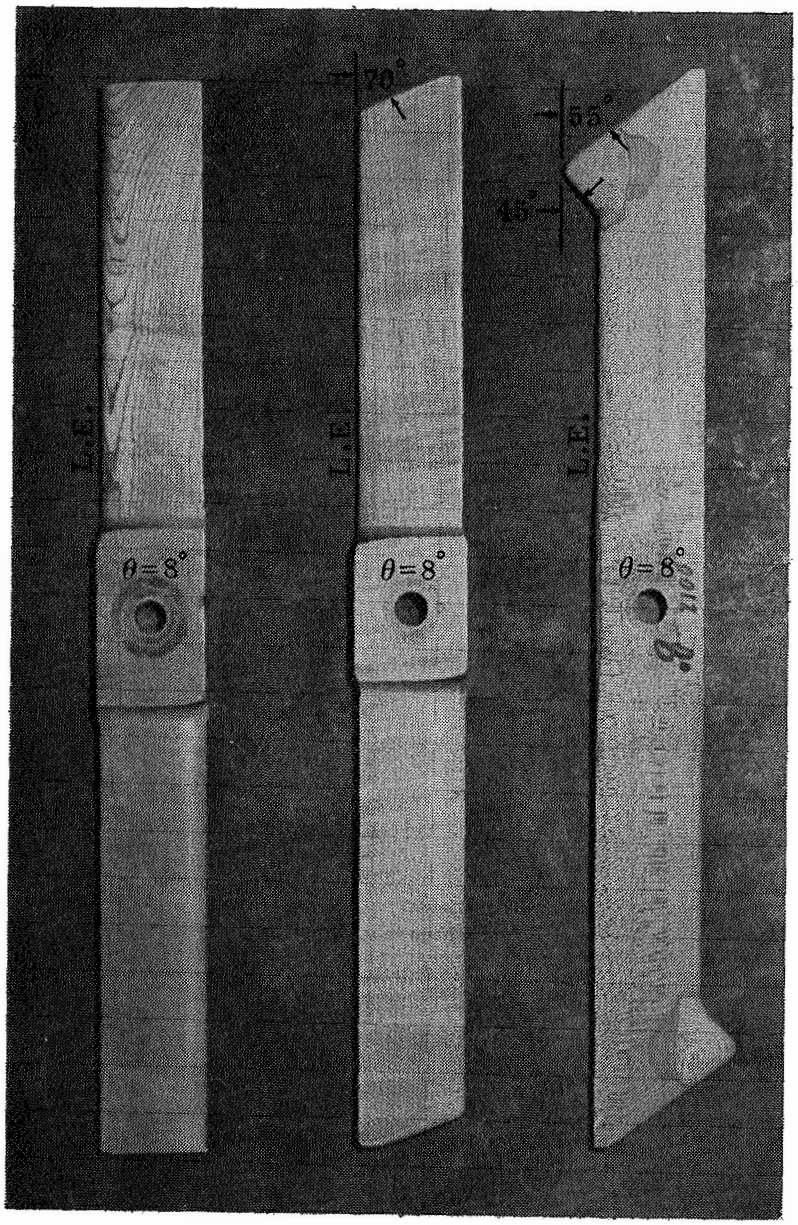

Radius	20.3 cm
Chord	4.14 cm
Airfoil	NACA 0012
Twist	None

Figure 8. Model Rotors Used for the Compressibility and Noise Investigation (Rotor Group 3).

2.5 Noise Equipment

The equipment utilized in the noise survey consisted of a B&K Model 4145 2.54 cm diameter free-field microphone with a random incidence corrector and windscreen. The noise data were recorded on a Nagra III 6.35 mm tape recorder at 38.1 cm/sec. The microphone-recorder system was calibrated for each of the three rotor noise surveys by a B&K Model 4220 pistonphone.

III. EXPERIMENTAL VORTEX STABILITY INVESTIGATION

Utilizing the schlieren system and the propellers and rotors in Figure 6, the effects of number of blades, collective pitch, and tip speed on vortex stability were investigated. The two- and four-bladed propellers and rotor shown were used to determine the effect produced by the number of blades. Both propellers had a fixed-pitch of 14 cm. The two- and four-bladed rotors had fixed-pitch angles of 8 and 12 deg, respectively. The three fixed-pitch four-bladed rotors with pitch angles of 4, 8, and 12 deg were used to determine the effect of collective pitch. The effect of tip speed was investigated with the two-bladed rotor at tip Mach numbers of 0.75, 0.85, 0.95, and 0.99.

With the exception of the tip speed portion of the investigation, all the tests were conducted at 12,000 rpm. This rpm corresponds to a tip Mach number of 0.60 for the 16.5 cm radius propellers and 0.74 for the 20.3 cm radius rotors. The tip Reynolds number for the propellers and rotors was 3.65×10^5 and 7.2×10^5, respectively.

3.1 Flow Visualization Procedure

The schlieren system used in this investigation produces a black and white image of the rotor wake that depicts the density gradient in the direction perpendicular to the knife edge. For comparative purposes photographs were taken of both the vertical and horizontal density gradient in the wake. All the wake photographs presented in this report depict the vertical density gradient since it produced the best image of the wake.

Except for the single-bladed wake analysis discussed in Section 4.2.2, no external heat source was used to aid the flow visualization of the tip vortex throughout this investigation. At tip Mach numbers greater than 0.40, the density gradient through the vortex core was great enough so that it could easily be visualized without the aid of an external heat source.

The following procedure was used for taking Polaroid photographs of the wake. With the rotor at the desired operating rpm, the sensitivity of the schlieren system was checked. If the schlieren image was either too dark or too light, the correct contrast was obtained by adjusting the knife edge. The time delay circuit, which changed the phasing between the flashing stroboscopic light source and the rotating rotor, was then adjusted so that the rotor could be observed at the desired azimuth with respect to the focal plane. A photograph of the wake was obtained by switching the strobe light

to the single flash mode, exposing the Polaroid film, and triggering a single flash.

3.2 Test Results and Discussion

3.2.1 General wake features. - Several significant observations about the wake's distortion, asymmetry, and stability can be made from the schlieren photographs in Figures 9 through 12. Each propeller and rotor was photographed at four different azimuths 90 deg apart to obtain a front, rear, right, and left view of the wake. In each figure, the front view (ψ = 0 deg) is the mirror image of the back view (ψ = 180 deg) and the right view (ψ = 90 deg), the mirror image of the left view (ψ = 270 deg). Photographing the various views at different instants of time indicated that the large scale vortex interactions between adjacent vortex filaments from neighboring rotor blades did not change with respect to time relative to a reference frame rotating with the rotor. In addition to the large scale interactions, small random sinusoidal fluctuations are observed along the vortex filament. These small-scale unstable interactions are similar to those that have been observed in fixed-wing investigations (Refs. 1 through 3).

Both the propellers and rotors generated asymmetrical rotor wakes at hover due to the pairing of adjacent tip vortices. This finding is in agreement with the results from a water tunnel investigation where wake asymmetry was always present in the lower portion of the wakes generated at hover. Wake asymmetry is especially noticeable for the highly loaded propellers (Figures 9 and 11) because of their greater wake pitch. Based on free-wake calculations for a two-bladed rotor, it was anticipated that the wakes would be symmetrical. Further investigation showed that the asymmetry resulted from small differences in blade loading. The blade with slightly more loading in the tip region imparts a greater impulse to the tip vortex passing underneath it which has been generated by the preceding blade. This results in more pitch in this vortex's trajectory. Verification of this is included in Section VI. This finding was unexpected since the fixed-pitch propellers and rotors were all accurately machined. The small difference in blade loading that does exist would necessarily be attributed to manufacturing tolerance or a slight difference in blade flexibility. Based on this finding, it appears that the wake is very sensitive to small differences in the blade-load distributions, and that it would be difficult to achieve wake symmetry.

3.2.2 Interaction between two tip vortices. - In the region of maximum wake contraction, vortex interaction causes two adjacent vortices, generated by neighboring rotor blades, to

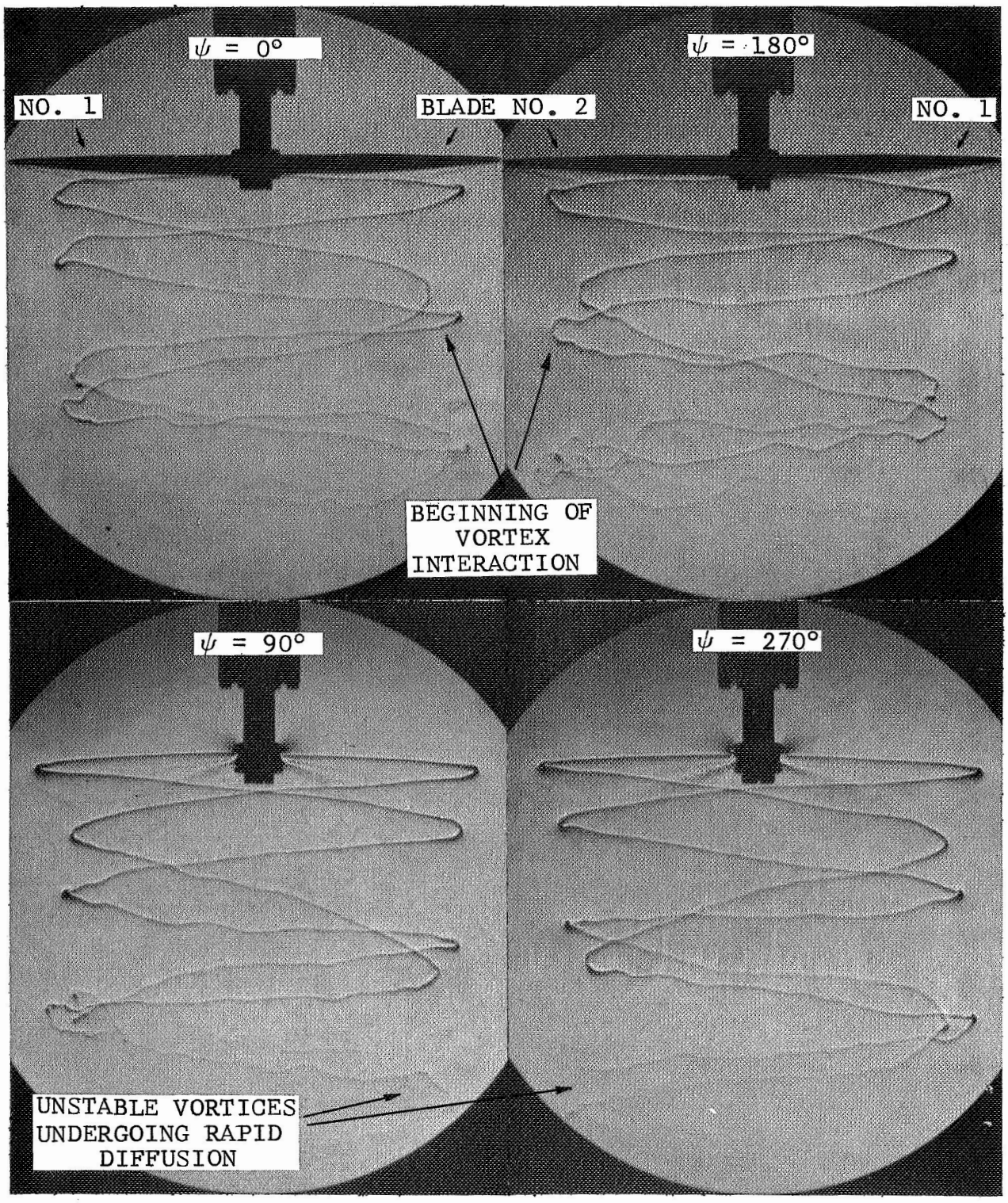

Figure 9. Photographs of the Two-Bladed Propeller Wake (Rotor Group 1) - R = 16.5 cm, M_T = 0.60.

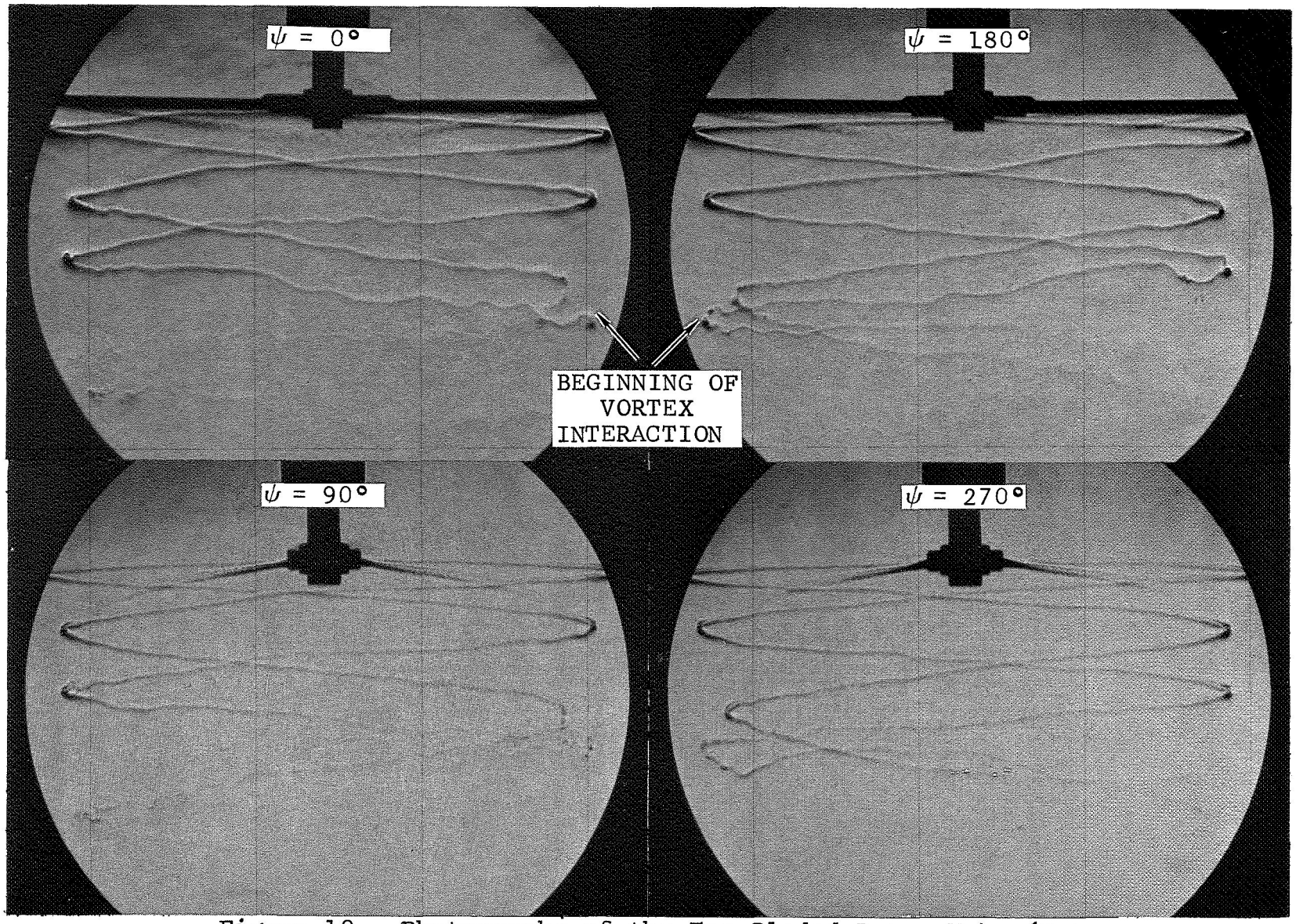

Figure 10. Photographs of the Two-Bladed Rotor Wake (Rotor Group 1) - R = 20.3 cm, θ = 8°, M_T = 0.74.

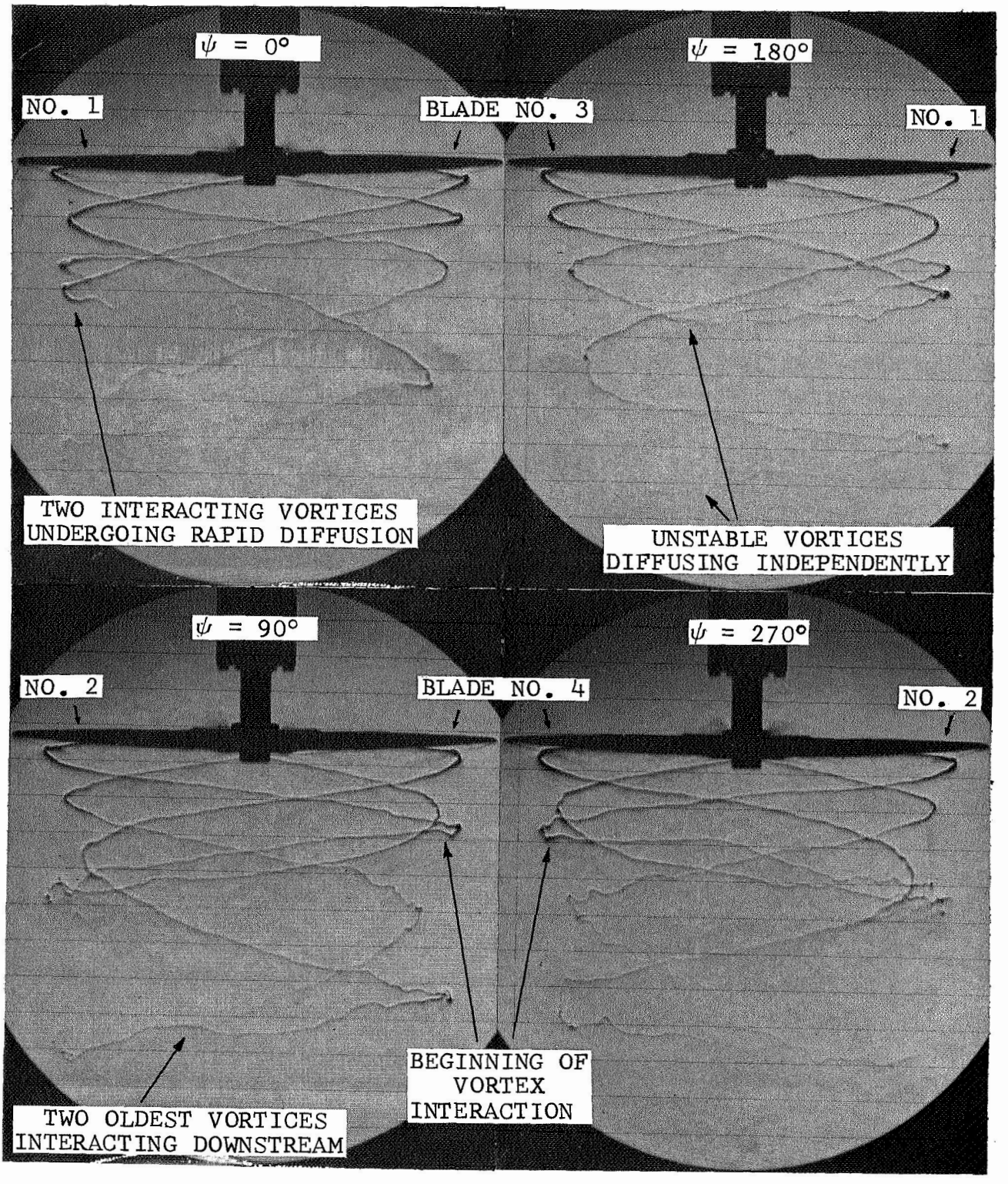

Figure 11. Photographs of the Four-Bladed Propeller Wake (Rotor Group 1) - R = 16.5 cm, M_T = 0.60.

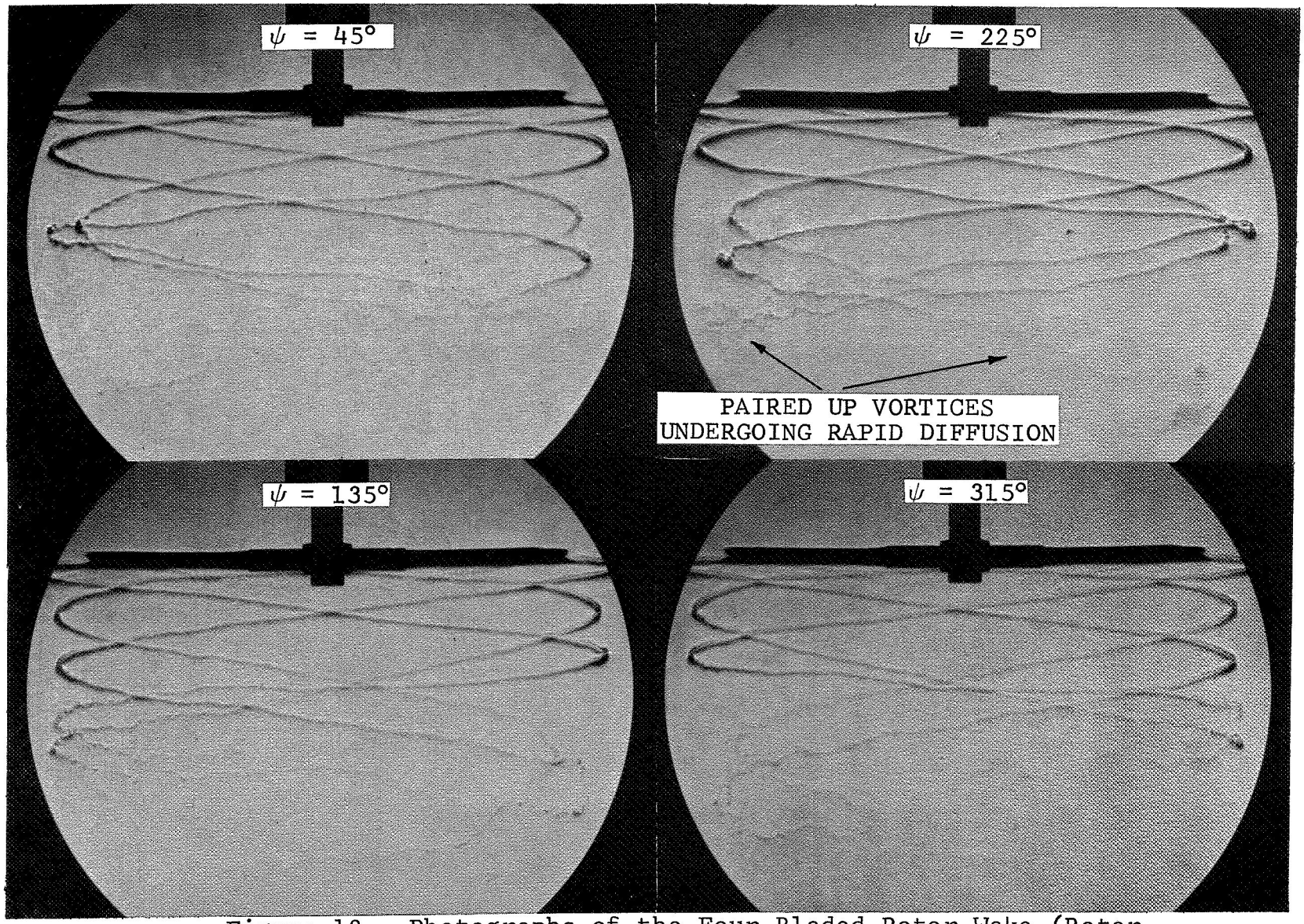

Figure 12. Photographs of the Four-Bladed Rotor Wake (Rotor Group 1) - R = 20.3 cm, θ = 12°, M_T = 0.74.

begin revolving about their common centroid of vorticity. While this is occurring, the two vortices draw closer to each other, become unstable, and either destroy each other or combine to form one weak diffused vortex. This destructive process, resulting from the interaction of two vortices, occurred for both the two- and four-bladed propellers and rotors.

Reference 2 describes a similar destructive interaction between the two tip vortices shed from fixed-wing aircraft where, unlike the rotor wake, the circulation of the two vortices is of the opposite sense. In a related theoretical investigation (Ref. 10), Widnall describes various modes of instability for a helical vortex filament. The mutual induction mode of instability described by Widnall is comparable to the large-scale interaction between two tip vortices as described in this report. For a helical vortex this mode of instability appears as the pitch of the helix decreases, and the neighboring turns of the filament begin to interact strongly.

The following simplified analogy from Reference 16 helps explain how two adjacent tip vortices revolve about their common centroid of vorticity during vortex interaction. Consider two infinite parallel rectilinear vortices of different strengths, Γ_1 and Γ_2, rotating in the same direction as shown in Figure 13.

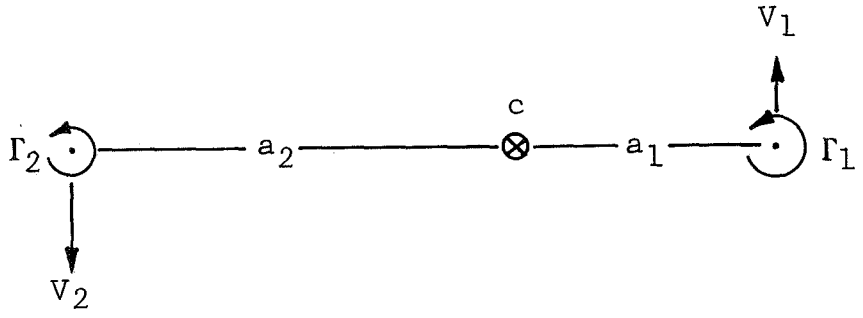

Figure 13. Two Infinite Rectilinear Vortices.

The distance between the two vortices is given as $a = a_1 + a_2$. The induced velocity at the center of vortex Γ_1 due to Γ_2 is given by

$$V_1 = \frac{\Gamma_2}{2\pi a} \tag{1}$$

Similarly, the induced velocity on vortex Γ_2 is due to Γ_1 and is given by

$$V_2 = \frac{\Gamma_1}{2\pi a} \tag{2}$$

Both of these velocities are perpendicular to, a, and are opposite to each other. By considering each vortex to have a mass proportional to its strength, a centroid of vorticity, c, which lies on the line joining the vortices, can be determined from the relation $\Gamma_1 a_1 + \Gamma_2 a_2 = 0$. Due to their mutual influence the two vortices move along circular paths about their common centroid of vorticity. For the simplified case where $\Gamma_1 = \Gamma_2$, the centroid of vorticity would be halfway between the two vortices. They would both revolve about this point on the same circular path with angular speed,

$$\omega = \frac{\Gamma}{\pi a^2} \tag{3}$$

The interaction between two tip vortices is also similar to the mutual interaction between two vortex rings moving along a common axis of symmetry as described in Reference 18. The rearward ring becomes smaller and moves more quickly while the forward one becomes larger and moves slowly. The smaller one can then pass through the larger one. Their roles then become reversed, and they move back and forth through each other.

3.2.3 Effects of number of blades. - An increase in the number of blades reduces the axial spacing between vortices, increases the angular rate at which they revolve about their centroid of vorticity, and causes them to become more unstable and diffuse sooner. Previously it was shown (Equation 3) that the angular rate at which two infinite rectilinear vortices revolve about their centroid of vorticity is directly proportional to the strength of the vortices and inversely proportional to the square of their separation. From this relationship one can easily see that the angular rate at which two tip vortices revolve about their centroid of vorticity will increase with the addition of more blades.

The tip vortex coordinates corresponding to the two-bladed propeller wake (Figure 14) clearly illustrate the destructive interaction between two vortices. The tip vortex from blade No. 2, which is deflected the most during blade passage, has more initial pitch in its trajectory than that from blade No. 1. When it is 1/2 of a revolution old it passes radially inside the tip vortex from blade No. 1. By the time it is 1-1/8 revolutions old, it is in the same horizontal plane as the tip vortex from blade No. 1. Due to the mutual interaction of the two vortices, they begin revolving about their common centroid of vorticity at about one-half revolution per rotor revolution. This continues for about 1 to 1-1/2 revolutions of the wake during which time the vortices become unstable, and undergo rapid diffusion. Instability appears as

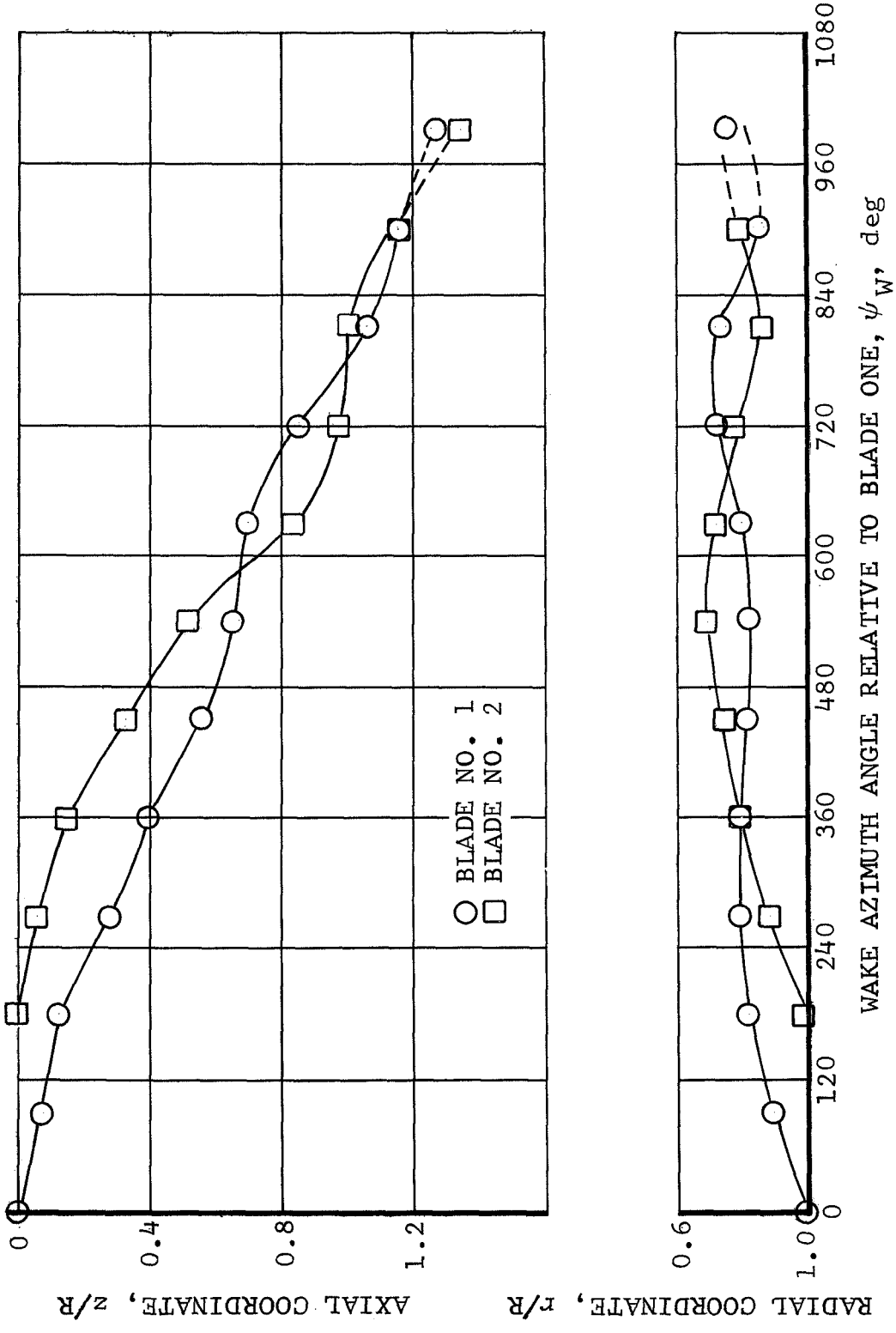

Figure 14. Two-Bladed Propeller Tip Vortex Coordinates (Rotor Group 1) - R = 16.5 cm, M_T = 0.60.

sinusoidal fluctuations of the tip vortex that grow with time. A detailed discussion of this short-wave instability, which is characteristic of all curved vortex filaments, can be found in Reference 17. As these fluctuations grow the vortices draw close together and appear to touch each other. Once they touch there is rapid diffusion of the vorticity in the opposing flow region between the two vortices. The vortices then appear to breakup or combine to form one weak diffused vortex. Whatever remains of the vortices dissipates further downstream. As seen in Figure 9 the vortices cannot be observed after the wake is 2-1/2 to 3 revolutions old.

For the two-bladed rotor in Figure 10 vortex interaction is similar to that of the propeller. The most noticeable difference is that the rotor's vortices diffuse about half a revolution earlier. This can probably be attributed to a more intense interaction between adjacent revolutions of the wake because of the closer spacing of vortices.

For the four-bladed propeller and rotor shown in Figures 11 and 12, the wake is more difficult to analyze than for the two-bladed case. The tip vortices, which are much closer together because of the decreased azimuth between blades, interact, become unstable, and diffuse sooner. Previously, it was observed that the vortices for the two-bladed case dissipated together at the same axial distance below the rotor. For the four-bladed case, two of the four vortices dissipate together about 1-1/2 wake revolutions (based on the older of the two vortices) below the rotor while the other two dissipate further downstream. This is easily seen in Figure 15 where the four-bladed propeller's tip vortex coordinates are plotted. The tip vortex from blade No. 2 has the greatest impulse imparted to it during blade passage. When it is 1/4 of a revolution old it passes radially inside the tip vortex from blade No. 1. By the time it is 5/8 of a revolution old it has moved down to the same axial position as the tip vortex from blade No. 1. The two vortices begin revolving around their common centroid of vorticity about once every rotor revolution which is twice the rate associated with the vortices generated by the two-bladed propeller. From Equation 3 this rate is calculated to be four times that of the two-bladed propeller if one assumes the strength of the tip vortex from the two-bladed propeller to be approximately equal to that of the tip vortex from the four-bladed propeller, and the spacing between vortices for the two-bladed propeller to be twice that of the four-bladed propeller. Upon close inspection of the propeller wakes one can see that in the region of maximum wake contraction the spacing between vortices for the two-bladed case is only about a third greater than the spacing between vortices for the four-bladed case. Using this value for the

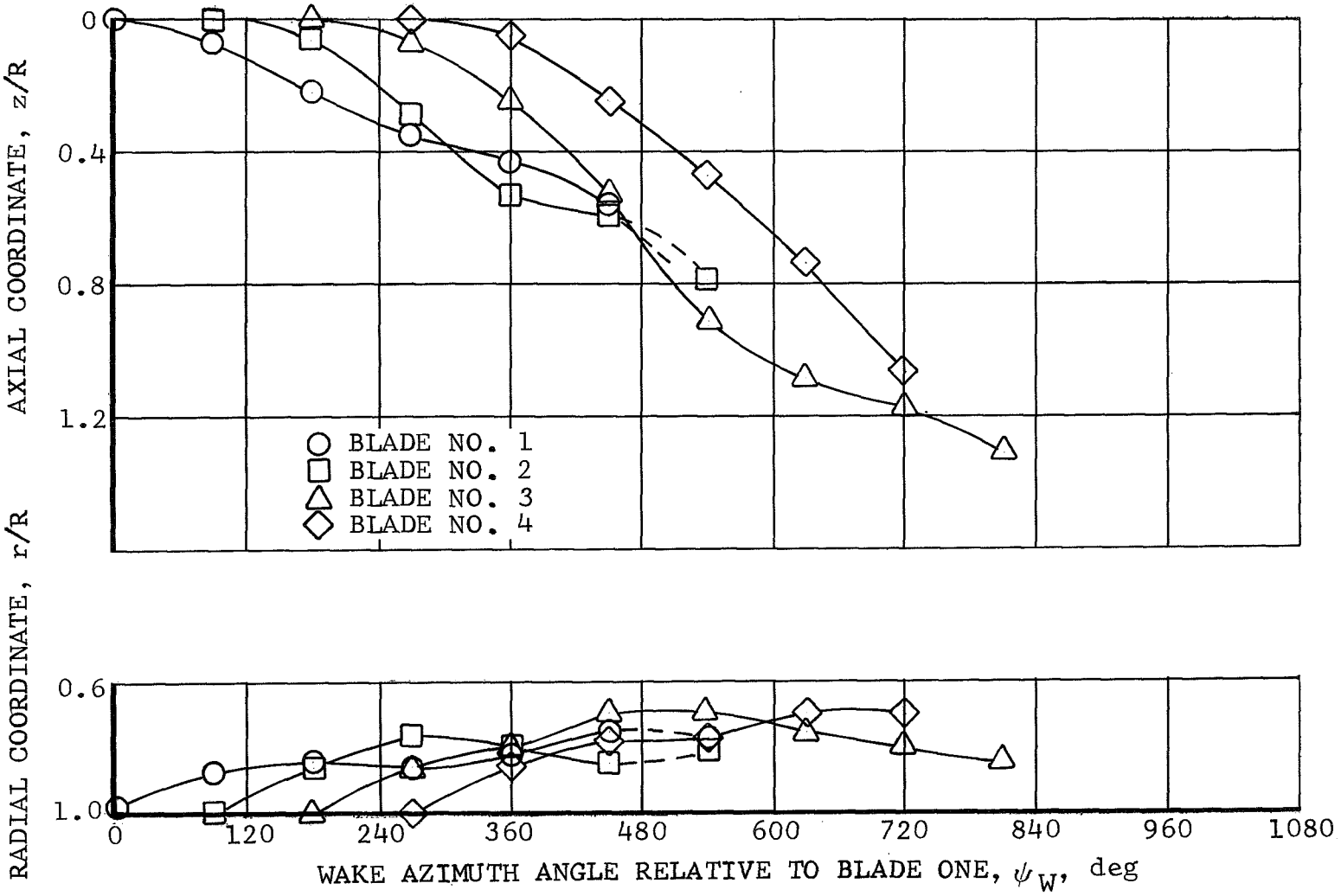

Figure 15. Four-Bladed Propeller Tip Vortex Coordinates (Rotor Group 1) - R = 16.5 cm, M_T = 0.60.

spacing between vortices, Equation 3 predicts two vortices from the four-bladed propeller to revolve about their centroid of vorticity at only about twice the rate of the two-bladed propeller which is in agreement with experimental results.

It is interesting to observe that the vortices generated by blade No. 3 and blade No. 4 are unable to pair up immediately as they pass downstream. They either break up independently under their own self-induced effects and any other destabilizing influence present, or pair up and interact with one another further downstream. For the rotor wake (Figure 12) these two vortices pair up downstream. This is more likely to occur for the rotor than for the propeller because of the closer spacing between vortices. In the case of the propeller (Figure 11) both possibilities are observed. In the photograph taken with the rotor located at ψ = 180 deg, the vortices appear to diffuse and breakup independently; whereas, in that taken at ψ = 90 deg, the vortices are able to stay intact until they pair up downstream.

3.2.4 Effects of collective pitch. - Schlieren photographs of the wakes generated by the four-bladed rotor at collective pitch angles of 4, 8, and 12 deg are shown in Figure 16. From the photographs one can see that as the collective pitch decreases the axial spacing between vortices decreases along with the vortex strength, and the tip vortices become increasingly unstable and diffuse more rapidly. This is especially obvious at a collective pitch of 4 deg. Two mechanisms are believed to be responsible for the faster diffusion of the tip vortex with a reduction in collective pitch. One is the interaction between two tip vortices as described in Section 3.2.2, which increases in intensity with a reduction in the axial spacing between vortices. The other is an instability related to the axial flow in the vortex core. The existence of this instability is primarily based on the experimental results of several fixed-wing investigations.

Logan (Ref. 19) measured the axial flow in the vortex generated by a one-twelfth scale semiwing using a five-holed static pressure probe. Over the downstream interval considered (10 to 26 chord lengths) an axial velocity deficit was found that diminished with distance for weak vortices and remained essentially unchanged for strong vortices. In a full-scale investigation, MacCready (Ref. 2) observed the axial motion of buoyant balloons in the vortex core toward the wing at a velocity equal to 11 percent of the aircraft speed. Chigier and Corsiglia (Ref. 20) measured the velocity components in the vortex core up to 12 chord lengths downstream for two model wings (CV-990 wing and a rectangular wing) using a three-wire anemometer. For the CV-990 wing, an axial velocity deficit

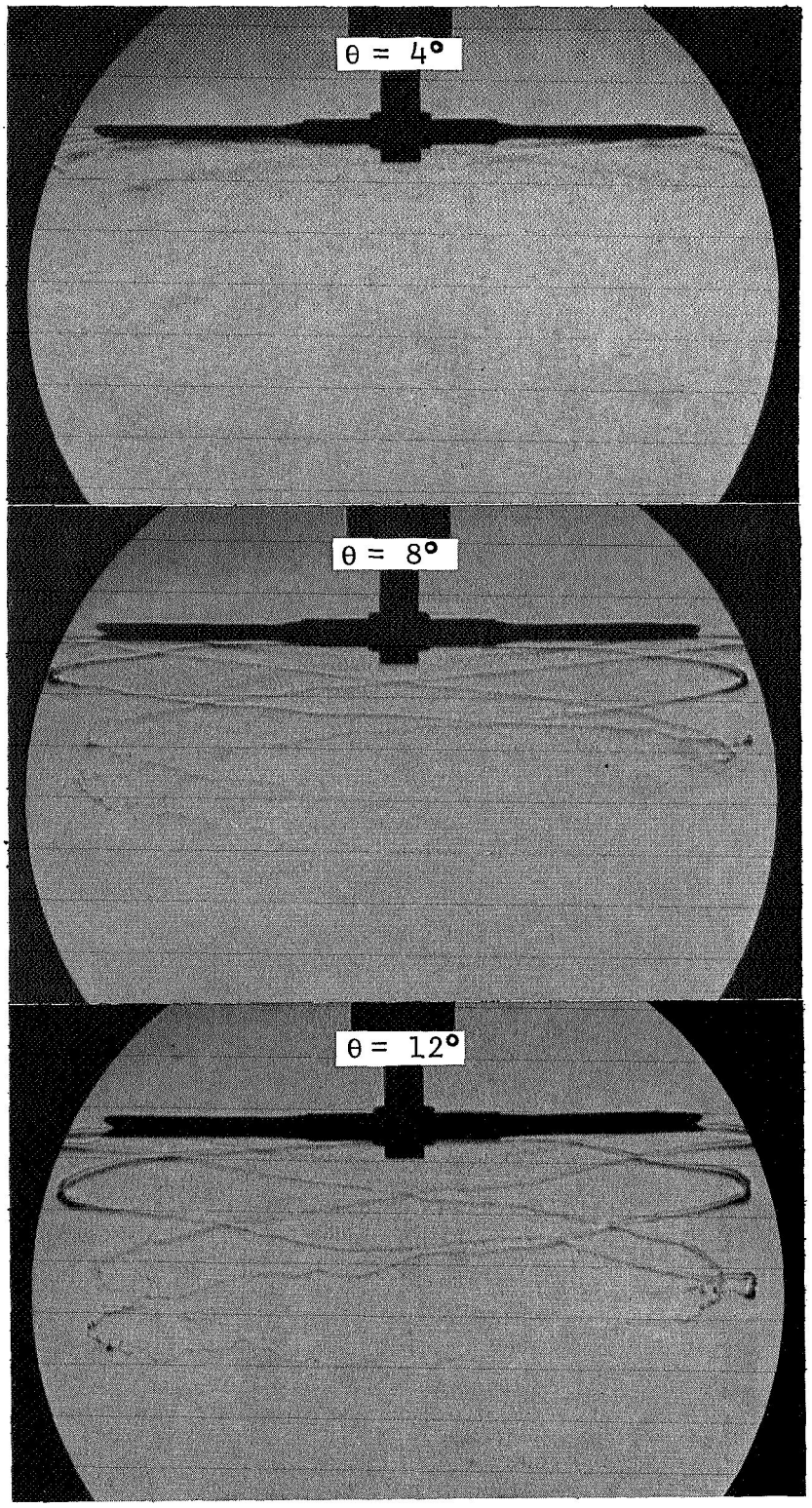

Figure 16. Photographs of the Wake Generated by the Four-Bladed Rotor at Various Collective Pitch Angles (Rotor Group 1) - R = 20.3 cm, M_T = 0.74.

was measured in the core at all angles of attack. For the cleaner rectangular wing, the axial velocity changed from a deficit at low angles of attack to an excess at angles greater than 9 deg. Boatwright (Ref. 14) surveyed the wake generated by a full-scale rotor at two thrust coefficients using a split-film total vector anemometer. The axial velocity in the vortex core was found to be toward the blade and was greater at the higher of the two thrust coefficients investigated. He concluded that the stability of the vortex was strongly related to the axial flow in the region of the vortex core.

Most of these investigations show the axial velocity in the core to be toward the lifting surface. It is felt that an axial velocity deficit has a stabilizing influence on the tip vortex. At low collective pitch angles, where the axial velocity deficit is believed to diminish quickly, vortex instability is more prominant, and could be more dominant than that due to the interaction between two vortices. In References 21 and 22, White, Balcerak, and Rinhart reported on the vortex dissipation due to axial mass flow injection into a vortex core. For high mass flow rates, they found that vortex dissipation was greater than predicted by theory and proposed that the difference might be due to an instability associated with the axial velocity in the core. Mass injection into a vortex core with an axial velocity deficit would tend to eliminate the deficit and possibly trigger vortex instability at high mass injection rates. In view of the uncertainty regarding the axial flow, additional research is necessary to further quantify the effects of collective pitch on the axial velocity in the vortex core and the related vortex stability.

3.2.5 Effects of tip speed. - The schlieren photographs in Figure 17 were taken of the two-bladed 20.3 cm radius rotor at four different tip speeds from 258 m/sec to 344 m/sec. This corresponds to a tip Mach number of 0.75 to 0.99 respectively. It is observed that: (1) the general trajectory of the tip vortex does not change with tip speed, and (2) vortex instability (i.e., unstable sinusoidal fluctuations) occurs close to the rotor once a strong shock wave forms on the lower surface of the NACA 0012 airfoil. This instability was only observed at Mach numbers above $M_T = 0.75$. The wake generated at $M_T = 0.55$ (not shown here) looks almost identical to that at $M_T = 0.75$. As the shock wave increases in intensity with tip Mach number its ability to induce instability increases. Later it will be seen that this trend is not discernable for the Wortmann FX69-H-098 airfoil which develops a weak shock on its lower surface.

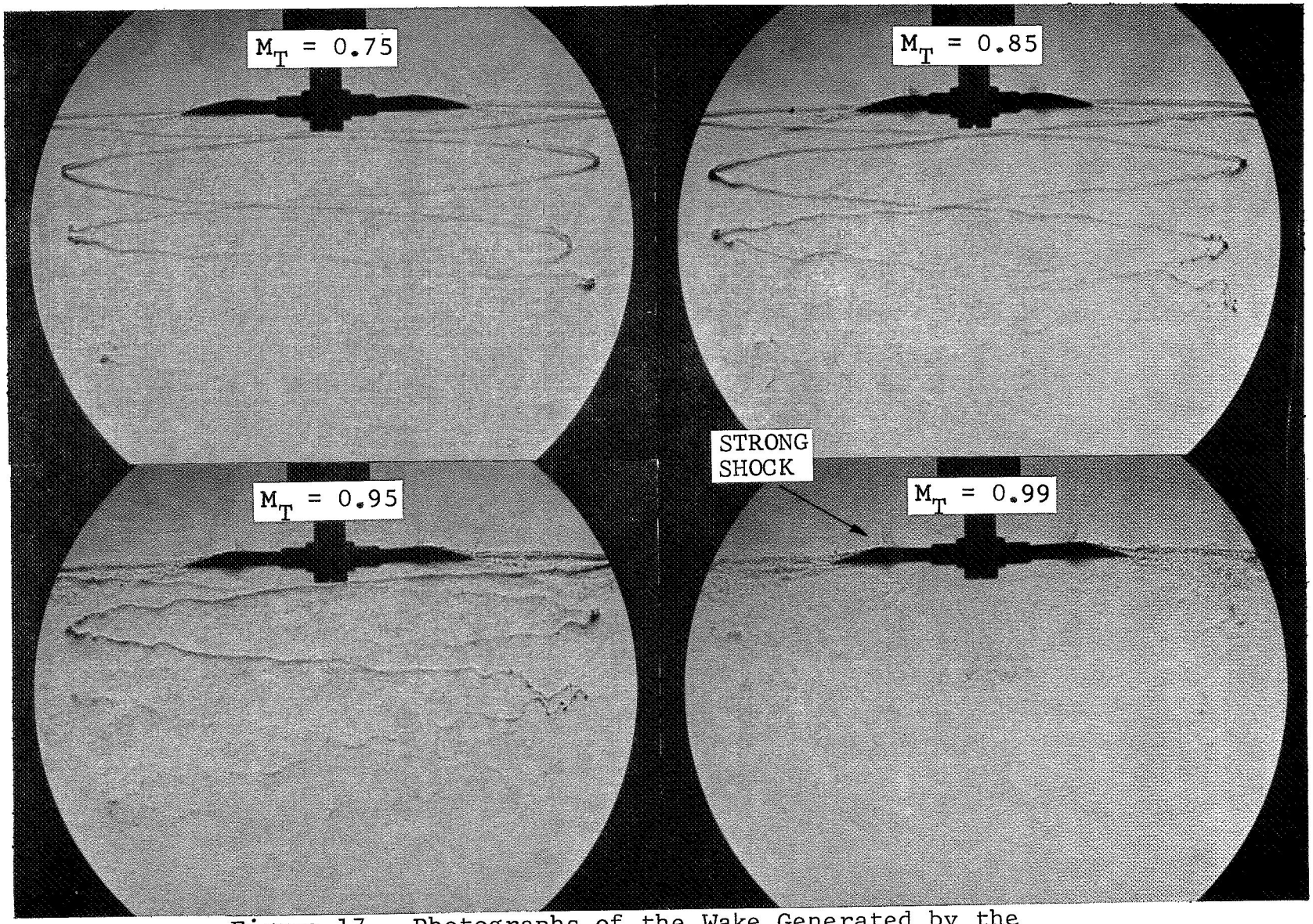

Figure 17. Photographs of the Wake Generated by the Two-Bladed Rotor at Various Tip Mach Numbers (Rotor Group 1) - R = 20.3 cm, $\theta = 8°$.

Shock formation, both above and below the blade tip, becomes quite predominant as the tip speed increases. At M_T = 0.99 the strong shock formation produces separation which interferes with the formation of the tip vortex. The flow behind the shock is very turbulent and the wake that develops from it dissipates rapidly.

IV. EXPERIMENTAL TIP SHAPE INVESTIGATION

A swept and double-swept tip shown in Figure 8 were chosen for comparison with the square tip, primarily because the results could then be correlated with full-scale experimental data (Refs. 12 and 13) which were available for these tip shapes. The three tip shapes were analyzed by measuring their performance, photographing their wakes, and measuring the velocity distribution in their tip vortex. Performance was measured at tip speeds of 106, 129, and 152 m/sec. At 152 m/sec schlieren photographs were taken of the wakes generated by the three tip shapes for collective pitch angles of 8, 10, 12, and 14 deg. These photographs were used to help verify the measured performance trends. Measurements of the velocity distribution in the tip vortex generated by the tips were taken with the stationary, hot-wire probe over the interval from ψ_W = 45 deg to ψ_W = 450 deg. This was done at a collective pitch of 12 deg and a tip speed of 152 m/sec.

For the 72.4 cm radius, single-bladed rotor hot-wire measurements in the vortex core were taken with the rotating probe at collective pitch angles of 4, 6, 8, and 10 deg for a tip speed of 30.4 m/sec.

4.1 Testing Procedures

4.1.1 Performance measurements. - Prior to a performance run, the desired collective pitch angle was set for each blade by measuring off the flat-surfaced blade grip with a clinometer. This was done with each blade positioned at the same azimuth location. Using this method, collective pitch angles could be set to an accuracy of ±0.2 deg.

Before taking a performance measurement, it was necessary to run the rotor up to the desired rpm and back to zero to eliminate ball-bearing hysteresis. Once the hysteresis was eliminated, the bridge outputs for thrust and torque measurements were zeroed with the rotor at rest. The rotor was then run up to the desired test rpm. After the inflow through the rotor stabilized, thrust and torque data were recorded. The rotor was then brought back to rest, and the bridge outputs were checked for zero shifts. Ambient temperature and pressure were recorded during the test.

Thrust and torque calibration readings were recorded after each test point. The thrust load cell was calibrated by setting weights on the rotor shaft. The torque cell was calibrated by applying a known force to a known moment arm. The accuracy of the thrust and torque measurements was considered to be within ±2 percent.

4.1.2 Hot-wire anemometer measurements. - Two hot-wire anemometer methods were utilized for measuring velocities in the wake. One of these methods used a stationary hot-wire probe to record periodic velocities at a fixed point in space while the other utilized a probe that rotated with the blade to record steady velocities at a fixed position relative to the rotating blade.

Stationary hot-wire probe: Figure 18 shows the stationary probe located below the blade. The hot-wire, which lies in a horizontal plane, is parallel to the y-axis. It is sensitive to the component of velocity normal to its axis and relatively insensitive to that component of flow along its axis which is assumed to be small. Prior to taking velocity measurements, the hot-wire was calibrated against a cistern-type manometer from zero to 91 m/sec. The probe was then positioned at the desired axial position below the rotor. Once the rotor was at operating rpm the relationship of the hot-wire to the tip vortex was observed on the viewing screen of the schlieren system. The probe was then traversed radially to position the hot-wire along the trajectory of the tip vortex. As the tip vortex passed over the hot-wire twice each revolution, the velocity distribution in the vortex core was observed on an oscilloscope.

Rotating hot-wire probe: Steady velocity measurements were obtained with the setup shown in Figure 19. Here the hot-wire, whose orientation is also parallel to the y-axis, rotates with the blade on a telescoping tube that can position it radially. With this apparatus the maximum circumferential velocity in the vortex core can be measured close to the blade when the vortex is still in the plane of rotation. For this rig the hot-wire was calibrated against the rotor's tip speed using the following procedure. The blade was set at zero collective pitch so no flow would pass through the rotor, and the probe was located well above and aft of the blade at a radial position equal to that of the blade tip. The rotor was then operated at known values of the tip speed; and the hot-wire, which was aligned radially for calibration purposes, recorded the tip speed. The probe was then turned 90 deg so that the hot-wire was aligned perpendicular to the traversing rod. Now, at operational rpm (ΩR = 30.4 m/sec), the only cooling of the wire was due to the 30.4 m/sec flow parallel to its axis. Although the wire was relatively insensitive to this component of flow, it was large in magnitude and thus the resultant cooling had to be taken into account. This cooling, which was equivalent to 7 percent of the tip speed, had to be subtracted from the measurements of the velocity in the tip vortex.

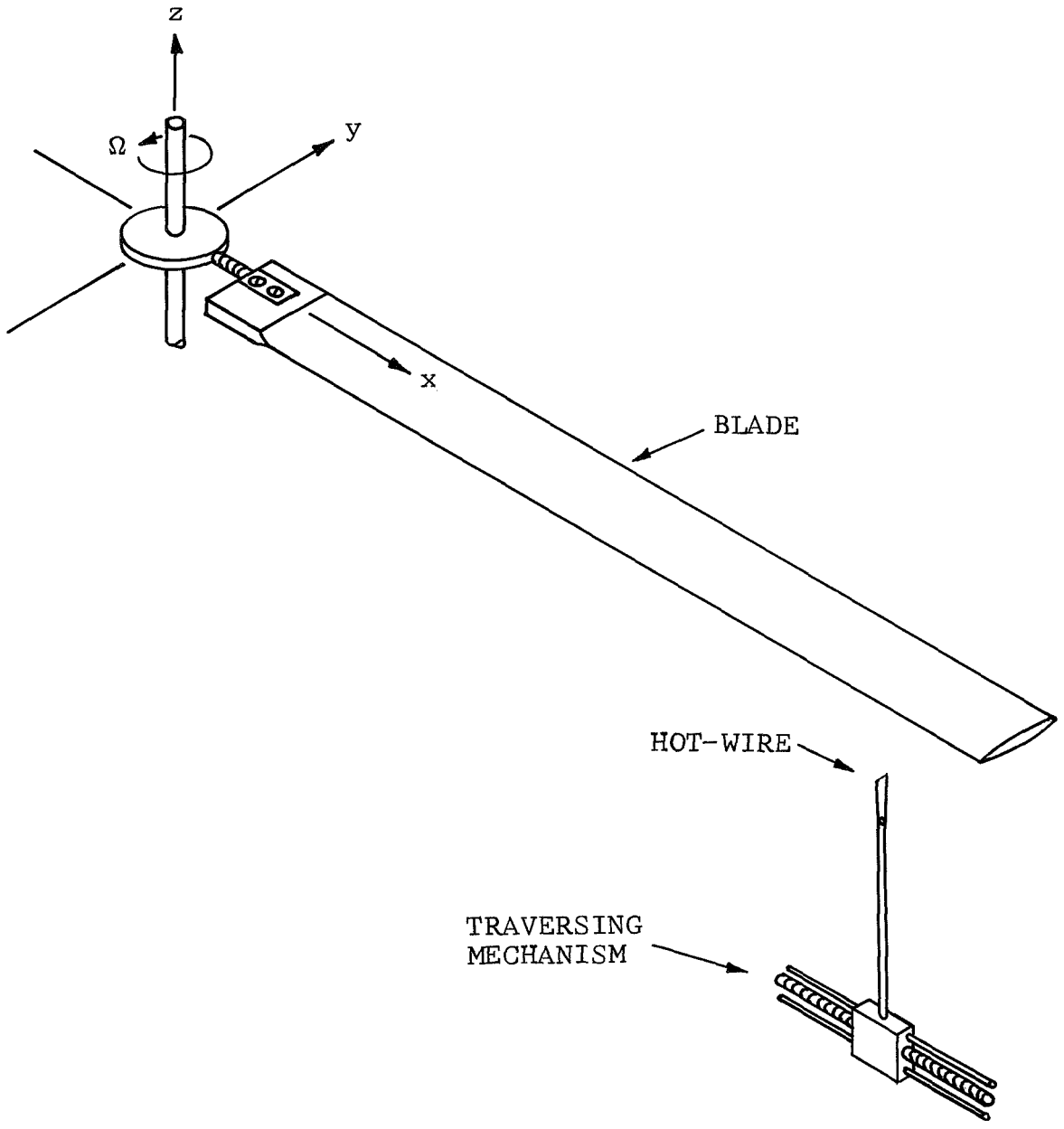

Figure 18. Stationary Hot-Wire Probe.

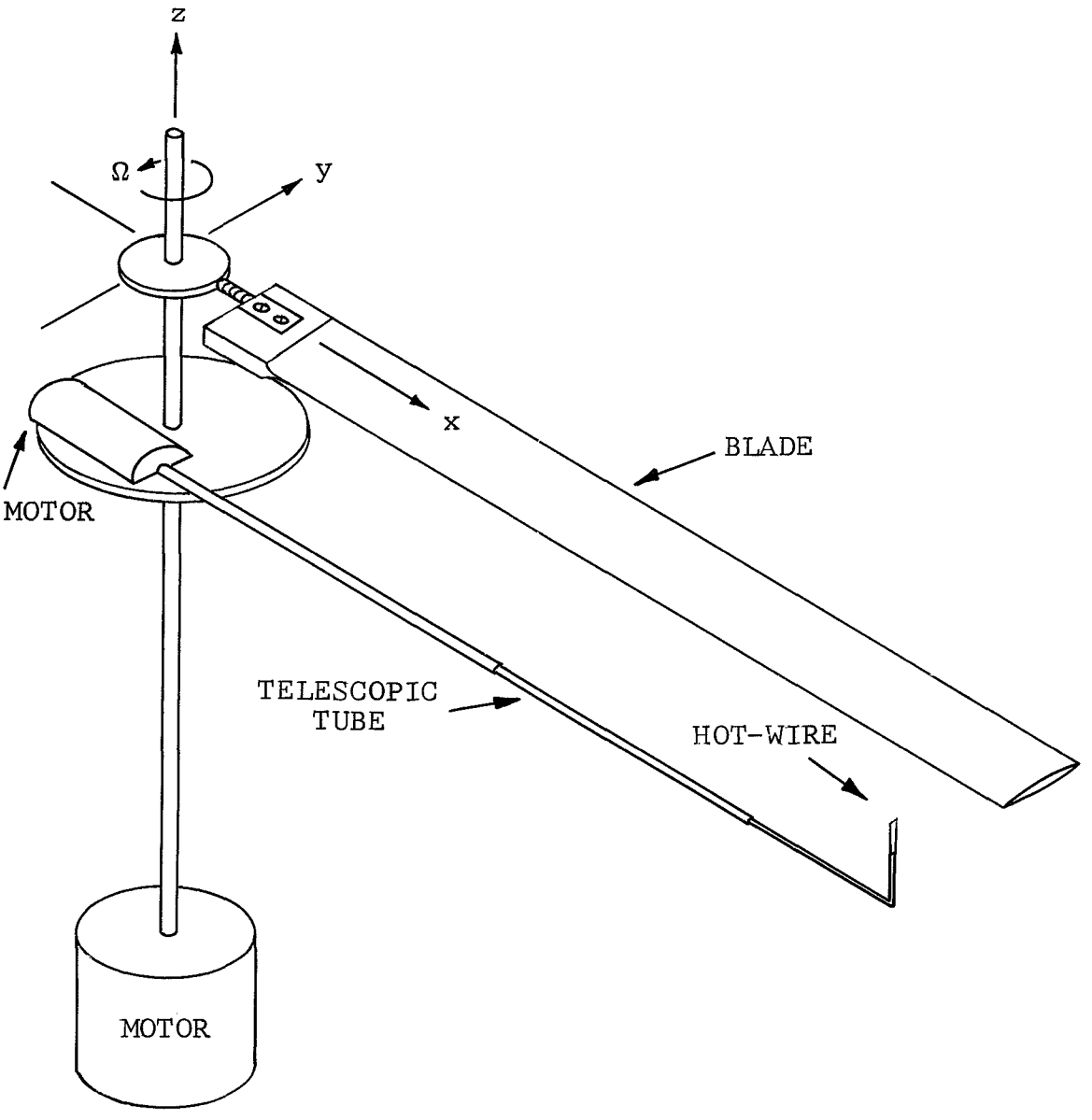

Figure 19. Rotating Hot-Wire Probe.

The following procedure was used for positioning the hot-wire in the vortex after the desired collective pitch was set with a clinometer. With the rotor at operating rpm the hot-wire probe was traversed radially until it intersected the vertical centerline of the vortex. This could be observed with the schlieren system. To aid the flow visualization it was necessary to place a heating element close to the blade tip. Once the probe was located along the vertical centerline of the vortex the rotor was stopped to manually change the vertical position of the hot-wire. The hot-wire was moved either up or down to position it in the center of the core. When the hot-wire was correctly positioned, the heating element was removed to eliminate any velocity measurement error that might be introduced by its presence.

4.2 Test Results and Discussion

4.2.1 Performance measurements. - Performance characteristics for the three tip shapes are shown in Figure 20 for tip speeds of 106, 129, and 152 m/sec. It is observed that the swept tip shows at least a 3 percent performance improvement over the square tip at medium thrust coefficients. For a hovering helicopter this is equivalent to a 12 percent increase in payload. The double-swept tip shows a small improvement of about 1 percent over the square tip at 129 and 152 m/sec for lower thrust coefficients. At very high thrust coefficients the square tip's performance is superior to both the swept and double-swept tip. This is because the tip vortex generated by these two tips breaks down at high angles of attack. For the swept tip, vortex breakdown occurs at a collective pitch setting of 12 deg as seen in the sequence of schlieren photographs in Figure 21. For pitch angles less than 10 deg, there appears to be a fairly laminar, concentrated vortex core. At 12 deg vortex breakdown is visible. It appears as a sudden divergence in the size of the vortex core, and a reduction in the maximum induced circumferential velocity. This agrees with data from a wind-tunnel tip shape study conducted by McCormick, et.al., (Ref. 11). For a 60 deg swept tip, they also found that there was a sudden divergence of the vortex core size and a reduction of the maximum circumferential velocity at an angle of attack of approximately 12 deg. Their measurements were taken with a vortex probe at a distance four-chord lengths behind the trailing edge.

Due to the vortex breakdown a large portion of the vortex-induced lift is eliminated, and the performance of the swept tip deteriorates below that of the square tip. Vortex-induced lift is additional lift produced near the blade tip by the strong tip vortex being shed. Most of this lift occurs in the

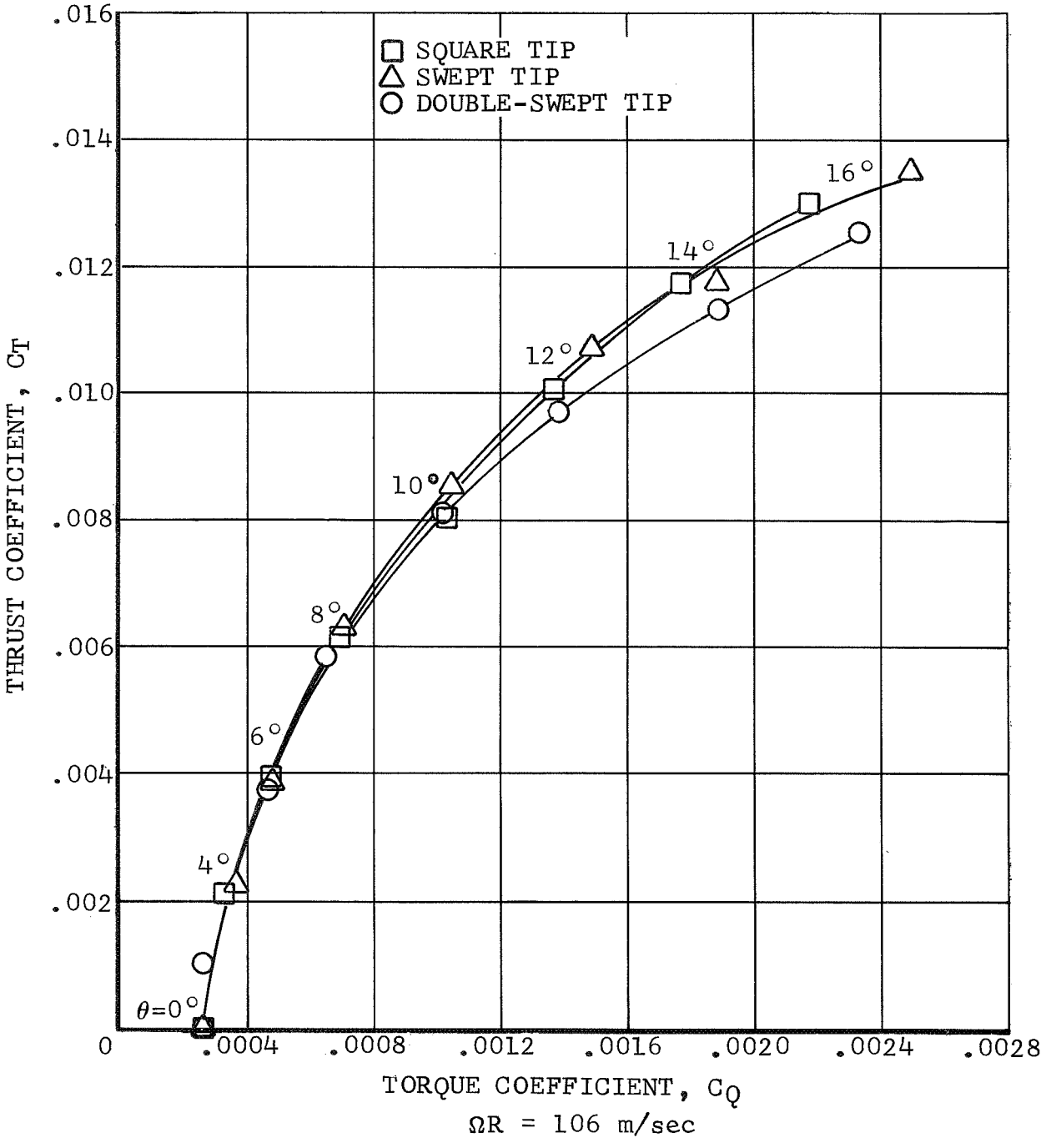

Figure 20. Effect of Tip Shape on Experimental Performance of Model Rotors (Rotor Group 2) - R = 35.0 cm.

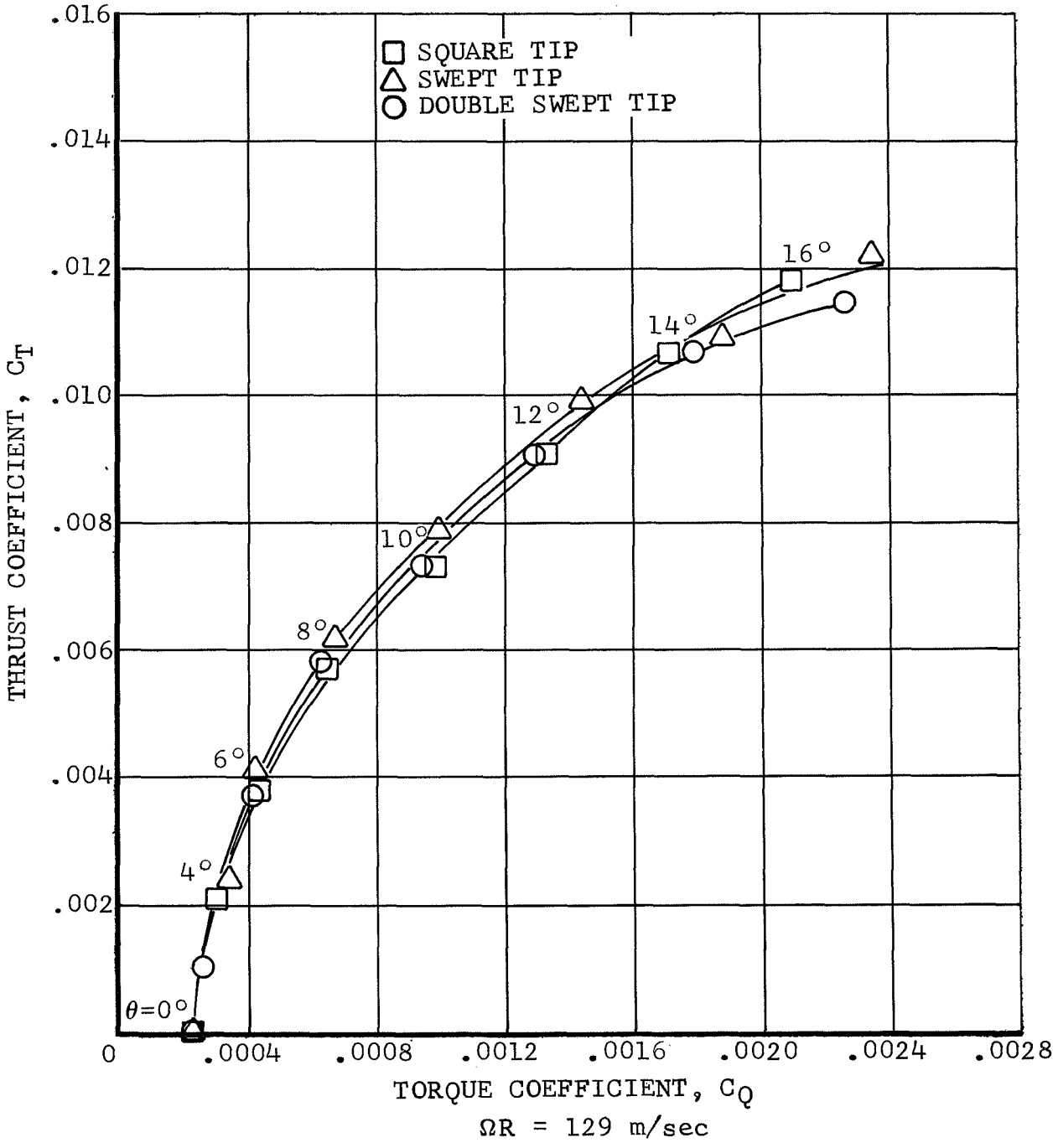

Figure 20. Continued.

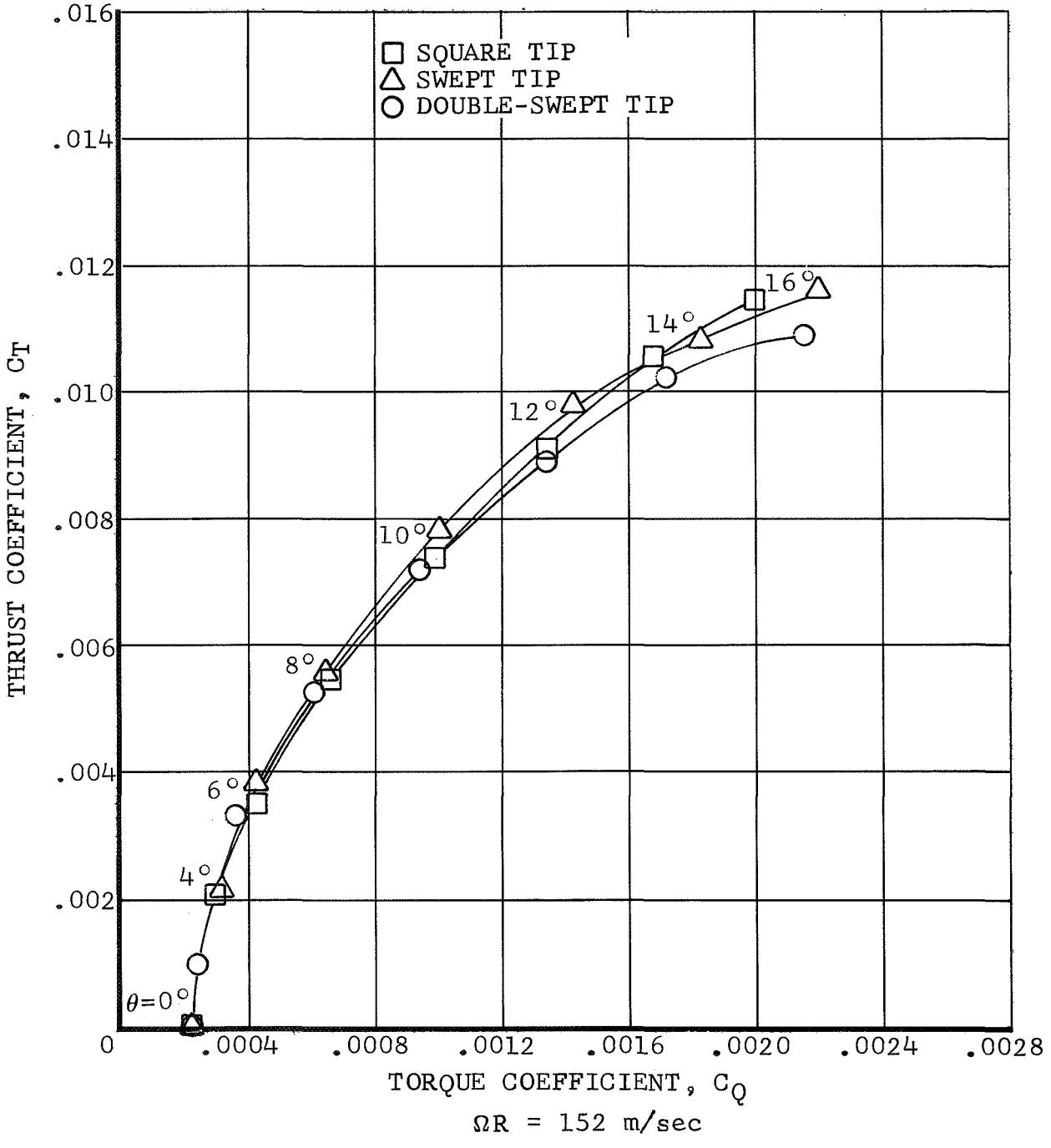

Figure 20. Concluded.

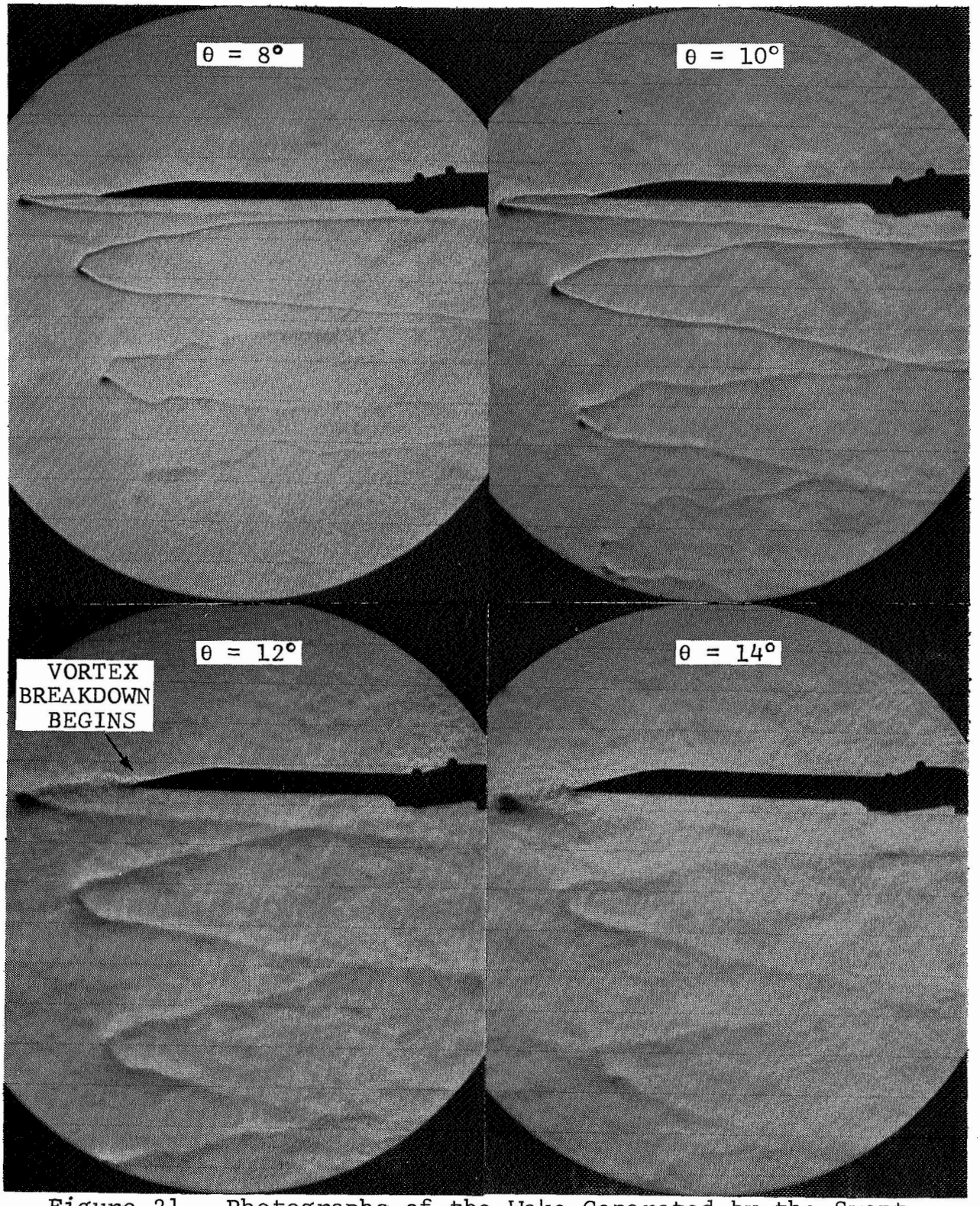

Figure 21. Photographs of the Wake Generated by the Swept Tip at Various Collective Pitch Angles (Rotor Group 2) - R = 35.0 cm, ΩR = 152 m/sec.

vicinity of the trailing edge. Its percentage of the total lift increases with angle of attack. Because of the vortex-induced lift any tip shape modification that causes vortex breakdown at the tip will also adversely affect the rotor performance at high thrust coefficients.

In Reference 23, Wentz and Kohlman give a detailed explanation of vortex breakdown for delta wings. They present vortex breakdown positions as a function of angle of attack and sweep angle. The angle of attack where breakdown occurs increases with increasing sweep for sweep angles less than 75 deg. For angles greater than 75 deg, breakdown occurs at a constant angle of attack, independent of sweep. Their data predict vortex breakdown to occur at an angle of attack of 12 deg for the sweep angle of 58 deg on the swept and double-swept tip.

For the double-swept tip, vortex breakdown occurs at a lower collective pitch than for the swept tip. This agrees with the earlier deterioration in performance for this tip. As seen in Figure 22, at a pitch of 8 deg there is a concentrated vortex core. At 10 deg vortex breakdown is observed. The occurrence of breakdown at a collective pitch 2 deg lower than for the swept tip is attributed to lower downwash in the tip region of the double-swept tip. The lower downwash manifests itself in reduced pitch of the helical wake (compare Figures 21 and 22) and results in higher angles of attack for a given collective pitch.

No vortex breakdown occurs for the square tip as seen in Figure 23. A concentrated vortex is present at all the collective pitch angles shown. The vortex strength and resulting vortex induced lift keep increasing in intensity with an increase in collective pitch. The vortex core remains very concentrated until blade stall occurs at a collective pitch of 17 deg.

Present hover performance programs do not account for vortex induced lift in the tip region. This is mainly because a rotor blade has a high aspect ratio and vortex induced lift is generally associated with low aspect ratio wings. However, when one considers that a rotor blade's lift is concentrated in the tip region, it appears reasonable that vortex induced lift can be quite substantial. Because of this additional lift, measured hover performance at high thrust coefficients would most likely be greater than that calculated using two-dimensional airfoil theory.

Based on the performance results it is seen that the swept tip offers a performance improvement over the square tip at low to medium disk loadings. At high disk loadings, low

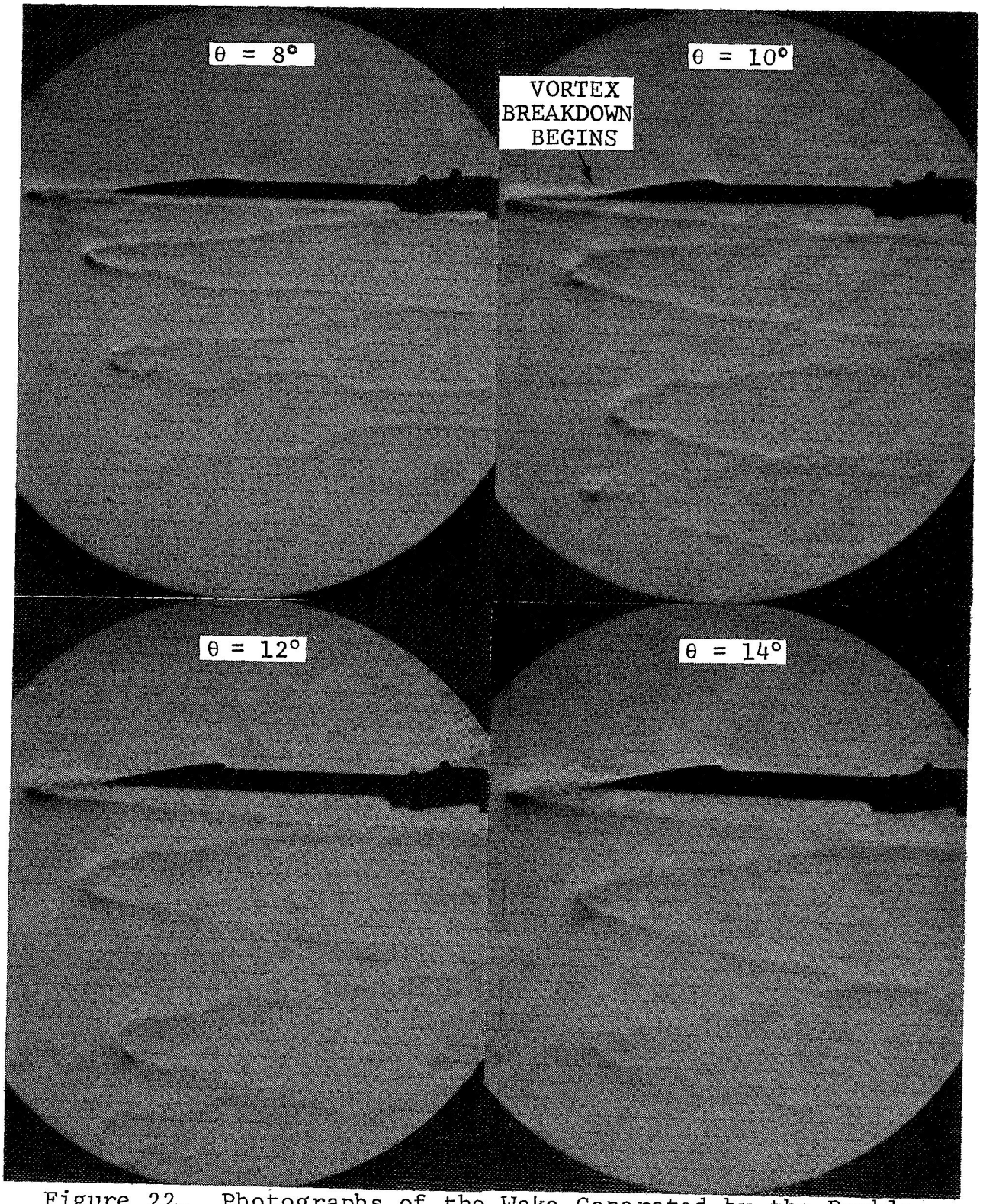

Figure 22. Photographs of the Wake Generated by the Double Swept Tip at Various Collective Pitch Angles (Rotor Group 2) - R = 35.0 cm, ΩR = 152 m/sec.

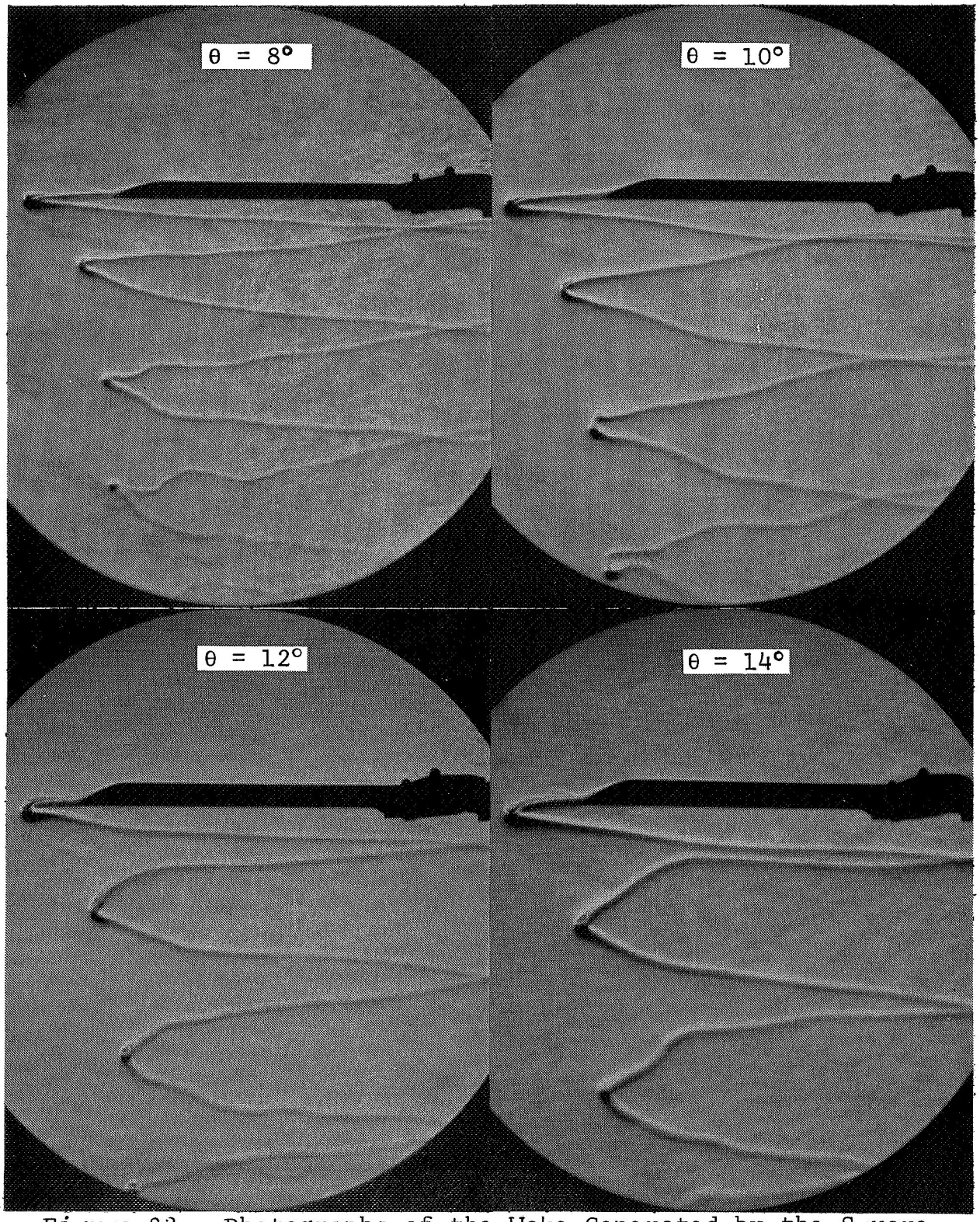

Figure 23. Photographs of the Wake Generated by the Square Tip at Various Collective Pitch Angles (Rotor Group 2) - R = 35.0 cm, ΩR = 152 m/sec.

sweep angles--less than about 70 deg--appear undesirable since they lead to early vortex breakdown which is detrimental to performance. These results appear to be especially applicable to tail rotors which operate at very high thrust coefficients during maximum yaw-rate turns in hover. A minimum amount of sweep (high-sweep angle) would most likely offer some performance improvement and still not produce vortex breakdown at high disk loadings.

Although the double-swept tip only provided a small performance improvement over the square tip at low disk loadings in hover, during high speed forward flight it provides compressibility relief over a larger portion of the blade than the swept tip. A further discussion of this is included in Reference 12.

The performance results for the three tips are in general agreement with the full-scale results of Reference 13, where Spivey concluded that the swept and double-swept tips were better than the square tip at low tip Mach numbers and low mean lift coefficients, and that the square tip was better at high mean lift coefficients. At high tip Mach numbers and high mean lift coefficients he found the swept and double-swept tip to be better than the square tip.

One aspect of the swept and double-swept tip that was not discussed in the previous paragraphs is the clipped region at the trailing edge as seen in Figure 7. One can see that the edge of these tips terminates perpendicular to the trailing edge. By clipping the tip, the low Reynolds number trailing edge region is eliminated. This region appeared to stall early, thus diffusing the vortex and increasing the drag.

4.2.2 Hot-wire anemometer measurements. - The analysis of the hot-wire traces that were taken with the stationary and rotating probe was based on the following assumptions:

1. The vortex core was assumed to be symmetrical over the interval investigated.

2. The hot-wire is assumed to be parallel to the vortex being measured; that is, the curvature of the vortex is small along the length of the wire.

3. The cooling produced by the axial velocity in the vortex core is assumed to be small since the wire is relatively insensitive to this component of flow.

4. The stagnation temperature change in the vortex is assumed to be small.

5. The translational velocity of the vortex across the stationary probe was assumed to be constant during the time required for the vortex to cross the hot-wire.

Stationary hot-wire probe: The trajectory of the tip vortex was very repeatable close to the rotor. When the hot-wire was positioned along the trajectory of the vortex in this region--at ψ_W = 45 deg as shown in Figure 24--the center of the vortex consistently intersected the wire twice every revolution of the rotor. The repeatability of the vortex trajectory decreases with downstream distance. With the hot-wire positioned in the wake at ψ_W = 420 deg, the vortex only intersects the hot-wire intermittently. Because of this, the sampling time required to obtain useful data increases.

The vector sum of the maximum circumferential velocity in the vortex core and the translational velocity of the vortex are measured as the vortex intersects the wire as seen in Figure 25. The hot-wire signal differs considerably depending on what portion of the core passes over the wire. If the inside portion of the core passes over the wire (Point A), the wire measures the quantity $V_\theta + V_\tau$; whereas, if the outside edge of the core passes over the wire (Point B), the quantity $V_\theta - V_\tau$ is measured. The case of primary concern is when the center of the core intersects the wire (Points C and D). When this occurs the quantity $\sqrt{V_\theta{}^2 + V_\tau{}^2}$ is measured as the near and far edge of the core intersect the wire.

A typical velocity distribution measured by the hot-wire as the center of the core intersects the wire is shown in Figure 26. The trace shown here, which is representative of those measured close to the blade, moves from left to right. The hot-wire first senses the induced velocity from the blade bound vortex as it passes over the probe. Then, as the tip vortex intersects the wire, two peaks appear which represent the edge of the core and correspond to Points C and D in Figure 25. Inside the vortex core, the circumferential velocity increases from zero at the center to a maximum at the core's boundary. Outside the core the circumferential velocity is inversely proportional to the radial distance. The maximum circumferential velocity in the core is obtained by subtracting the translational velocity of the vortex across the wire from the peak velocity at the edge of the core.

Figure 27 shows the velocity distribution measured for the three tip shapes at ψ_W = 45 deg for a collective pitch of 12 deg. It is observed that the maximum circumferential velocity is greatest for the square tip and lowest for the double-swept tip. At a collective pitch of 12 deg, it is recalled

SQUARE TIP

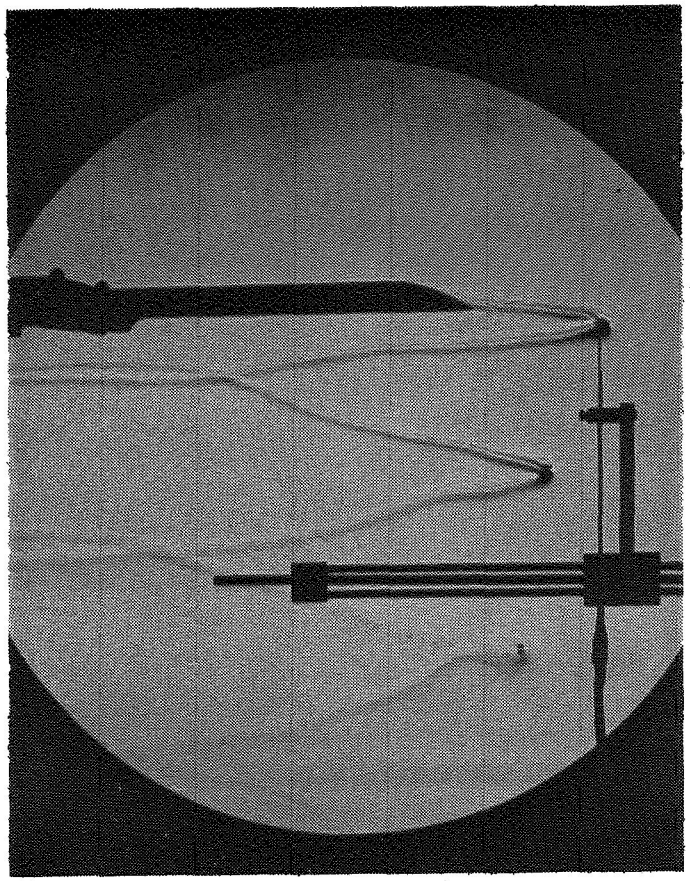

PROBE LOCATION, $\psi_W = 45^o$

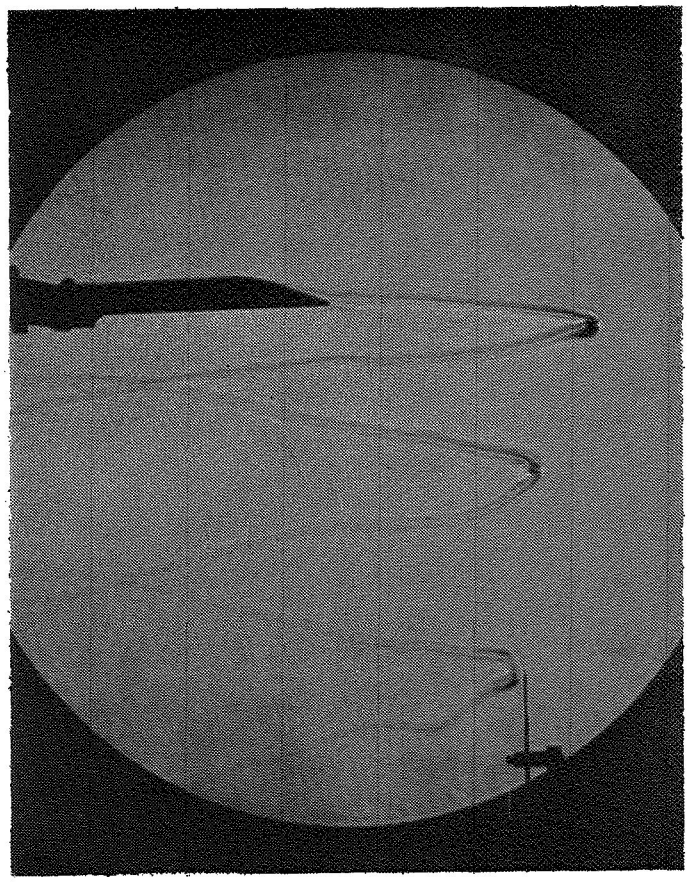

PROBE LOCATION, $\psi_W = 420^o$

Figure 24. Photographs of the Hot-Wire Anemometer Located in the Wake for Tip Vortex Velocity Measurements (Rotor Group 2) - R = 35.0 cm, ΩR = 152 m/sec.

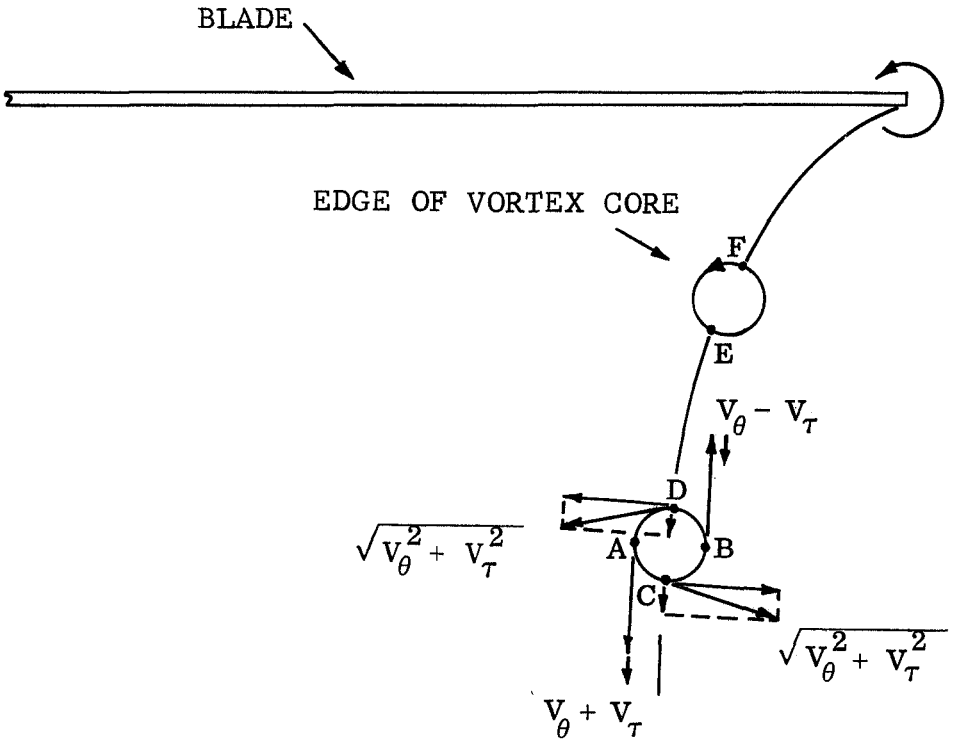

Figure 25. Analysis of the Vortex Core Intersecting the Hot-Wire.

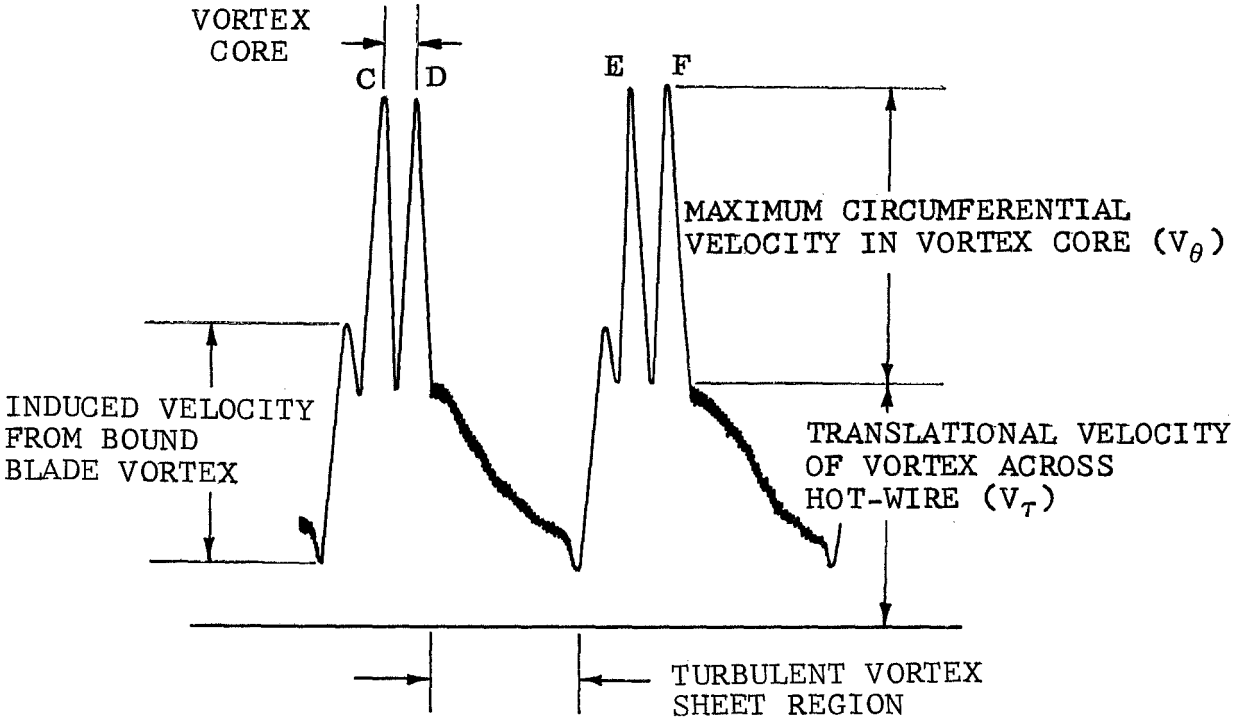

Figure 26. Hot-Wire Anemometer Measurement of Velocity Distribution through Tip Vortex

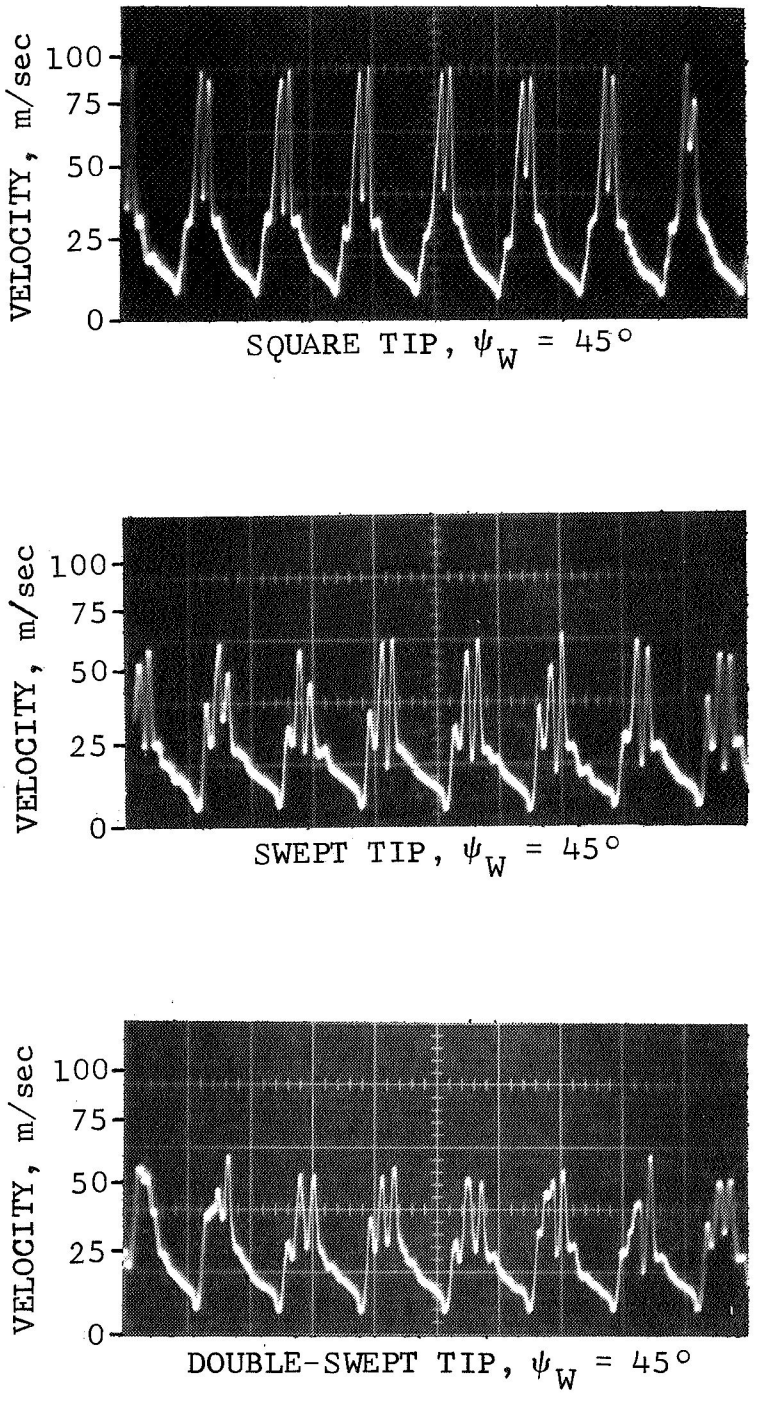

Figure 27. Hot-Wire Anemometer Measurements of the Velocity Distribution Through the Tip Vortex. (Rotor Group 2) - R = 35.0 cm, θ = 12°, ΩR = 152 m/sec.

that vortex breakdown was present for both the swept and double-swept tip, and that the degree of breakdown was more severe for the latter. This accounts for the lower maximum circumferential velocity in the core of the vortex generated by these two tips. From the velocity trace it is also seen that the more diffused vortex generated by the double-swept tip has the largest core size.

Figure 28 shows the velocity distribution measured further downstream for the square tip at ψ_W = 420 deg for the swept tip at ψ_W = 270 deg. In this region, where the vortex intermittently intersects the hot-wire, only one velocity trace through the center of the vortex core is present for the square tip. For the younger vortex generated by the swept tip, three intersections of the vortex core are observed. It is also seen that the magnitude of the maximum circumferential velocity for the swept tip has significantly decreased relative to the square tip. The character of the traces is slightly different from those obtained close to the rotor, since the induced velocity from the bound blade vortex is less significant.

Figure 29 shows the maximum circumferential velocity in the vortex core versus vortex age for the square and swept tip. The data, which were taken at intervals corresponding to about $\Delta\psi_W$ = 50 deg, all fell within the band shown. The magnitude of the maximum circumferential velocity varied within this band width due to a certain amount of unsteadiness in the inflow through the rotor. For the square tip the ratio of the maximum circumferential velocity to tip speed of 38 percent at ψ_W = 45 deg agrees favorably with that measured by Cook (Ref. 15) at high disk loadings. He recently conducted a similar investigation using a full-scale one-bladed rotor.

On several occasions it was noticed that when the hot-wire probe was traversed radially to intersect the tip vortex trajectory, the trajectory appeared to be pushed by the probe. This only occurred in the lower wake after the tip vortex was a revolution old. No noticeable interference from the probe was observed close to the rotor. The image of the tip vortex before and after intersecting the probe appeared to be identical.

Some velocity measurements were also attempted at lower collective pitch angles. As the pitch angle was decreased it became increasingly difficult to obtain velocity traces through the center of the vortex core. This was especially noticeable at pitch angles less than 7 deg where high velocity peaks corresponding to the edge of the core were usually recorded. Cook (Ref. 15) also encountered the same difficulty at low pitch angles.

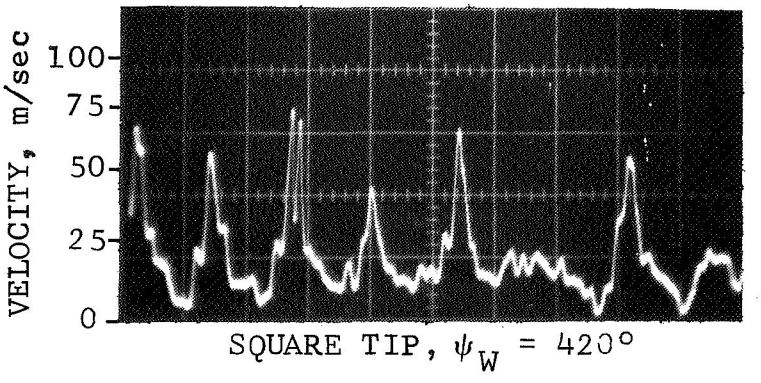

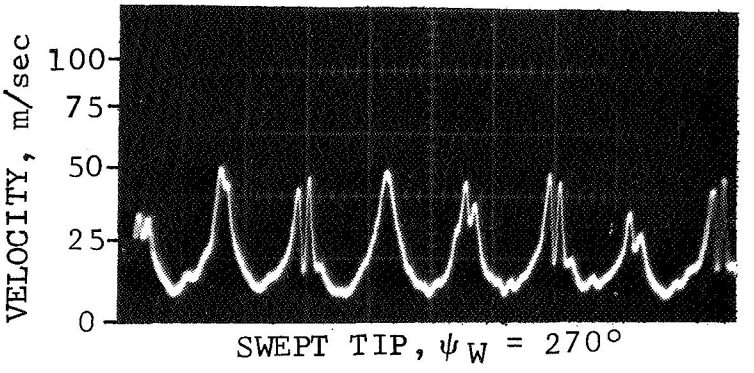

Figure 28. Hot-Wire Anemometer Measurements of the Velocity Distribution Through the Tip Vortex (Rotor Group 2) - R = 35.0 cm, θ = 12°, ΩR = 152 m/sec.

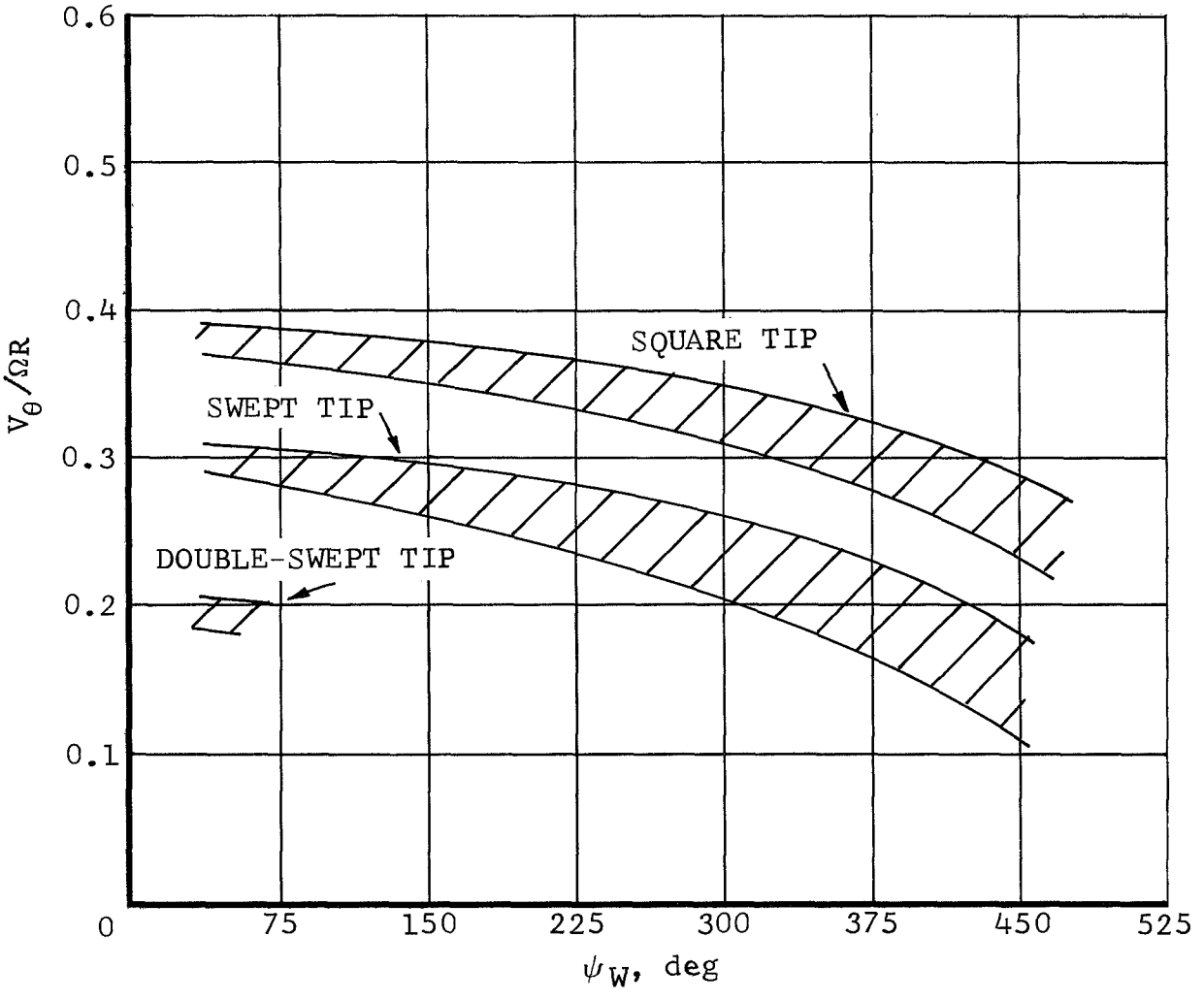

Figure 29. Maximum Circumferential Velocity Versus Vortex Age (Rotor Group 2) - R = 35 cm, θ = 12°, ΩR = 152 m/sec.

Rotating hot-wire probe: Figure 30 shows the hot-wire positioned in the vortex at various distances behind the blade and the corresponding hot-wire anemometer measurements. A well-defined vortex exists two-chord lengths behind the blade. It is seen that the velocity measured by the hot-wire fluctuates with time over a wide interval.

Ideally, if the hot-wire could be positioned along the edge of the vortex core, a steady velocity would be recorded equal to the maximum circumferential velocity. In reality, there is some motion of the vortex relative to the hot-wire that increases with vortex age. This accounts for the large fluctuations present in the velocity trace. When the hot-wire intermittently lies along the narrow edge of the vortex core, peak velocities are measured. The frequency at which peak values occur decreases as the probe is positioned further behind the blade. When the hot-wire passes into the center of the core, the velocity approaches zero. In order to determine the magnitude of the maximum circumferential velocity, the peak values of the velocity trace were reduced by 7 percent to account for the cooling produced by the 30.4 m/sec flow along the axis of the wire.

Velocity measurements in the tip vortex at collective pitch angles of 4, 6, 8, and 12 deg are shown in Figure 31. The maximum circumferential velocity, which is given as a fraction of the tip speed, increases nearly linearly with collective pitch. Over the short distance measurements were taken, there appears to be very little if any reduction of the maximum circumferential velocity.

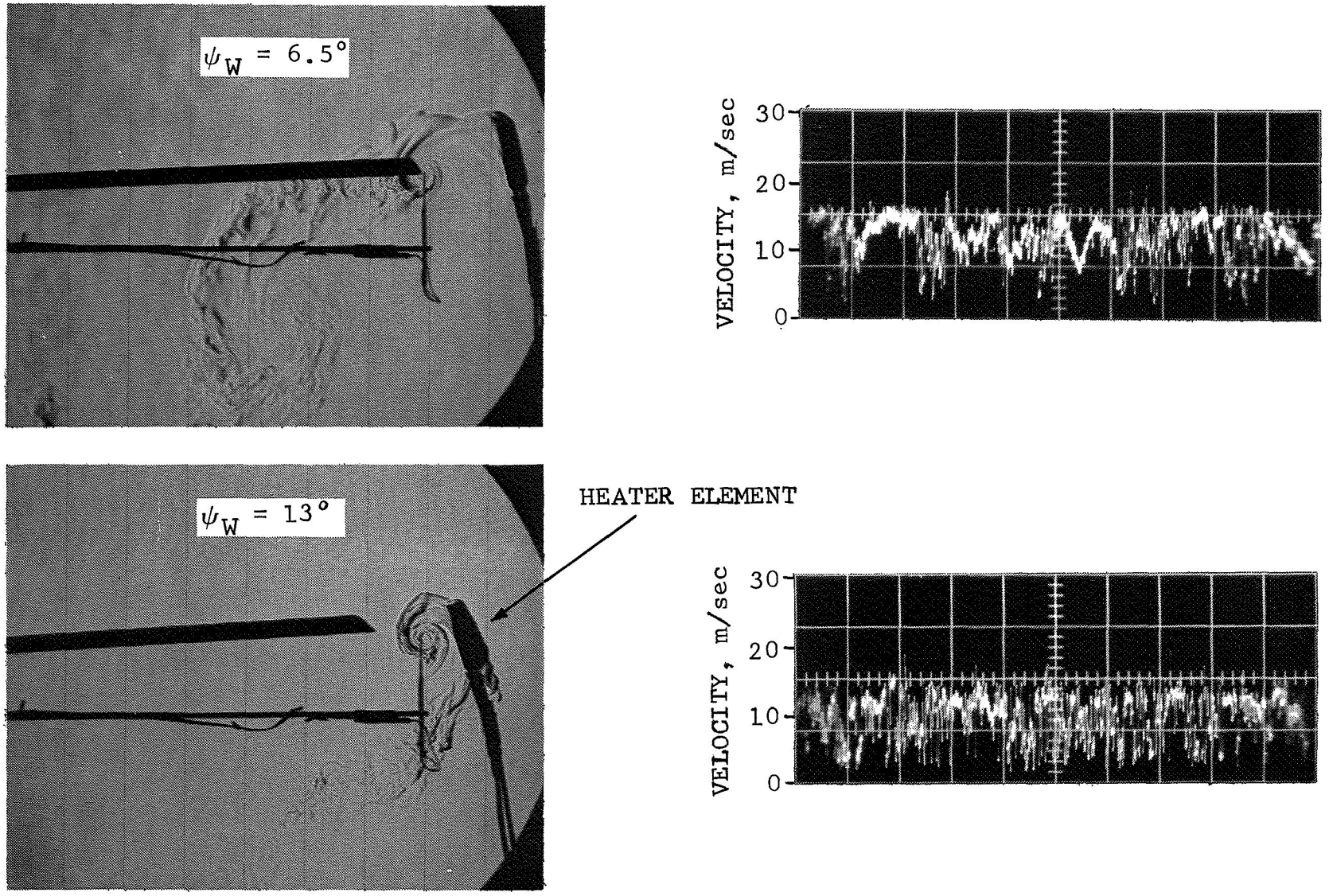

Figure 30. Circumferential Velocity in Vortex at Various Locations Behind the Rotor Blade (Rotor Group 2) - R = 72.4 cm, θ = 10°, ΩR = 30.4 m/sec.

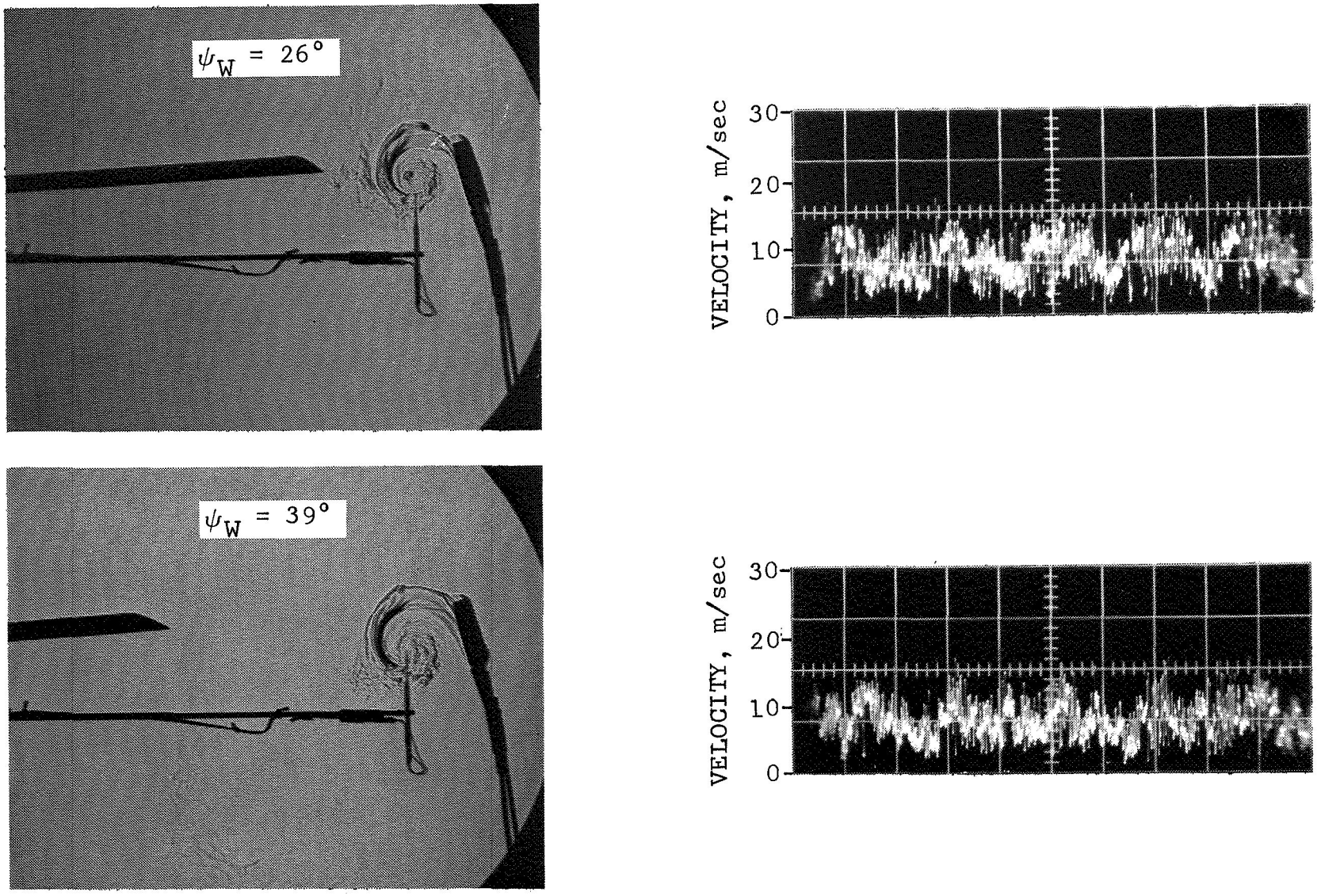

Figure 30. Concluded.

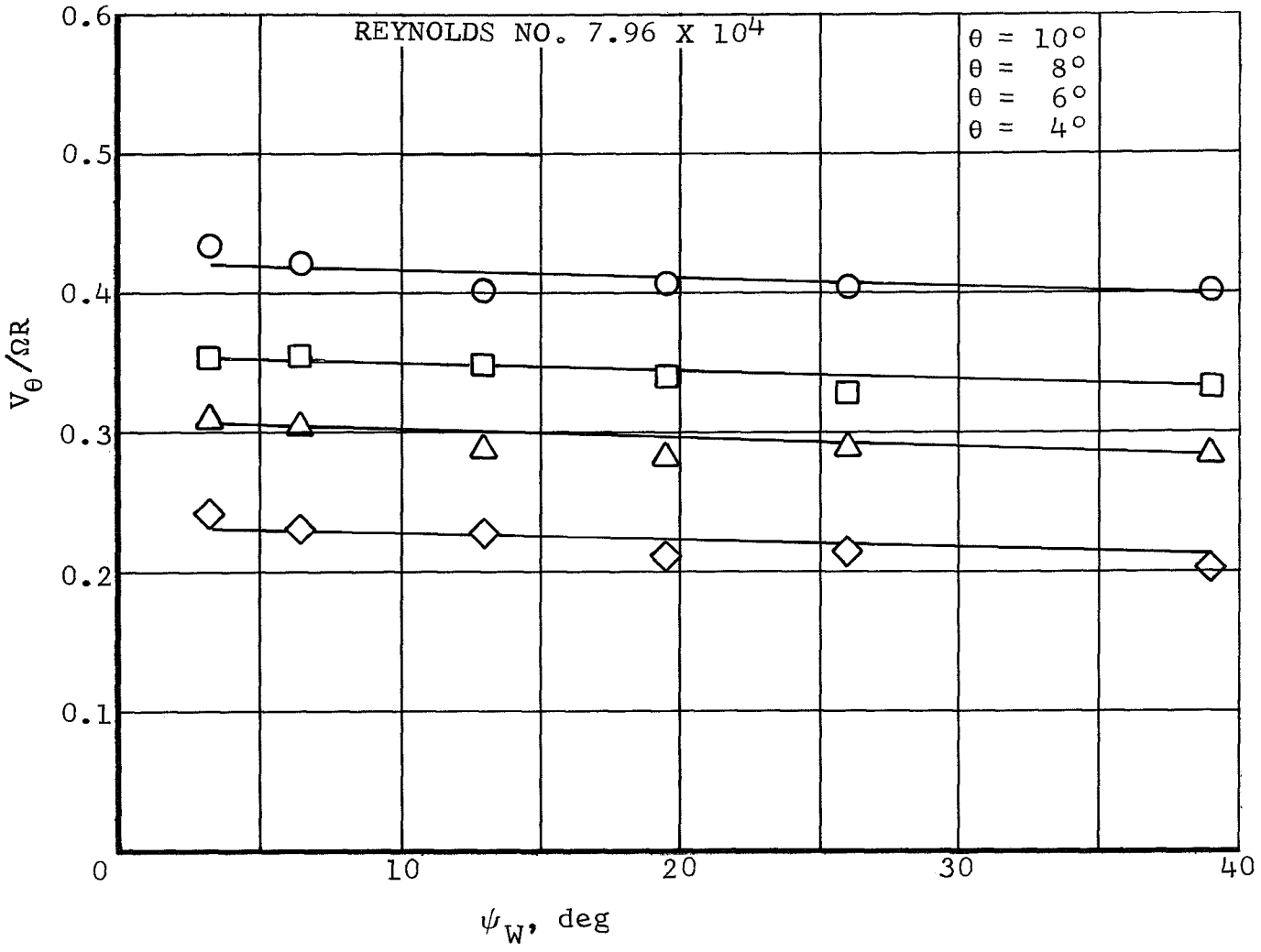

Figure 31. Maximum Circumferential Velocity at Various Locations Behind the Rotor Blade (Rotor Group 2) - R = 72.4 cm, ΩR = 30.4 m/sec.

V. COMPRESSIBILITY AND NOISE INVESTIGATION

The purpose of this investigation was to observe the shock wave produced by two different airfoil profiles (NACA 0012 and a Wortmann FX69-H-098) and three tip shapes (square, swept, and double-swept) at a tip Mach number of 0.95. The acoustic levels produced by the three tip shapes were measured and recorded for tip Mach numbers of 0.65, 0.75, 0.85, and 0.95. Particular attention was given to the relationship between the shock wave propagating radially outward from the tip and the rotational noise. The rotors used in this section are shown in Figure 8.

5.1 Testing Procedure

5.1.1 Flow visualization of shock waves. - The schlieren system was employed to photograph the profile and planform image of the shock generated by two square tip rotors--one with an NACA 0012 airfoil profile and the other with a Wortmann FX69-H-098 airfoil. For the three tip shapes only the planform image was photographed.

Photographs of the profile image were taken with the drive motor in the upright position; however, to photograph the planform image the drive motor had to be mounted horizontally. Some difficulty was encountered taking photographs of the wake with the motor in the horizontal position. At high tip Mach numbers the rotor wake would impinge upon one of the parabolic mirrors. This induced some vibration in the mirrors, thus altering the sensitivity of the schlieren system and making it difficult to obtain good photographs. To alleviate this problem, the rotor's axis of rotation was slanted 10 deg to the collimated light beam.

5.1.2 Noise measurements. - The acoustic levels generated by the square, swept, and double-swept tips were measured and recorded with the system described in Section 2.5. To measure directivity, a cylindrical grid as shown in Figure 32 was established with its origin at the rotor hub. The grid consisted of three equally spaced arcs in the plane of the rotor shaft. The radial distances of the arcs were 3-, 4-, and 5-rotor diameters respectively. Each arc, extending from 60 deg below the rotor plane to 60 deg above, was broken down into increments of 20 deg. This resulted in twenty-one grid points at which noise measurements were taken for each of the four tip Mach numbers (0.65, 0.75, 0.85, 0.95).

The recorded analog data were digitized and processed with a Bell Helicopter Company acoustic analyses computer program. Employing a fast Fourier transform, the program

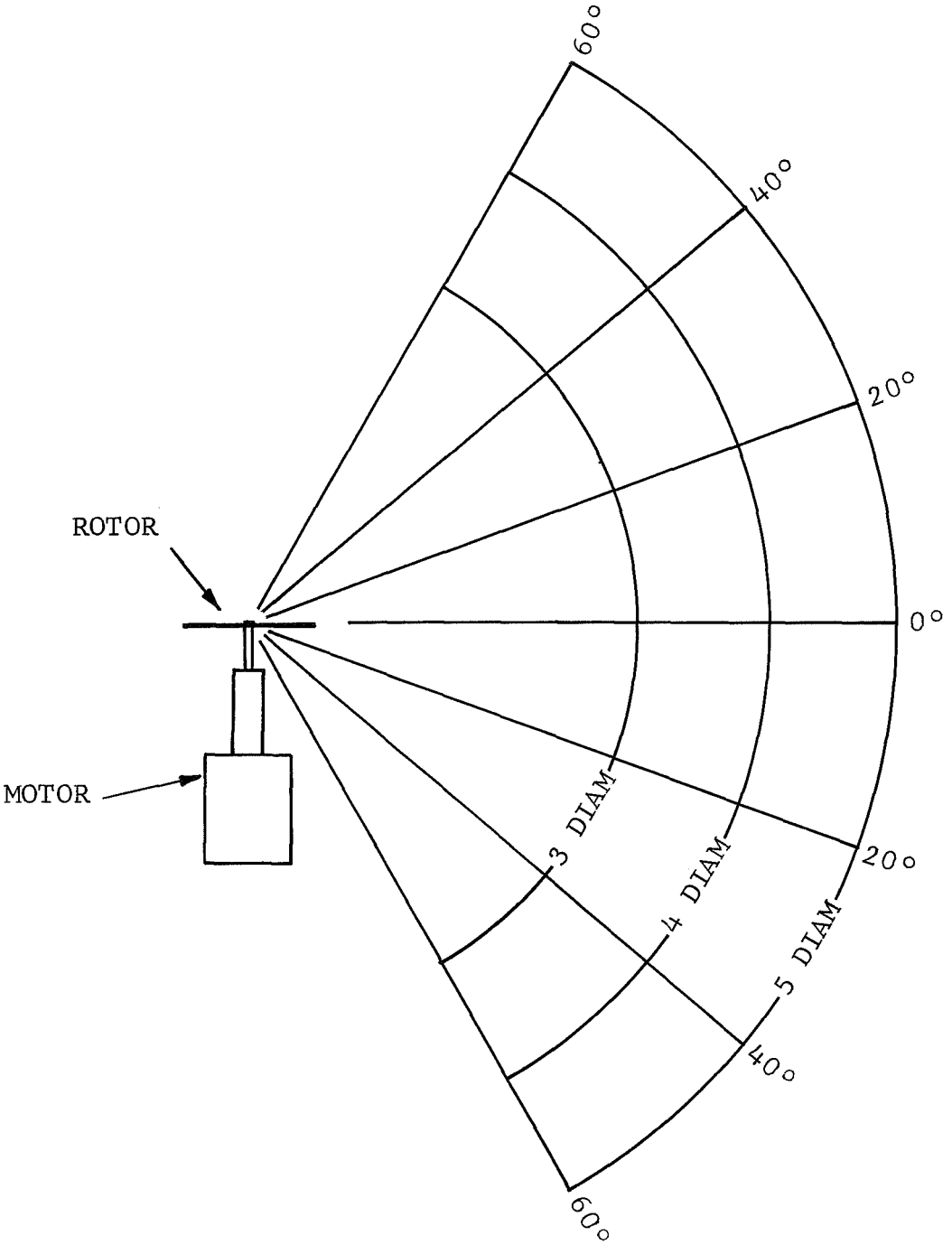

Figure 32. Cylindrical Grid Used for Noise Measurements.

generates octave, third-octave, and arbitrary narrow band descriptions of the acoustic data. All three descriptions were utilized in the noise investigation. The narrow band descriptions were computed for a 10 Hz constant band-width filter; examples of which are shown in Figure 33.

5.2 Test Results and Discussion

5.2.1 Shock wave formation. - The shock wave produced by a rotating source propagates radially outboard at the speed of sound. Because of the rotational motion of the source, the planform view of the shock wave appears as an Archimedes spiral. This phenomenon is analogous to that of a fireworks pinwheel. Figure 34 illustrates the three-dimensional nature of the shock wave generated by a rotating rotor blade. The shock formation along the upper and lower surface of the blade in the tip region would look like that shown in sectional view A-A. The planform view illustrates how the shock formation spirals radially out from the tip. Although it is difficult to predict how the shock above and below the airfoil combine outboard of the tip, it is believed that the resulting shock front would resemble sectional view B-B. The portion of the arc representing the shock front ahead of the plane of rotation (z-positive) would most likely be larger than that behind the plane of rotation since the shock on the upper surface of the airfoil is more intense than that on the lower surface. The most intense region of the spiral shock formation--in and ahead of the plane of rotation--correspond to where the higher harmonic sound measurements recorded by Hubbard and Lassiter (Ref. 24) were the strongest. They recorded the sound generated by a two-bladed propeller at supersonic tip speeds and found that a larger amount of the sound energy appeared in the higher order harmonics as the tip speed increased and that these higher order frequencies were strongest in and ahead of the plane of rotation.

In the following schlieren photographs, one can see that both the tip planform and airfoil profile influence the characteristics of the spiral shock wave. Figure 35 shows both the profile and planform view of the spiral shock wave produced by the NACA 0012 and Wortmann FX69-H-098 airfoil profiles. The profile view of the wake generated by the 0012 airfoil shows a shock front projecting vertically from both the upper and lower surface of the airfoil--the latter being the weaker. In the profile view, the sonic lines spiraling radially outboard from above and below the airfoil divide the dark supersonic region in front of the shock from the light subsonic region behind the shock. For the Wortmann FX69-H-098 airfoil a strong shock is observed only on the upper surface of the airfoil in the profile view. The one distinct sonic line observed in the

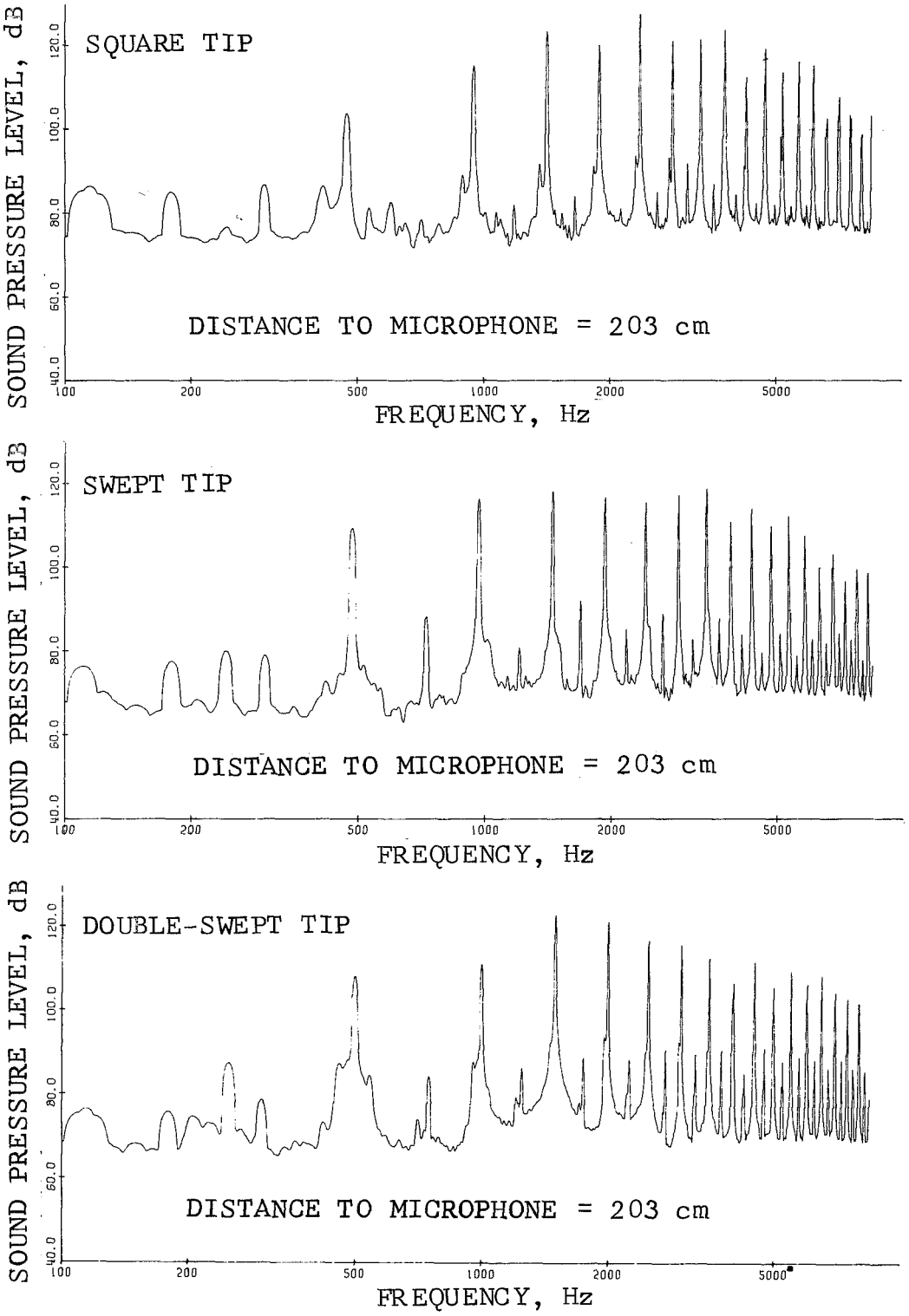

Figure 33. 10 Hz Narrow Band Width Analysis for the Various Tip Shapes (Rotor Group 3) - $\theta = 8°$, $M_T = 0.95$.

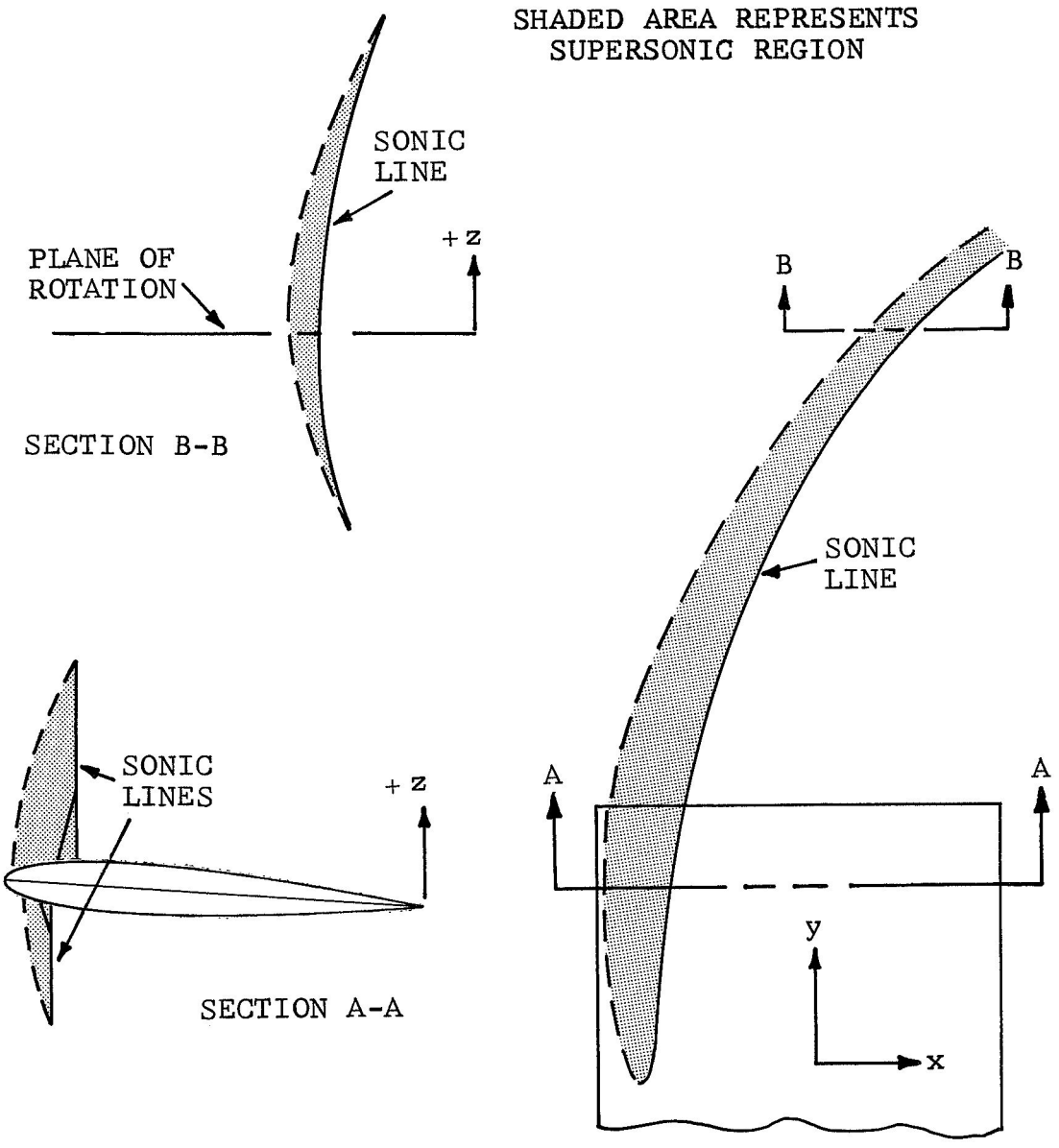

Figure 34. Shock Wave Produced by a Rotating Rotor Blade.

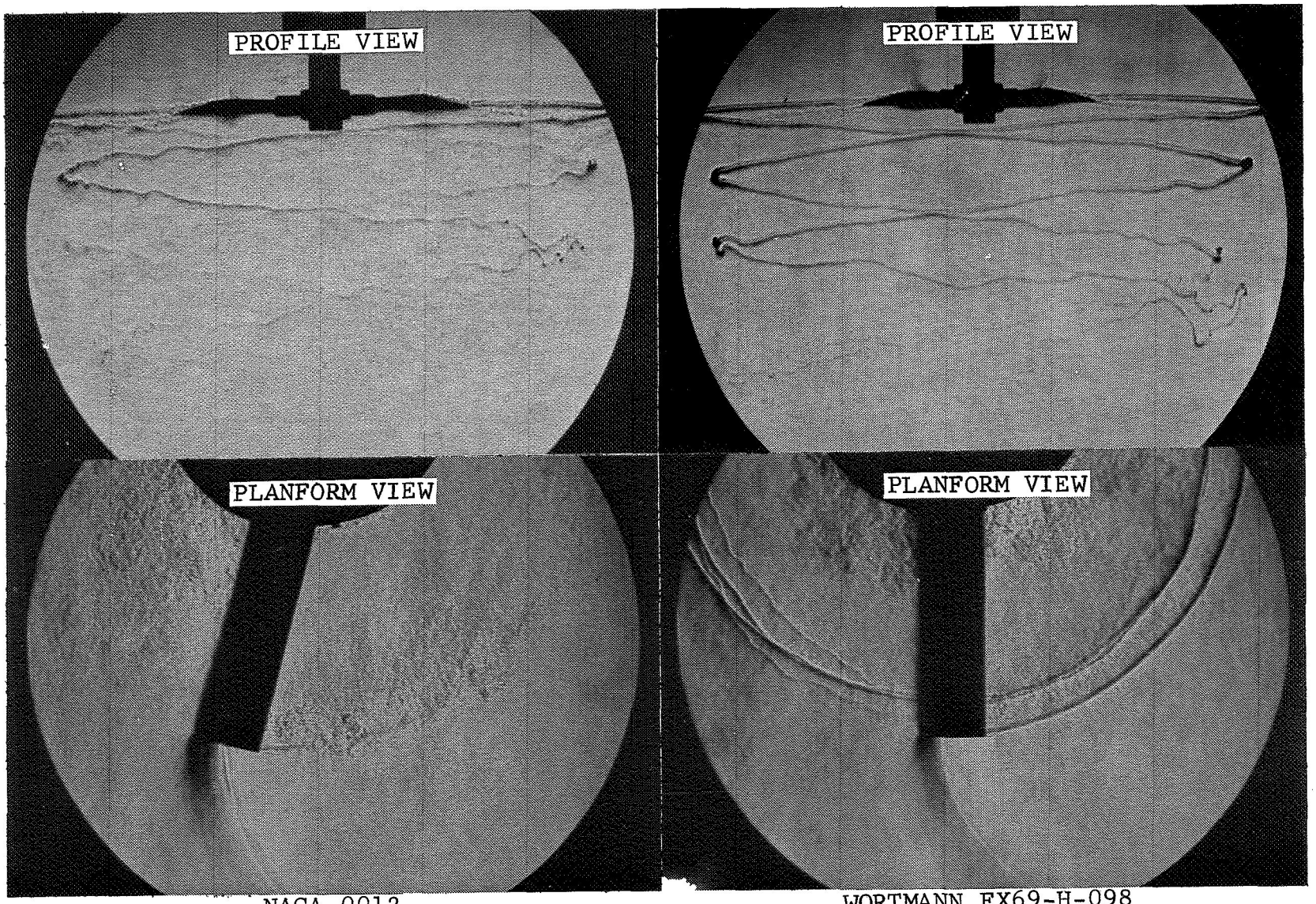

Figure 35. Shock Wave Generated by Two Different Airfoil Profiles (Rotor Group 3) - R = 20.3 cm, $\theta = 8°$, $M_T = 0.95$.

planform view, about one-third of a chord length behind the leading edge, would of necessity correspond to the strong shock propagating from the upper surface of the airfoil.

The profile view of the wake generated by the 0012 airfoil shows the tip vortex to be more unstable than that produced by the Wortmann FX69-H-098 airfoil. This instability is induced by the shock projecting from the lower surface of the airfoil. The Wortmann FX69-H-098, which has no observable shock on the lower surface of the blade to induce vortex instability, generates a relatively stable, intense vortex. The high concentration of turbulence around the rotor hub in the inplane views resulted from the heat dissipated by the drive motor which was operating at maximum output.

In Figure 36 the spiral shocks generated by the square, swept, and double-swept tip are shown for a tip Mach number of 0.95. It is seen that the tip shape exerts a strong influence on the formation and strength of the radial shock. The square tip exhibits the strongest shock pattern. The narrow shock produced by the double-swept tip was concentrated in the vicinity of the trailing edge. Although the double-swept tip produced the weakest shock, it also produced the least amount of thrust--about 60 percent of that produced by the swept tip. The square tip, which had the strongest shock, produced about 90 percent as much thrust as the swept tip.

5.2.2 Noise measurements. - The results of the directivity measurements provided no clear distinction between the three tip shapes. It is felt that room acoustics exerted a strong effect on the spatial sound characteristics and muddled the directivity patterns of the rotors. Data from the grid point located in the rotor plane, five-rotor diameters (203 cm) from the hub, were used to represent the spectral results.

Figure 37 presents the octave sound pressure levels of the three tip shapes for the four tip Mach numbers. It is seen that the square tip's sound pressure levels are about five decibels higher in the upper frequencies than the single or double-swept tip. It is felt that this results from the spiral shock formation discussed in the previous section. In the lower frequencies there is some variation between the tip shapes for different tip Mach numbers; but, in general, the square tip produces higher sound pressure levels than either the swept or double-swept tips.

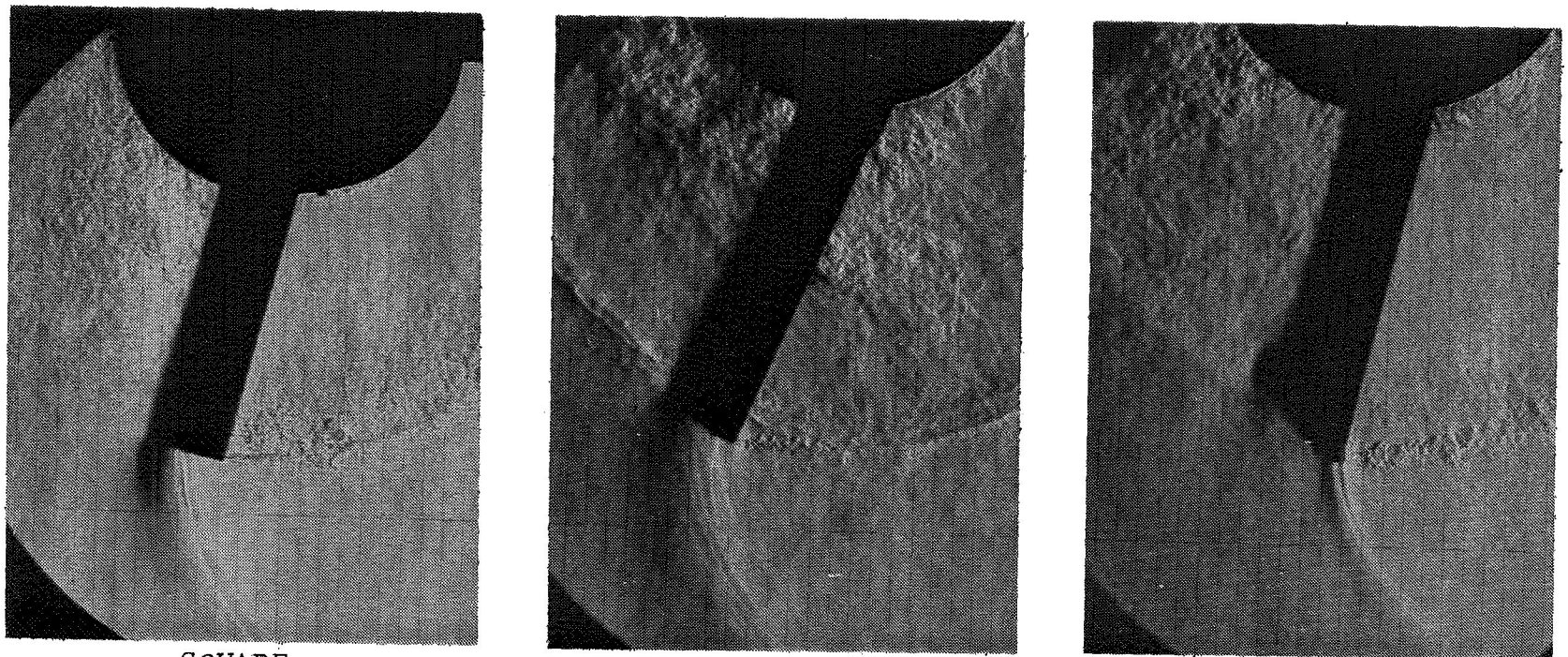

Figure 36. Planform View of the Shock Wave Generated by Various Tip Shapes (Rotor Group 3) - R = 20.3 cm, θ = 8°, M_T = 0.95.

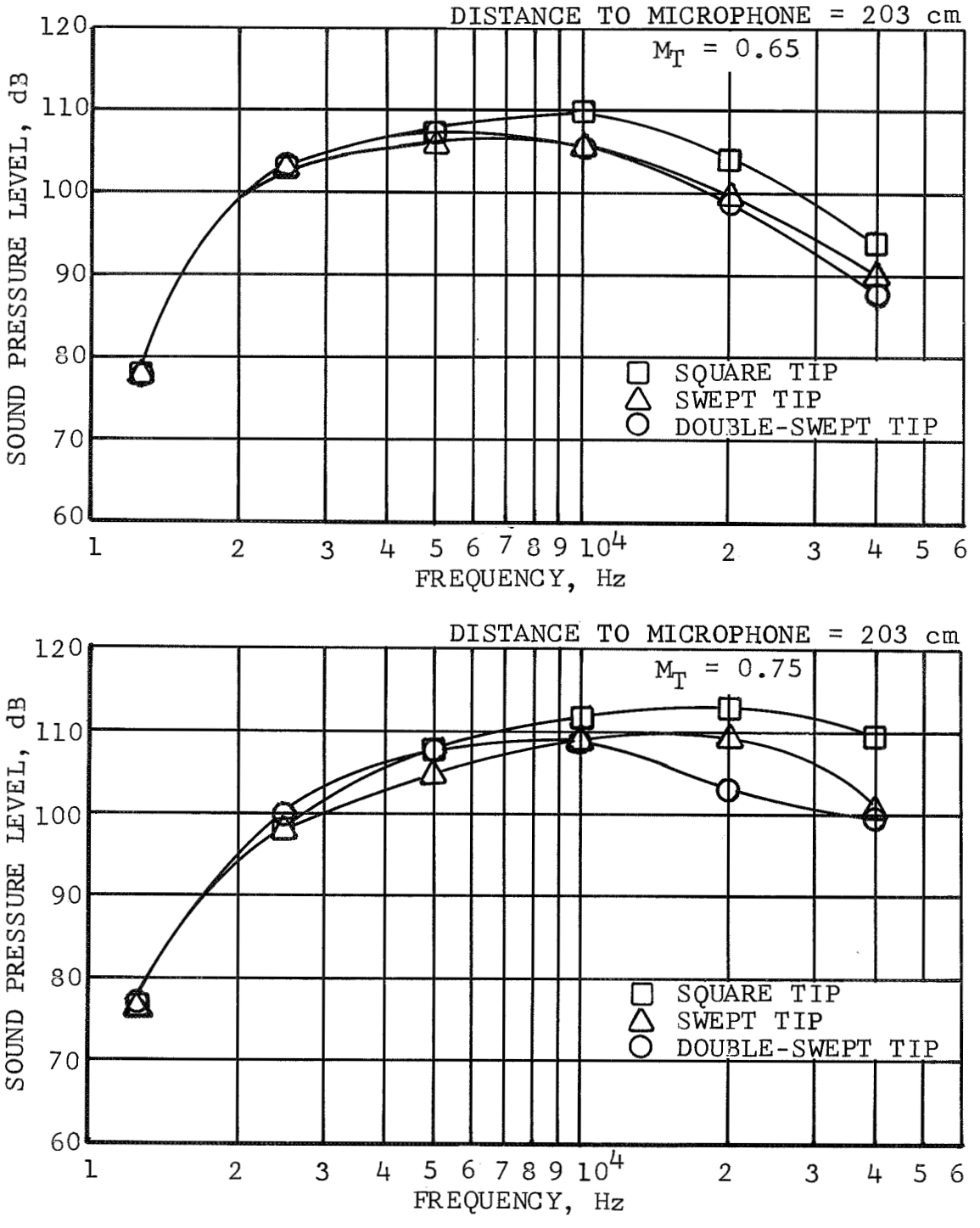

Figure 37. Octave Band Sound Pressure Level Comparisons for Various Tip Shapes (Rotor Group 3) - R = 20.3 cm, θ = 8°

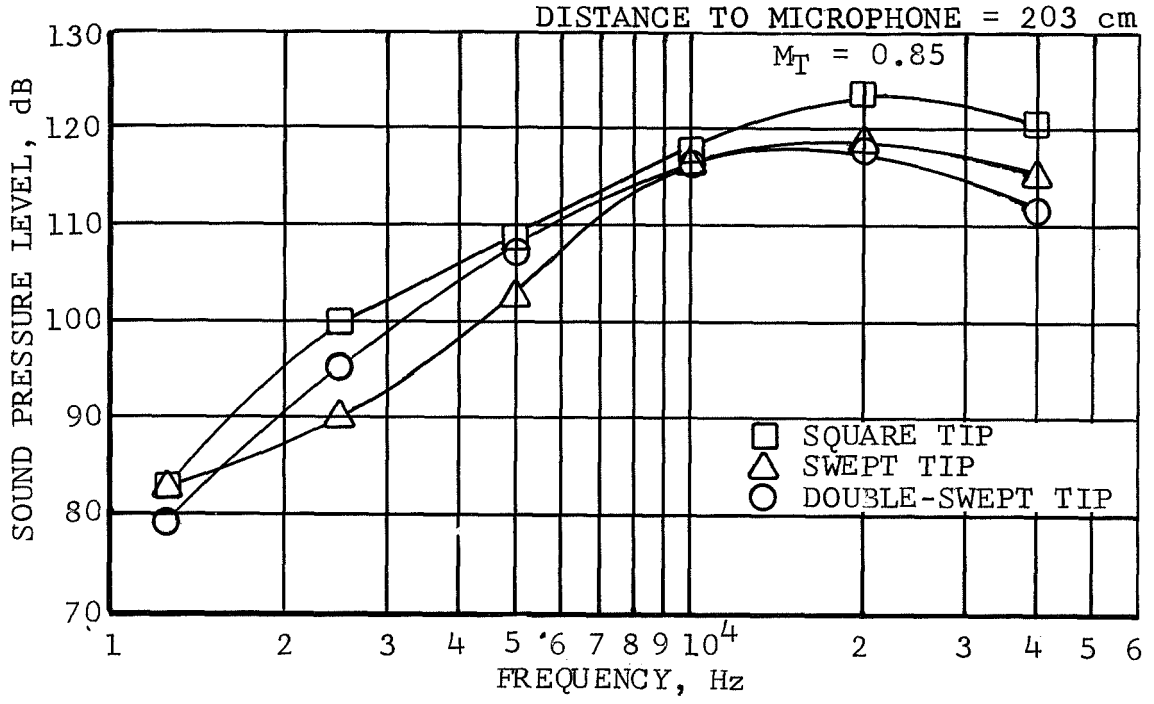

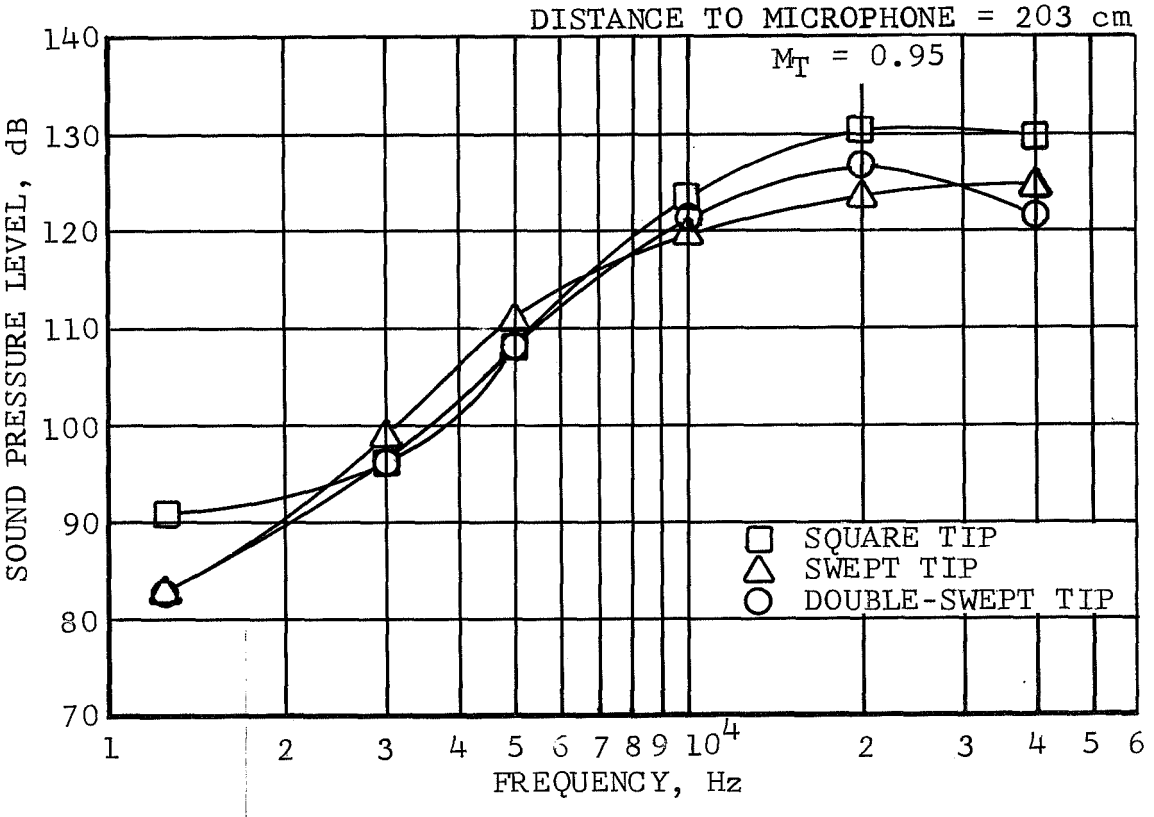

Figure 37. Concluded.

VI. ANALYSIS OF VORTEX STABILITY RESULTS

6.1 Vortex Stability Analysis

Crimi's free-wake analysis which is documented in Reference 5 was used to investigate the interaction and stability of a hovering rotor's tip vortex. In Crimi's method, each blade is represented by a bound vortex filament. The helical tip vortex trailing from each blade is represented by a finite number of vortex filaments. The motion of each filament is induced by all the other vortex filaments and the bound blade vortex filaments. As vortex interaction occurs, the helical tip vortex becomes distorted. The distortion process continues until the geometry of the wake does not change significantly from one iteration to the next. With a two-bladed rotor, convergence can usually be obtained for 2-1/2 revolutions of the wake. It is interesting to note that the tip vortex for the two-bladed rotor could only be observed with the schlieren system for about 2-1/2 revolutions. It diffused rapidly after this point. In Crimi's program, representation of the inboard vortex sheet and viscous dissipation of the tip vortex are neglected. For this analysis, their effects were not considered to be of major importance.

The Euler method of numerical integration is used for computing the distorted wake geometry in Crimi's free-wake analysis. For better accuracy the second order Runge Kutta method of numerical integration was used in this analysis. The procedure involves using the Biot-Savart law to calculate the induced velocities at the end points of all vortex filaments representing the wake. These velocities are integrated over a small time increment to obtain a new wake geometry. Another set of induced velocities are calculated for the new wake geometry. This set is averaged with the respective preceding velocity components, and then integrated again over the time increment to obtain a refined wake geometry.

The wakes calculated for comparison with experimental results consisted of seven revolutions with twelve vortex filaments or time increments per revolution. To assure adequate convergence, the iteration procedure was continued for 96 time increments. Profile drawings of the calculated wakes were obtained to qualitatively compare with experimental results. Although the calculated wakes consisted of seven revolutions, only four were plotted. The last three revolutions were quite erratic and their main purpose was to help provide better convergence for the upper portion of the wake.

6.2 Vortex Stability Results and Discussion

Using the Euler method of numerical integration, the trajectory of the tip vortex after the first revolution, did not correlate well with experimental observations. This is attributed to the rapid accumulation of errors associated with the Euler method of integration. A more detailed explanation of this is included in Reference 25 where several vortex interaction problems are analyzed using various numerical methods. With the more accurate second order Runge Kutta method of integration, the trajectory of the tip vortex, after the first revolution, differed significantly from that calculated using the Euler method. The wake converged upon a trajectory similar to that observed experimentally. One peculiarity associated with the calculated trajectory was a one-per-rev, combined axial and radial oscillation of the tip vortex after it was 1-1/2 revolutions old. This oscillation, which was superimposed on the interaction of two vortices revolving about their common centroid of vorticity, was not observed experimentally. The cause of this discrepancy is uncertain. Although the possibility exists that it could be characteristic of a symmetrical wake, more likely it results from inadequate representation of the far wake or from numerical integration problems arising during the calculation of the tip vortex trajectory. These numerical problems become more acute as the number of blades increases or the collective pitch decreases. A detailed investigation of this discrepancy was beyond the scope of this program.

6.2.1 Wake asymmetry analysis. - The wake profile shown in Figure 38 was calculated for a two-bladed UH-1B rotor. It is seen that, unlike the experimental wakes, the wake is perfectly symmetrical. Vortex interaction between adjacent revolutions of the tip vortex occurs on both sides of the wake at the same axial distance below the rotor. The interaction differs considerably from the experimental results where the two vortices pair up. Based on the schlieren pictures, wake asymmetry was believed to result from asymmetrical rotor loading. To verify this, wake trajectories were calculated for an asymmetrically loaded rotor. This was simulated by making the bound vortex strength of one blade, Γ_2, 10 percent greater than the other. The resulting wake shown in Figure 38 now looks similar to that seen experimentally. It is no longer symmetrical and the trajectory of the weaker tip vortex, Γ_1, is displaced further by the following blade's stronger bound vortex. The extra axial displacement enables it to pass inside the other tip vortex when it is about one revolution old. After this happens, the two vortices pair up and revolve about their common centroid of vorticity as they pass downstream. Toward the bottom of the wake, this becomes less obvious due to the

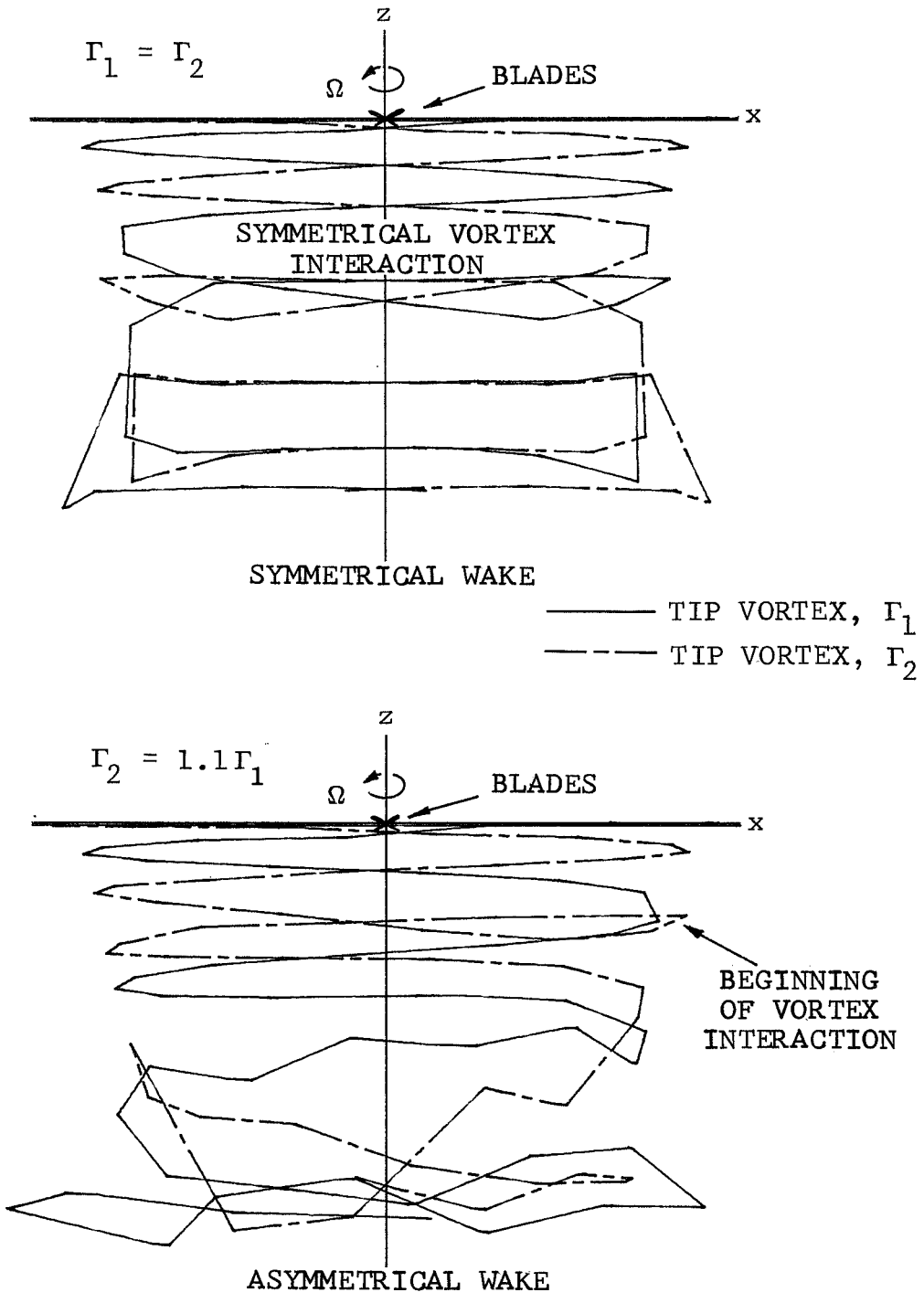

Figure 38. Calculated Free Wakes
UH-1B, 3180-kg Lift

numerical problems associated with the free-wake program. Large wake distortions are present that most likely result in tip vortex breakup.

6.2.2 Proposed mechanism for initiating the interaction between two tip vortices. - Crimi's free-wake program can lend some insight into the vortex interaction that originates in the region of maximum wake contraction and the vortex instability that follows. With this program it can be shown that two vortices pair up and begin revolving about their centroid during the transition from contracting to expanding radial flow. As long as there is strong radial contraction, this will not occur.

To illustrate how the transition from wake contraction to expansion takes place, the free-wake program was used to calculate the induced velocity components in cylindrical coordinates on all the wake points for a two-bladed rotor. Only four revolutions of the wake were used in this analysis and the iteration procedure was terminated after 60 time increments. The results are qualitatively the same if more revolutions of the wake are considered. Figure 39 shows the induced radial velocities, V_r, on the wake points representing the helical tip vortex from one blade before and after wake distortion occurs. Prior to wake distortion, the induced radial flow is inboard on the upper half of the helix and outboard on the lower half. Any revolution of the helix will produce radial contraction on that portion of the helix above it and radial expansion on that portion below it. This is characteristic of any finite helical vortex, inclusive of the wake below a hovering rotor. The induced velocity distribution for the tangential component, V_t, and the downwash component, V_z, are not of importance and are shown here purely for general interest. As an element of the tip vortex generated by a hovering rotor blade passes downstream, it experiences the transition from radial contraction to expansion. During the transition its rate of descent is decreased and its relative position to that segment of the tip vortex directly above it (which has been generated by the following blade 1/2 a revolution later) is such that they begin revolving about their centroid of vorticity. Although the velocity distributions are quite erratic after the wake has converged upon a distorted geometry, there are certain gross similarities between the radial flow distribution before and after wake distortion.

For example, the induced radial flow is still inboard over the first revolution and a half of the helix. Despite the erratic pattern of the radial flow over the rest of the wake, the gross radial flow direction is still outboard and the transition from contraction to expansion is much sharper due to the strong vortex interaction.

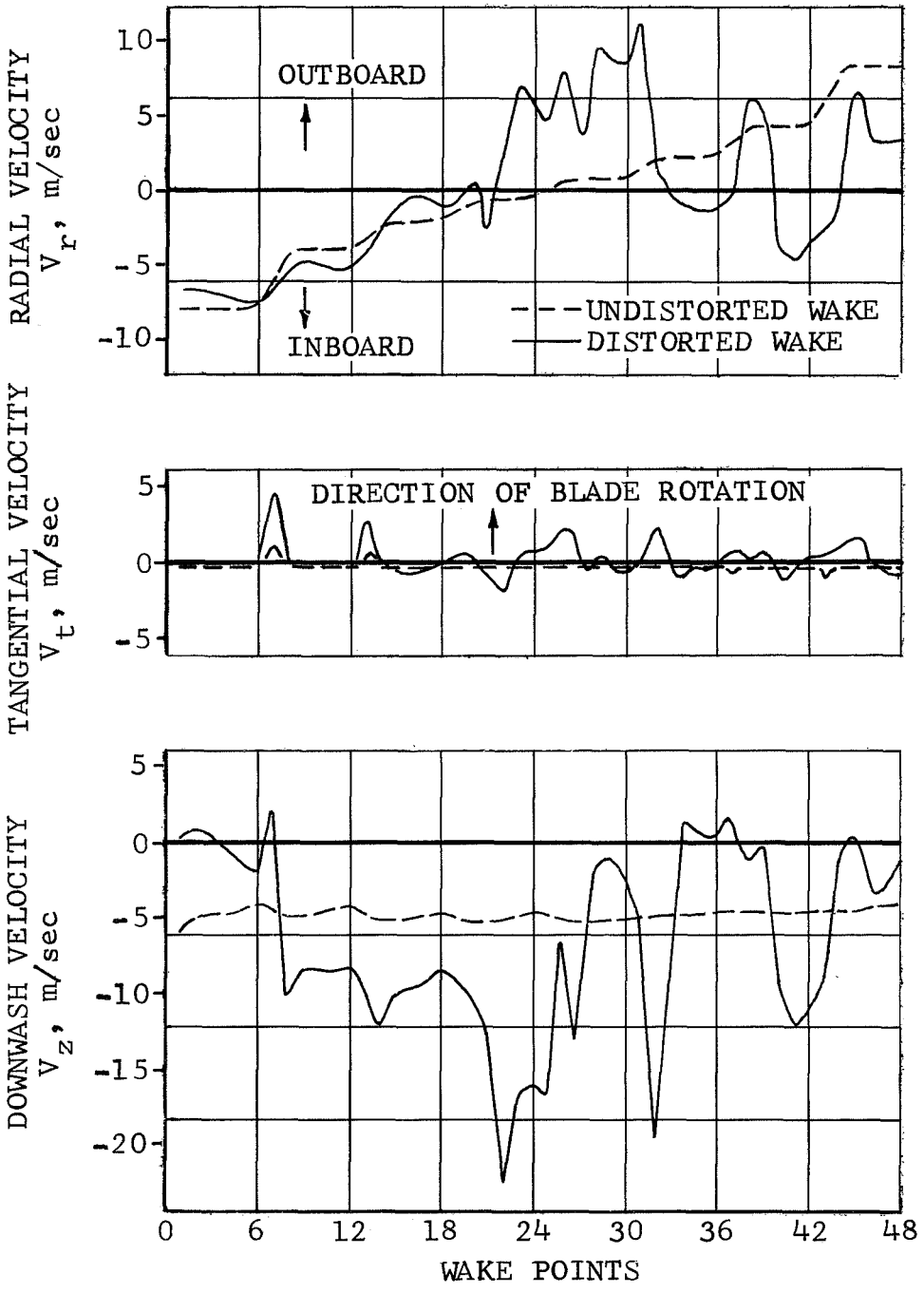

Figure 39. Induced Velocity Components on Wake Points.

As wake contraction takes place, the downwash velocity from the rotor is increasing in the direction of flow, and it provides a favorable velocity gradient which aids vortex stability. After the wake has reached maximum contraction and begins its erratic expansion, the downwash velocity decreases in the direction of flow. This would probably favor vortex instability. Also, the induced velocity distribution along the tip vortex path after wake contraction takes place is quite erratic and any perturbations present would probably be amplified and aid vortex breakup.

VII. CONCLUSIONS

1. The principal conclusions to be drawn from the vortex stability investigation are as follows:

   a. All the wakes observed were asymmetrical due to small differences in loading between blades. The tip vortex preceding the blade with the greatest loading is deflected the most during blade passage and is the first to undergo vortex interaction.

   b. Vortex interaction, where two vortices revolve about their common centroid of vorticity at a rate proportional to their strength and inversely proportional to the square of their separation, always occurs between vortices generated by neighboring rotor blades.

   c. As the number of blades increase, or as the collective pitch decreases, the angular rate at which two vortices revolve about their common centroid of vorticity increases and vortex instability and diffusion occur sooner.

   d. The mechanism believed to be responsible for initiating large scale vortex interaction is the transition from a strong radial wake contraction to an erratic radial wake expansion.

   e. For the two-bladed propeller and rotor, both vortices always paired up and destroyed each other through vortex interaction.

   f. For the four-bladed propeller and rotor, two neighboring vortices always paired up and destroyed each other while the other two passed further downstream and either broke up independently or paired up and destroyed each other.

   g. At high tip Mach numbers unstable sinusoidal fluctuations of the tip vortex occur close to the rotor. These appear to be induced by the strong shock formation projecting from the lower surface of the airfoil in the vicinity of the tip.

   h. The free-wake analysis describes in a qualitative manner tip vortex interaction during hover. However, the accuracy of the analysis, especially in the far-wake region, is highly dependent on the method of integration.

2. The following conclusions can be drawn from the tip shape investigation:

   a. The combined use of the schlieren and hot-wire anemometer method in hover provide a valuable means for investigating the wake characteristics of various tip shapes, and relating them to their performance characteristics.

   b. At low to medium thrust coefficients, the 58 deg swept tip shape outperformed both the square and double-swept tip over the tip speed range investigated.

   c. For a swept tip, high sweep angles are required to avoid tip vortex breakdown at high thrust coefficients. Once vortex breakdown occurs there is a significant reduction in rotor performance.

   d. Tip vortex induced lift in the tip region was found to be substantial for square tip rotors at high thrust coefficients.

3. The compressibility and noise investigation yielded these conclusions:

   a. The formation and strength of the spiral shock wave were strongly affected by the tip's airfoil profile and tip shape.

   b. The 70 deg swept tip produced less noise and better performance than the square tip at high tip Mach numbers.

VIII. RECOMMENDATIONS

1. Experimental investigations need to be conducted to determine vortex decay rates, as a function of number of blades and collective pitch, for various tip shapes.

2. Using the techniques developed in this investigation, the performance and flow field characteristics of other promising tip shapes need to be investigated.

3. Programs used to calculate hover performance need to account for vortex induced lift at high thrust coefficients.

4. Further schlieren studies need to be conducted to investigate the shock formation and noise characteristics associated with other tip shapes and airfoil profiles.

5. A free-wake analysis that can accommodate vortex diffusion and instability needs to be developed for accurately representing a hovering rotor's wake.

REFERENCES

1. Widnall, S. E.; Bliss, D.; and Zalay, A.: Theoretical and Experimental Study of the Stability of a Vortex Pair. Symposium on Aircraft Wake Turbulence (Seattle, Washington), September 1970.

2. MacCready, P. B.: An assessment of Dominant Mechanisms in Vortex-Wake Decay. Symposium on Aircraft Wake Turbulence (Seattle, Washington), September 1970.

3. Olsen, J. H.: Results of Trailing Vortex Studies in a Towing Tank. Symposium on Aircraft Wake Turbulence (Seattle, Washington), September 1970.

4. Levy, M. A.; and Forsdyke, A. C.: The Steady Motion and Stability of a Helical Vortex. Proceedings of the Royal Society, Series A, Vol. 120, 1928.

5. Crimi, P.: Theoretical Prediction of the Flow in the Wake of a Hovering Rotor. CAL Report BB-1994-S-1 and BB-1994-S-2, Cornell Aeronautical Laboratory, Inc., September 1965.

6. Tanner, W. H.; and Wohlfeld, R. M.: Vortex Field, Tip Vortex, and Shock Formation on a Model Propeller. Proceedings of the CAL/AVLABS Symposium on Aerodynamics of Rotary Wing and VTOL Aircraft, Vol. 1, June 1969.

7. Landgrebe, A. J.: An Analytical and Experimental Investigation of Helicopter Rotor Hover Performance and Wake Geometry Characteristics. USAAMRDL Technical Report 71-24, Eustis Directorate, USAAMRDL, June 1971.

8. Clark, D. R.; and Landgrebe, A. J.: Wake and Boundary Layer Effects in Helicopter Rotor Aerodynamics. AIAA 4th Fluid and Plasma Dynamics Conference, (Palo Alto, California), June 1971.

9. Landgrebe, A. J.: The Wake Geometry of a Hovering Helicopter Rotor and Its Influence on Rotor Performance. AHS Paper 620, Presented at the 28th Annual National Forum of the American Helicopter Society, May 1972.

10. Widnall, S. E.: The Stability of a Helical Vortex Filament. Journal of Fluid Mechanics, Vol. 54, pp. 641-633, 1972.

11. McCormick, B. W.; Spencer, R. H.; and Sternfield, H.: Tip Vortex Thickening for Application to Helicopter Rotor Noise Reduction. USAAVLABS Report 66-1, September 1966.

12. Spivey, R. F.: Blade Tip Aerodynamics - Profile and Planform Effects. Presented at the 24th Annual National Forum of the American Helicopter Society, May 1968.

13. Spivey, W. A.: New Insights into the Design of Swept-Tip Rotor Blades. Presented at the 26th Annual National Forum of the American Helicopter Society, June 1970.

14. Boatwright, D. W.: Measurement of Velocity Components in the Wake of a Full-Scale Helicopter Rotor in Hover. USAAMRDL Technical Report 72-33, Eustis Directorate, USAAMRDL, June 1972.

15. Cook, C. V.: The Structure of the Rotor Blade Tip Vortex. Presented at AGARD Specialists' Meeting on Aerodynamics of Rotary Wings, (Marseille, France), September 1972.

16. Prandtl, L.; and Tietjens, O. G.: Fundamentals of Hydro- and Aeromechanics. Dover Publications, 1934.

17. Betchov, R.: On the Curvature and Torsion of an Isolated Vortex Filament. Journal of Fluid Mechanics, Vol. 22, pp. 471-479, 1965.

18. Lamb, H.: Hydrodynamics. Cambridge University Press, 1932.

19. Logan, A. H.: Vortex Velocity Distributions at Large Downstream Distances. Journal of Aircraft, Vol. 8, No. 11, November 1971.

20. Chigier, N. A.; and Corsiglia, V. R.: Wind-Tunnel Studies of Wing Wake Turbulence. Journal of Aircraft, Vol. 9, No. 12, December 1972.

21. Rinehart, S. A.; Balcerak, J. C.; and White, R.P.: An Experimental Study of Tip Vortex Modification by Mass Flow Injection. RASA Report 71-01, January 1971.

22. White, R. P.; and Balcerak, J. C.: An Investigation of the Mixing of Linear and Swirling Flows. RASA Report 72-04, February 1972.

23. Wentz, W. H.; and Kohlman, D. L.: Vortex Breakdown on Slender Sharp-Edged Wings. Journal of Aircraft, Vol. 8, No. 3, pp. 156-161, March 1971.

24. Hubbard, H. H.; and Lassiter, L. S.: Sound from a Two-Blade Propeller at Supersonic Tip Speed. NACA TR-1079, 1952.

25. Jones, J. P.; and Noak, M.: Some Problems in the Numerical Solution of Vortex Motion Equations. Proceedings of the 3rd CAL/AVLABS Symposium on Aerodynamics of Rotary Wing Aircraft, Vol. III, Cornell Aeronautical Laboratory, Inc., (Buffalo, New York), June 1969.

NATIONAL AERONAUTICS AND SPACE ADMINISTRATION
WASHINGTON, D.C. 20546

OFFICIAL BUSINESS
PENALTY FOR PRIVATE USE $300

SPECIAL FOURTH-CLASS RATE
BOOK

POSTAGE AND FEES PAID
NATIONAL AERONAUTICS AND
SPACE ADMINISTRATION
451

U.S.MAIL

POSTMASTER: If Undeliverable (Section 158
Postal Manual) Do Not Return

"The aeronautical and space activities of the United States shall be conducted so as to contribute . . . to the expansion of human knowledge of phenomena in the atmosphere and space. The Administration shall provide for the widest practicable and appropriate dissemination of information concerning its activities and the results thereof."

—NATIONAL AERONAUTICS AND SPACE ACT OF 1958

NASA SCIENTIFIC AND TECHNICAL PUBLICATIONS

TECHNICAL REPORTS: Scientific and technical information considered important, complete, and a lasting contribution to existing knowledge.

TECHNICAL NOTES: Information less broad in scope but nevertheless of importance as a contribution to existing knowledge.

TECHNICAL MEMORANDUMS: Information receiving limited distribution because of preliminary data, security classification, or other reasons. Also includes conference proceedings with either limited or unlimited distribution.

CONTRACTOR REPORTS: Scientific and technical information generated under a NASA contract or grant and considered an important contribution to existing knowledge.

TECHNICAL TRANSLATIONS: Information published in a foreign language considered to merit NASA distribution in English.

SPECIAL PUBLICATIONS: Information derived from or of value to NASA activities. Publications include final reports of major projects, monographs, data compilations, handbooks, sourcebooks, and special bibliographies.

TECHNOLOGY UTILIZATION PUBLICATIONS: Information on technology used by NASA that may be of particular interest in commercial and other non-aerospace applications. Publications include Tech Briefs, Technology Utilization Reports and Technology Surveys.

Details on the availability of these publications may be obtained from:

SCIENTIFIC AND TECHNICAL INFORMATION OFFICE

NATIONAL AERONAUTICS AND SPACE ADMINISTRATION

Washington, D.C. 20546